STEAM JET EJECTOR COOLING POWERED BY LOW GRADE WASTE OR SOLAR HEAT

by

Adriaan Jacobus Meyer

Thesis presented in partial fulfilment of the requirements for the degree of MscEng in Mechanical Engineering
Stellenbosch University

Thesis supervisor:
Professor TM Harms

Thesis co-supervisor:
Mr RT Dobson

December 2006

DECLARATION

I, the undersigned, hereby declare that the work contained in this thesis is my own original work and that I have not previously, in its entirety or in part, submitted it at any university for a degree

Signature:_____ Date:_____

Adriaan Jacobus Meyer

ABSTRACT

A small scale steam jet ejector experimental setup was designed and manufactured. This ejector setup is of an open loop configuration and the boiler can operate in the temperature range of T_b = 85 °C to 140 °C. The typical evaporator liquid temperatures range from T_e = 5 °C to 10 °C while the typical water cooled condenser pressure ranges from P_c = 1.70 kPa to 5.63 kPa (T_c = 15 °C to 35 °C). The boiler is powered by two 4 kW electric elements while a 3 kW electric element simulates the cooling load in the evaporator. The electric elements are controlled by means of variacs.

The function and fluid dynamics of a steam jet ejector is explained by means of a theoretical model found in literature. The detailed operation of the steam ejector is further represented in the form of a literature study. The proper functioning of a steam jet ejector is dependant on the following parameters: the boiler temperature, the evaporator temperature, the critical condenser pressure, the primary nozzle exit position and the ejector throat ratio A_R. A condenser pressure higher than the critical condenser pressure and the super- heating of the primary steam has a negligible effect on the system's operation.

Experimental results conducted at a boiler temperature of T_b = 130 °C compare well to published experimental data conducted at similar operating conditions. This verifies the general operation of the experimental setup.

Primary nozzles with throat diameters of 2.5 mm, 3.0 mm and 3.5 mm are tested while the secondary ejector throat diameter remains unchanged at 18 mm. These primary nozzles allow the boiler to operate in the temperature range of 85 °C to 110 °C. When the nozzle throat diameter is increased, the minimum boiler temperature decreases. A primary nozzle with a 3.5 mm throat diameter was tested at a boiler temperature of T_b = 95 °C, an evaporator temperature of T_e = 10 °C and a critical condenser pressure of P_{crit} = 2.67 kPa (22.6 °C). The system's electric COP is 0.253.

In a case study, the experimental data of a solar powered steam jet ejector air conditioner is investigated. Solar powered steam ejector air conditioning systems are technically and economically viable when compared to conventional vapour compression air conditioners. Such a system can either utilise flat plate or evacuated tube collectors, depending on the type of solar energy available.

A steam ejector can be used for rapid subzero vacuum cooling. This was demonstrated through experiments in which 7 L of water could be cooled down from room temperature to 2.4 °C in less than 10 min. During this test, the evaporator vapour temperature reached temperatures as low as –8.5 °C.

OPSOMMING

‘n Kleinskaalse eksperimentele stoom ejektor opstelling is ontwerp en vervaardig. Hierdie ejektor opstelling gebruik ‘n ooplus konfigurasie en kan funksioneer met keteltemperature in die gebied van T_b = 85 °C to 140 °C. Die tipiese verdampertemperatuur gebied is T_e = 5 °C to 10 °C terwyl die tipiese druk gebied van die waterverkoelde konden-ser P_c = 1.70 kPa to 5.63 kPa (T_c = 15 °C to 35 °C) is. Stoom in die ketel word geproduseer deur twee 4 kW elektriese elemente. Die verdamper se verkoelingslas word gesimuleer deur ‘n enkele 3 kW elektriese element. Beide die elektriese elemente word beheer deur verstelbare transfor-mators.

‘n Teoretiese model vanuit die literatuur beskryf die funksie en vloeidinamika van die stoom ejektor. Die breedvoerige werking van ‘n stoom ejektor word verder verduidelik aan die hand van ‘n literatuurstudie. Die korrekte werking van ‘n stoom ejektor word bepaal deur die volgende parameters : die keteltemperatuur, die verdampertemperatuur, die kritiese kondensor druk, die primêre spuitstukuitlaat posisie en die ejektor keëlverhouding A_R. ‘n Kondensordruk hoër as die kritiese kondensordruk en die superverhitting van die primêre stoom het ‘n weglaatbare effek op die sisteem.

Eksperimentele resultate wat verkry is by ‘n keteltemperatuur van T_b = 130 °C vergelyk goed met gepubliseerde data uitgevoer by soortgelyke bedieningstoestande. Hierdie verifieer die algemene funksioneering van die eksperimentele opstelling.

Terwyl die sekondêre spuitstuk se keëldiameter onveranderd gehou is by 18 mm, is primêre spuitstukke met keëldiameters van 2.5 mm, 3.0 mm en 3.5 mm getoets. Die verskillende spuitstukke laat die ketel toe om in die temperatuur gebied van 85 °C to 110 °C te funksioneer. Indien die primêre spuitstuk diameter vergroot word, verlaag die minimum ketel temperatuur. ‘n Primêre spuitstuk met ‘n 3.5 mm keëldiameter is getoets by ‘n ketel temperatuur van T_b = 95 °C, ‘n verdamper temperatuur van 10 °C en ‘n kritiese kondensordruk van P_{crit} = 2.67 kPa (22.6 °C). Die sisteem se elektriese “COP” is 0.253.

In ‘n gevallestudie is die eksperimentele data van ‘n sonaangedrewe stoom ejektor lugverkoeler ondersoek. Sonaangedrewe stoom ejektor lugverkoeling is tegniese en ekonomiese haalbaar wanneer dit vergelyk word met konvensionele lugverkoeling. Die sisteem kan platplaat of ge-evakueerde buis sonverhitters gebruik afhangende van die tipe sonlig wat beskikbaar is.

‘n Stoom ejektor kan toegepas word op snel subzero vakuum verkoeling. Hierdie metode is gedemonstreer deur eksperimente waarin 7 L water afgekoel kon word vanaf kamertemperatuur tot 2.4 °C in minder as 10 minute. Tydens hierdie eksperiment het die verdamper damptemperatuur ‘n minimum –8.5 °C bereik.

ACKNOWLEDGEMENTS

I would like to thank the following people:

- Professor Thomas Harms, as thesis supervisor, for his guidance, encouragement and support during this project
- Mr Robert Dobson, as thesis co-supervisor, for his enthusiasm and advice from previous experience with steam jet ejectors
- Mr Cobus Zietsman and the team from SMD for their technical advice and support with constructing the experimental setup
- Johann Stander, for being such a patient and diligent proof reader
- To my family and friends for support, interest and prayers

It is the glory of God to conceal a matter,
but the glory of kings is to search out a matter

King Solomon

TABLE OF CONTENTS

LIST OF FIGURES

LIST OF TABLES

NOMENCLATURE

A	area	[m^2]
A_T	nozzle area ratio ($A_T = A_{exit}/A_t$)	[-]
A_{exit}	nozzle exit area	[m^2]
A_t	nozzle throat area	[m^2]
A_4	ejector profile throat area	[m^2]
A_R	ejector throat ratio	[-]
C_{sc}	solar collector constant	[W/°Cm^2]
d	diameter	[mm]
G	solar irradiation	[W/m^2]
h	specific heat	[kJ/kg]
h_g	specific heat in gas state	[kJ/kg]
h_f	specific heat in fluid state	[kJ/kg]
h_{fg}	specific heat of evaporation	[kJ/kg]
I	electric current	[A]
k	specific heat ratio	[-]
$\dot{m}$	mass flow rate	[kg/s]
P	pressure/electric power	[A]/[W]
P_{co}	limiting condenser pressure	[Pa]
P_c	critical condenser pressure	[Pa]
Q	heat	[J]
R_m	entrainment ratio	[-]
s	entropy	[kJ/kg-K]
T	temperature	[°C]
T_c	critical condenser temperature	[°C]
v	velocity	[m/s]
V	volume/electric volts	[m^3]/[V]
W	work	[J]

NOMENCLATURE, (continue)

Greek symbols

η	efficiency	[%]
ρ	density	[kg/m^3]
Ω	electric resistance	[ohms]

Subscripts

a	ambient
b	boiler
c	condenser
d	diffuser
e	evaporator / exit
f	fluid
elec	electrical
g	gas (vapour)
i	inlet
m	mixing chamber / mean
o	outlet
sc	solar collector
1	constant pressure mixing section
2	secondary nozzle throat
3	position before shock wave
4	position after shock wave / secondary nozzle throat
1’	primary nozzle exit
1”	secondary flow inlet
P	primary nozzle
t	throat
theo	theoretical

ABBREVIATIONS

AC	alternating current
CD	compact disk
CFC	chlorofluorocarbon
COP	coefficient of performance
HCFC	hydrochlorofluorocarbons
HFC	hydrofluorocarbons
ID	inner diameter
IR	infrared
OD	outer diameter
PC	personal computer
PCM	phase change material
PVC	polyvinyl chloride
UK	United Kingdom

1. INTRODUCTION

High oil prices can be good news – it drives the research into renewable energy alternatives. It further promotes the efficient use of energy and it encourages people to seek ways of utilising waste heat or energy.

Waste process heat and waste steam is common in industry and it can be applied for heating, cleaning and absorption cooling cycles along with other uses. The application of waste heat is determined by the temperature of the heat or steam. Waste heat has more uses at higher temperatures. Waste steam and process heat below 100 °C is often termed low grade waste heat.

The need for cooling is common in many industries and ranges from product refrigeration to space cooling. The main aim of this thesis is to investigate the use of low grade heat to drive a steam jet ejector cooling cycle.

A steam jet ejector that can operate at a boiler temperature of 100 °C or below can easily be powered by conventional flat plate solar water heaters. Since the cooling load is commonly synchronised with the availability of solar energy, this becomes an attractive application of solar energy.

The objectives of this project are:

1) *Design and build a small scale experimental steam jet ejector setup.*

   Chapter 2 will explain the thought process behind the design of such a system. It will further explain how such a setup was constructed as well as the experimental method that was followed.

2) *Explain the fluid dynamic theory relevant to the steam jet ejector.*

   Chapter 3 will explain the fluid dynamic theory based on present literature. This will include the efficiency of the primary nozzle, the mixing chamber and the diffuser. This theoretical model is compared to experimental results in chapter 5.

3) *Explain the function and fluid dynamics of a steam jet ejector in the context of a literature study.*

The work of various authors on small scale steam ejectors will be presented in chapter 4 in the form of a literature study. The

effect of the boiler and evaporator temperatures as well as the condenser pressure on the system performance is represented. Chapter 4 further aims to explain the mixing of the primary and secondary streams and the influence of the primary nozzle exit position based on published experimental results.

4) *Verify the operation of a small scale steam ejector system at familiar boiler temperatures.*

   The steam jet ejector is well documented in literature. This is, however, mostly for boiler temperatures in the range of T_b = 110 °C to 140 °C. The initial aim of Chapter 5 will be to compare experimental results obtained by the author for a boiler temperature of T_b = 130 °C to that of experimental data published in literature at the same operating conditions. This comparison aims to benchmark the operation of the constructed experimental setup.

5) *As the main aim of this thesis, investigate and document the proposed operation of the system at boiler temperatures less than 100 °C.*

   Chapter 5 will explain tests conducted on primary nozzles with different throat diameters. Tests on boiler temperatures would start at 110 °C. The primary nozzle throat diameter will be increased after every successful test. The aim would be to lower the boiler temperature as low as the other system parameters would practically allow for each primary nozzle that is tested. The experimental results of each nozzle and corresponding boiler temperatures are documented. A comparison to theory and other published data will be presented.

6) *Investigate the possibility of a solar thermal driven system.*

   Chapter 6 will be dedicated to the discussion of a solar powered steam ejector system. A case study will be conducted on an existing solar powered steam ejector air conditioner. Different types of solar collectors and different configurations for incorporating solar collectors to an ejector system will be investigated.

7) *Through the above lay, the foundation for further research in this field of endeavour and comment on any new applications thereof or insight gained into steam jet ejectors powered by low grade waste heat.*

2. THE STEAM JET SYSTEM

2.1 System Layout and Operation

A steam jet refrigerator was first developed by Le Blanc and Parson as early as 1900 (ASHRAE, 1969). It experienced a wave of popularity during the early 1930s for air conditioning systems of large buildings (Stoecker, 1959). The system was replaced with the more favourable vapour compression system. The latter system was superior in its coefficient of performance (COP), flexibility and compactness in manufacturing and operation (Eames et al., 1995a).

The steam ejector cycle is similar to the conventional vapour compression cycle except that the compressor is replaced by a liquid feed pump, boiler and ejector-pump. In brief, liquid refrigerant is vaporised at a high pressure in a boiler and fed to an ejector where it entrains a low pressure vapour originating from the evaporator. This combined flow is then compressed to an intermediate pressure equal to that of the condenser. This cycle has recently drawn renewed attention due to its simplicity of construction, ruggedness and few moving parts.

Figure 2.1 shows a schematic of the conventional ejector refrigeration cycle. The cycle typically consists of the boiler, the ejector, the condenser and the evaporator.

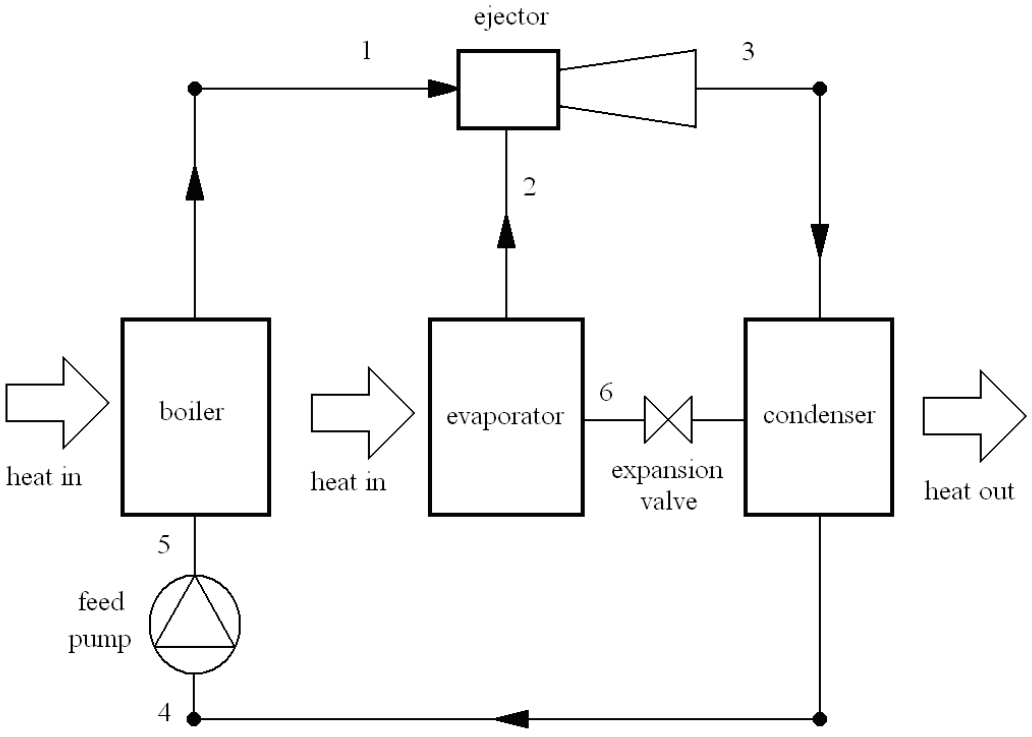

Figure 2.1: Ejector cycle (Chunnanond and Aphornratana, 2004b)

In figure 2.1, the liquid refrigerant boils in the boiler at a high pressure and temperature due to the application of heat. This high-pressure refrigerant vapour passes through line 1 and enters the primary nozzle of the ejector compressor. A typical ejector cross-section with pressure and velocity profiles is shown in figure 2.2. The primary stream accelerates and expands through a convergent-divergent (de Laval) nozzle to produce super-sonic flow (typical Mach number above 2), which creates a low pressure region. This partial vacuum created by the supersonic primary flow entrains refrigerant vapour from the evaporator through momentum transfer in line 2. The evaporator pressure falls and boiling of the refrigerant in the evaporator occurs at a low pressure and consequently at a low temperature.

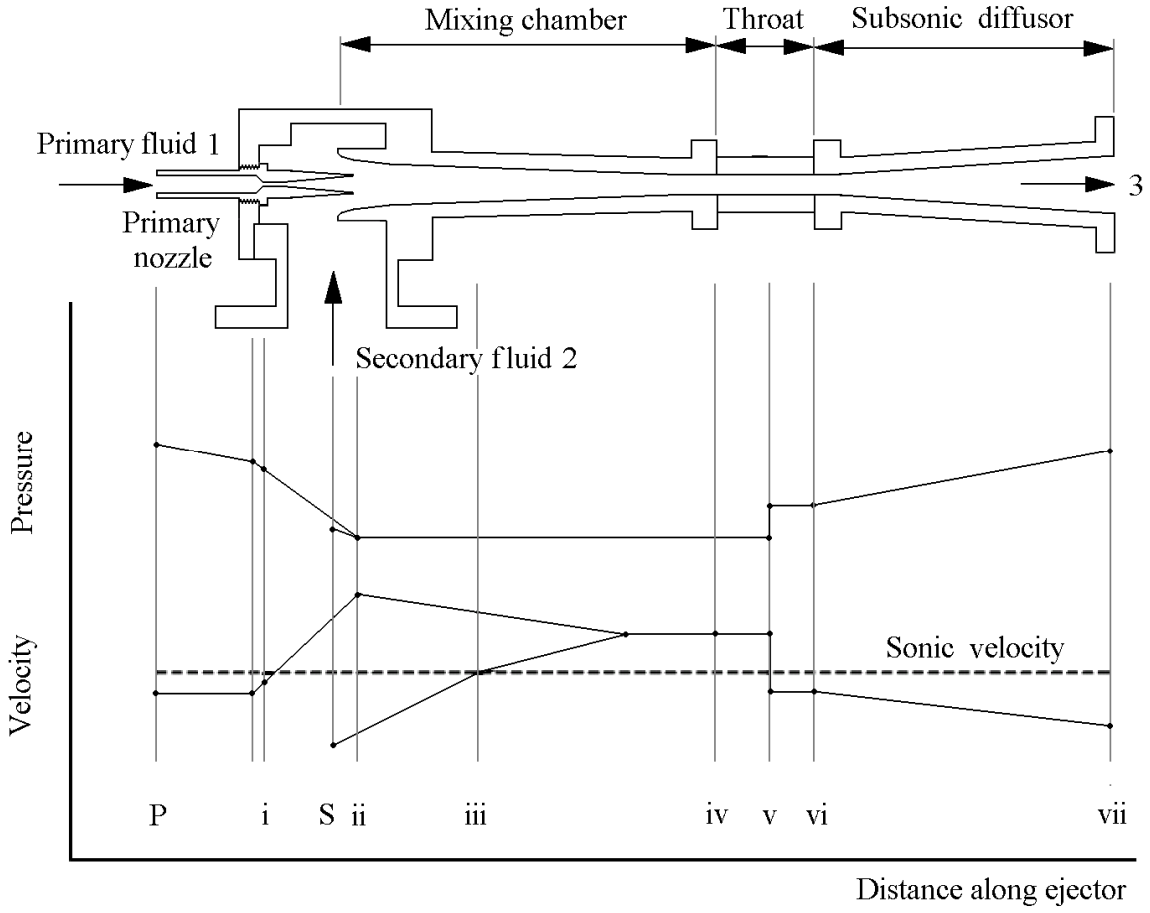

Figure 2.2: Typical ejector cross section and pressure and velocity profiles (Chunnanond and Aphornratana, 2004a)

The primary and secondary streams mix in the mixing chamber and enter a normally choked (sonic flow conditions at the throat) secondary converging-diverging nozzle (also referred to as the ejector profile). The flow expands in the diffuser part of this nozzle through a thermodynamic shock process. This shock wave causes a sudden rise in the static pressure and its location varies with the

condenser backpressure. The flow emerges from the shock wave with subsonic velocity and is compressed in the diffuser to the saturation pressure of the condenser.

From the diffuser exit, the mixed flow is fed directly to the condenser through line 3 where it is cooled and condensed. The condensate is returned to the evaporator via an expansion valve in line 6 and to the boiler through a feed pump in line 4. A full description of ejector principles and performance and industrial applications can be found in additional texts (e.g. Engineering Sciences Data Unit, 1986).

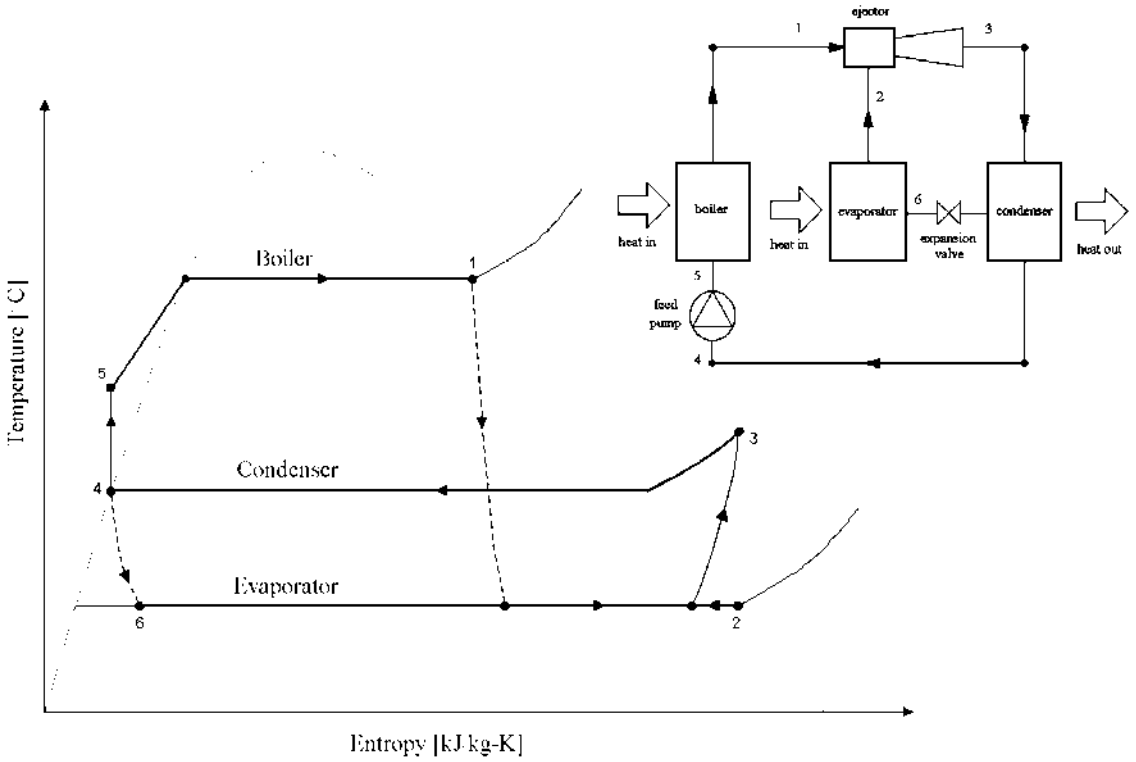

Figure 2.3: General steam ejector T-s diagram and corresponding system cycle (Van Wyk, 2000)

Figure 2.3 present a general thermodynamic analysis for the ejector cycle. Different working fluids can be used in an ejector cycle e.g. halocarbon compounds such as CFCs, HCFCs and HFCs, (Eames et al., 1995b) as well as butane, ammonia and water (Pridasawas, 2003a).

Water is by far the most environmentally friendly fluid. Using water as working fluid the evaporator temperature typically varies in the range 5 °C to 15 °C depending on the application. Typical condenser temperatures vary in the range 15 °C to 40 °C depending on the condenser type (wet or dry cooled), cooling water temperature and ambient conditions. In practical systems, the boiler temperature should be above 80 °C according to Eames et al. (1999). COP values for the cycle typically vary in the range of 0.1 – 0.6, depending on the operating conditions.

2.2 The Experimental Setup

A photo and accompanying schematic drawing of the experimental setup is included in figure 2.4 and 2.5 respectively.

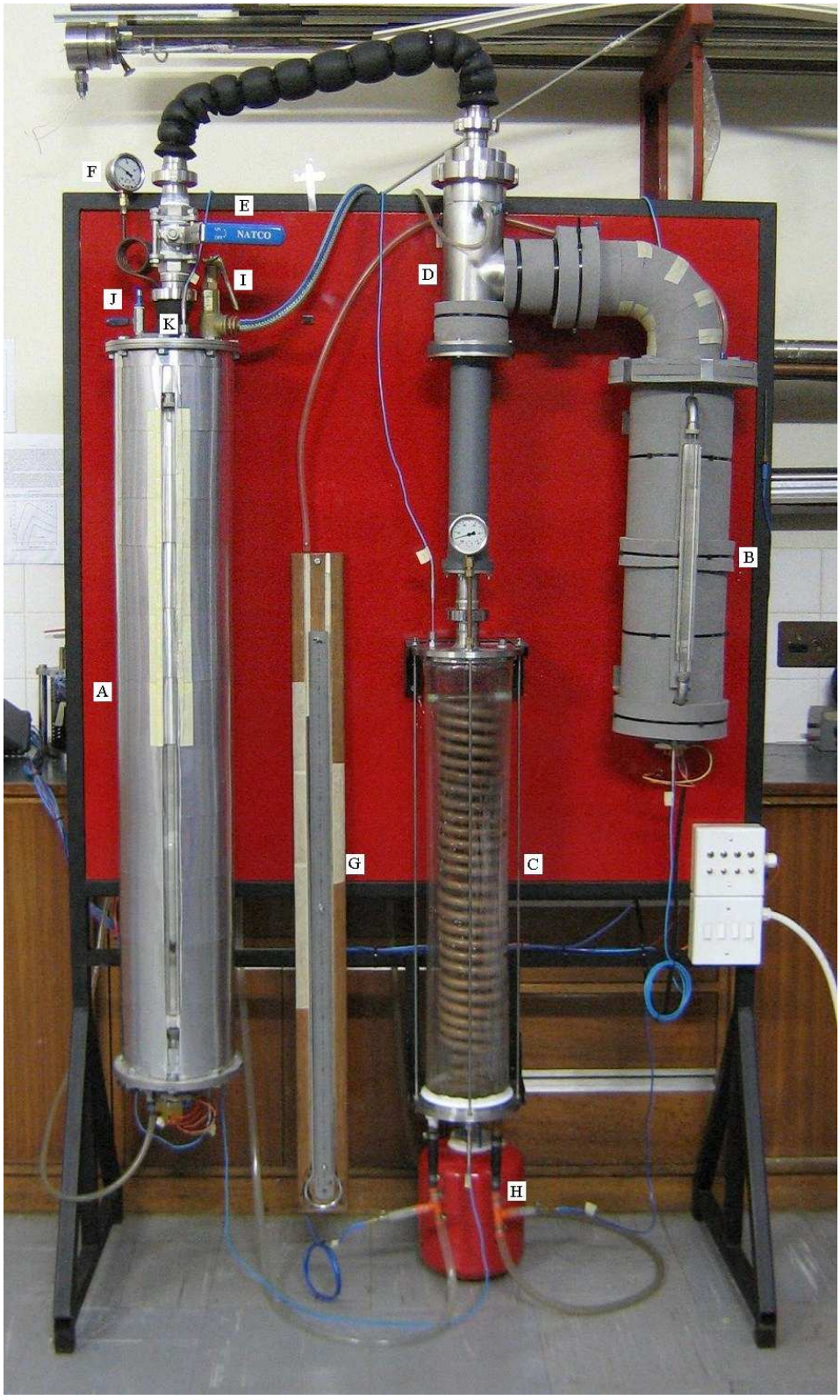

Figure 2.4: The ejector experimental setup

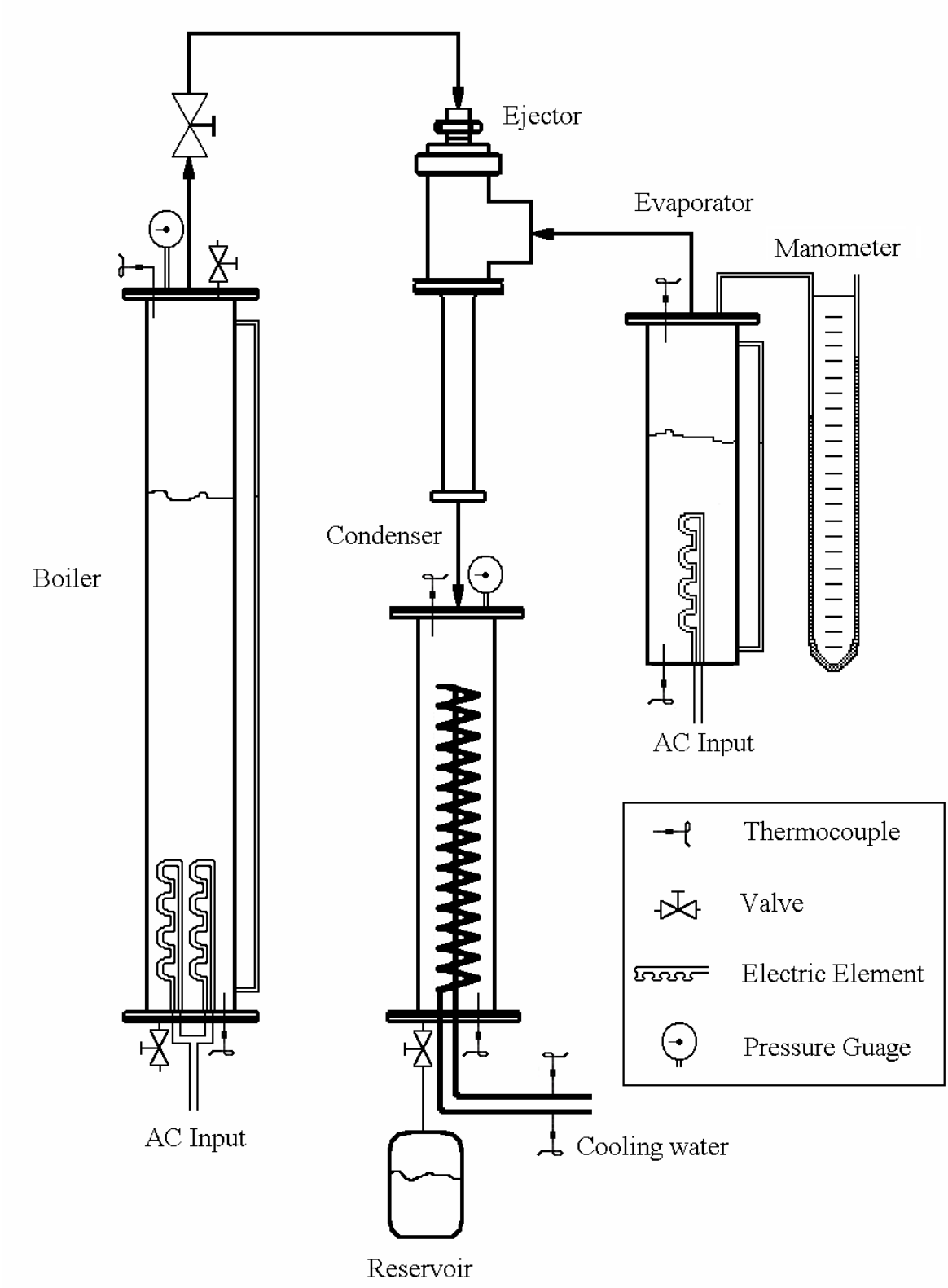

Figure 2.5: Schematic of the experimental setup

The design of the experimental setup was done with the aid of published work of Eames et al. (1995b) and Eames et al. (1999) as well as previous work done at Stellenbosch University (figure B.1, Van Wyk, 2000). The aim of the design was to keep the system as

simple as possible and use off-the-shelf components where feasible. More complex system schematics from other authors are included in figure B.2.

In reference to figure 2.5 the test facility consists of four principal components: a 8 kW electrical steam boiler (A), a 3 kW evaporator (B), a water-cooled condenser (C) and an ejector assembly (D) as labelled in figure 2.4. Detailed mechanical drawings of the experimental setup can be found in appendix C and on the data CD included at the back of the thesis.

2.2.1 The boiler (A)

The boiler was manufactured from a 150 mm ID stainless steel pipe 1250 mm in length and 2 mm wall thickness. The bottom and top ends of the pipe were fitted with bolted stainless steel flanges 8 mm in thickness as well as viton o-rings. Two 4 kW electric elements, a thermocouple, two thermostats and a drain valve were mounted on the bottom flange. The top flange was fitted with a variable pressure relief valve (I), an analogue pressure gauge (F), a steam pipe, a ball valve (E), a thermocouple (J) and a drain valve (K) as can be seen in figure 2.4 and figure 2.6. The boiler was insulated with 25 mm fibre wool insulation and aluminium cladding was used. This can be seen in figure 2.4.

Figure 2.6: The uninsulated boiler (insert right: boiler top enlarged)

The boiler water level is measured by means of a sight glass. The sight glass was manufactured from a 12 mm OD and 2 mm wall thickness glass tube. The boiler has a total volume of 22.1 L and the useable volume available between the top of the electric elements and the top of the sight glass is 15.2 L. The boiler was designed to operate at T_b = 80 °C to 140 °C and the corresponding pressure span of $P_b \approx$ 45 kPa to 360 kPa. At the maximum steam flow of 13.5 kg/h (8 kW boiler electric energy input and T_b = 140 °C) the boiler can produce steam for more than an hour. Steam leaves the boiler through a 40 mm ID, 2 mm wall thickness pipe and ball valve (E). The boiler was hydrostatically tested up to 400 kPa before it was fitted.

2.2.2 The evaporator (B)

The evaporator (figure 2.7) was manufactured from a 150 mm ID stainless steel pipe 600 mm in length and 2 mm wall thickness. The bottom end was welded closed and fitted with a 3 kW electric element and a thermocouple. The top end of the evaporator has bolted stainless steel flanges and an o-ring and is fitted with a thermocouple and mercury manometer (G). The water content is measured with a sight glass similar to that of the boiler. The total volume of the evaporator is 10.6 L and the useable volume between the top of the electric element and the top of the sight glass is 4.1 L.

Figure 2.7: Partly insulated evaporator

Water vapour flows from the evaporator to the ejector through a stainless steel pipe and elbow, both 100 mm ID. The connection between the evaporator pipe and ejector is done with a 100 mm ID stainless steel union. A connection pipe with a large diameter was chosen due to the high specific volume of steam at low temperatures (147.1 m^3/kg at 5 °C and 77.9 m^3/kg at 15 °C versus 1.67 m^3/kg at 100 °C). A large diameter pipe is necessary to ensure a low vapour velocity. With the evaporator operating at maximum electric input of 3 kW and at an evaporator temperature of 5 °C the steam velocity in the 100 mm ID pipe is 22.6 m/s.

The evaporator vapour and liquid temperatures are measured with separate thermocouples (figure 2.5). The pressure within the evaporator is determined by means of the steam tables as well as with the mercury manometer (G). A difference between these two pressures mentioned indicates the presence of air in the evaporator. The evaporator is insulated with 10 mm thick Armaflex insulation.

The electric element simulates the evaporator cooling load. This element is controlled with a variac.

2.2.3 The condenser (C)

A boiler unit from a previous experimental setup (figure B.1) was modified to a condenser (figure 2.8). A 150 mm diameter Perspex pipe 800 mm long and with 3 mm wall thickness is fitted with stainless steel flanges. Silicone was used to ensure an airtight joint between the Perspex and endplates. The top plate is fitted with a thermocouple and an analogue pressure gauge. This plate also connects to the bottom of the ejector through a 40 mm stainless steel pipe and union as can be seen in figure 2.8. The bottom plate has a drain valve, thermocouple and a cooling water inlet and outlet.

Inside the condenser is a copper cooling coil. This coil was manufactured from 15 mm OD plain copper pipe and wound in two spirals. The outer spiral has an OD of 120 mm and the inner spiral has an OD of 85 mm. 15 m of copper pipe was used and the wounded coil is approximately 700 mm long.

The temperature inside the condenser is controlled by the cooling water flow rate. The minimum temperature in the condenser is limited by the temperature of the cooling water. The total volume of the condenser is 14.1 L without the cooling coil. The volume of the condenser with the cooling coil fitted is 11.5 L. The cooling water inlet and outlet pipes are both fitted with thermocouples (figure 2.8c).

A receiver tank (H) with a capacity of 8 L is connected to the outlet of the condenser. This tank serves as a reservoir for the condensate.

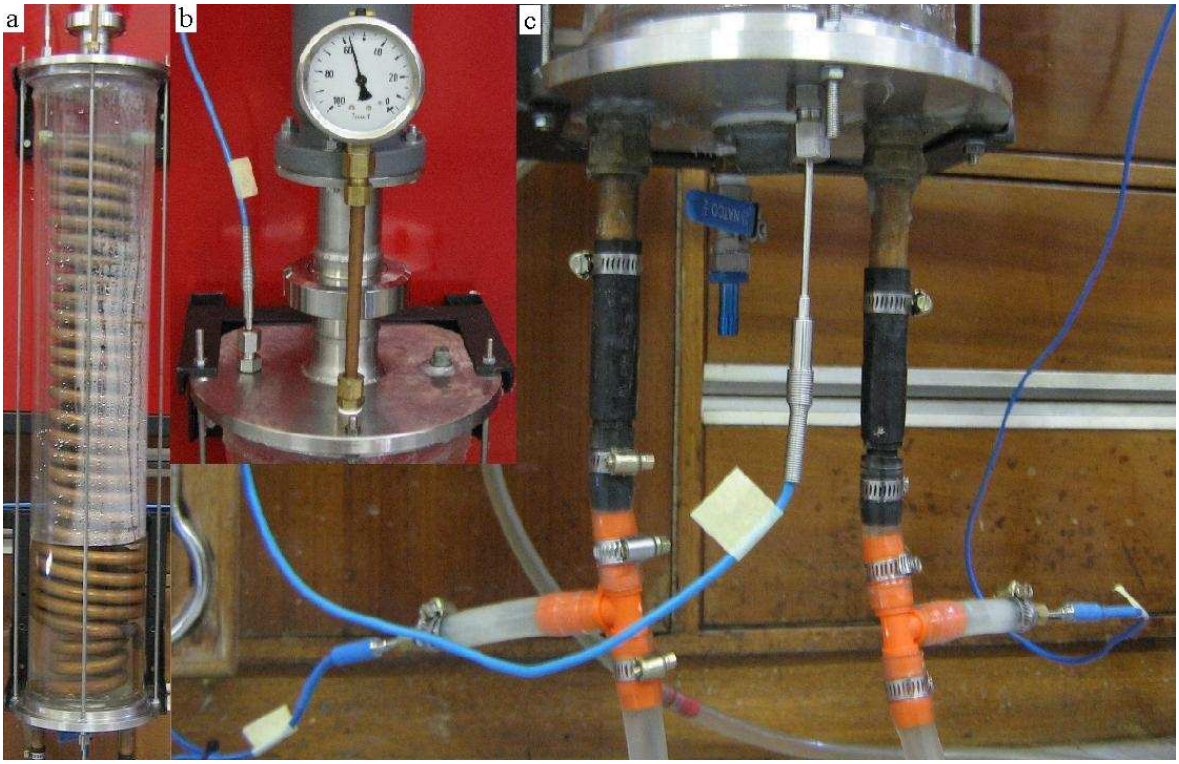

Figure 2.8: The condenser (reservoir not fitted)
a) Complete condenser
b) Condenser top with thermocouple and pressure gauge
c) Condenser bottom including drain valve, thermo-couple and cooling water pipes with thermocouples

2.2.4 The ejector (D)

Figure 2.9 shows a drawing and a photo of the ejector assembly. The outer body in which the nozzle is situated is made from a standard 100 mm ID, 2 mm wall thickness stainless steel T-piece. Two 100 mm ID unions connect the T-piece to the boiler and the evaporator. A ½" valve is located near the top of the T-piece and is used along with the vacuum pump to remove air from the system.

A flange and o-ring connects the bottom end of the T-piece to the secondary nozzle. The secondary nozzle is manufactured from a solid piece of PVC, 150 mm in diameter and 325 mm in length. This secondary nozzle has a throat length of 40 mm and a throat diameter of 18 mm. The secondary nozzle throat is a critical dimension in the proper operation of the system. The secondary nozzle profile was obtained from published data of Aphornratana and Eames (1997). Refer to appendix C for a detailed drawing of the secondary nozzle profile and other components.

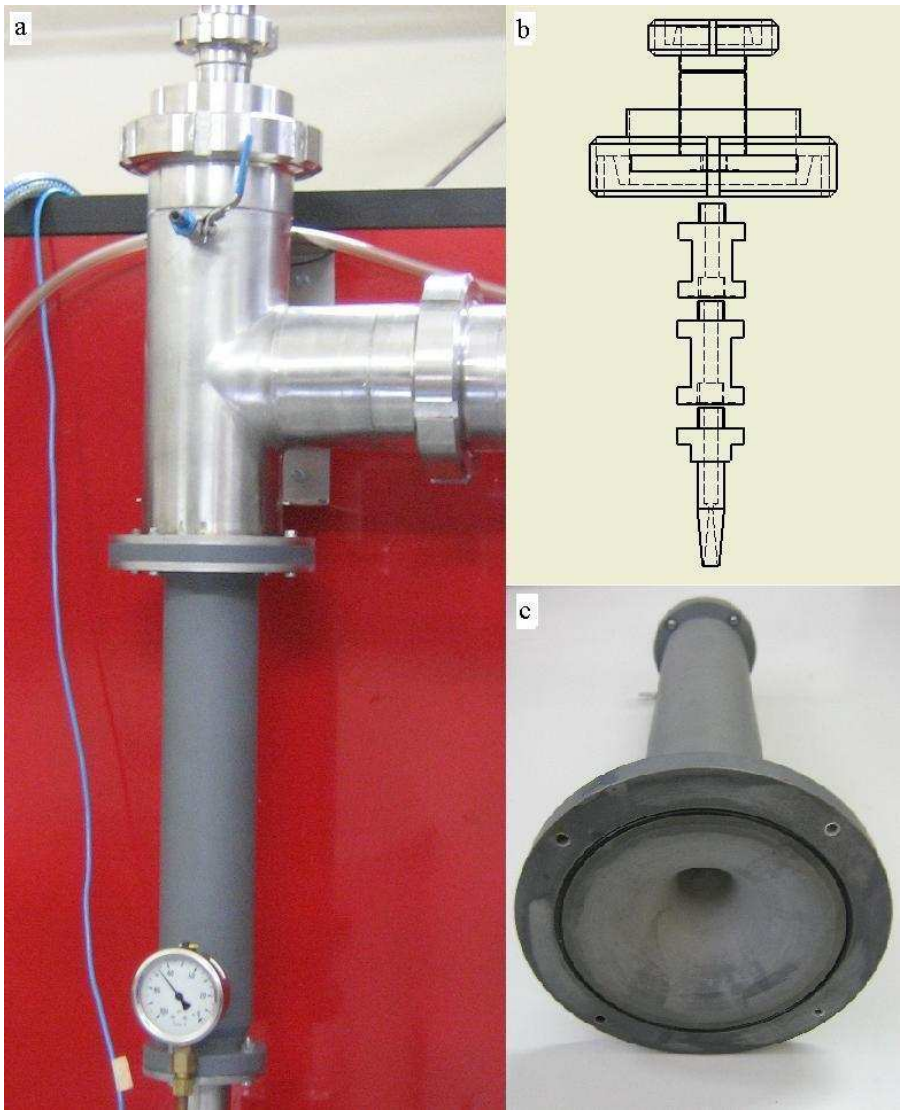

Figure 2.9: The ejector assembly
a) the complete ejector
b) the nozzle and spacers positions
c) the secondary nozzle (seen from above)

The nozzle and spacers are manufactured from brass and viton o-rings are used. The spacers and nozzle screw into a flange that is connected to the top end of the T-piece (figure 2.9 b, SteamJet06_05_01P – appendix C). There are six spacers (40, 45, 50, 60, 70 and 80 mm in length). By using different combinations of spacers, the primary nozzle position can vary relative to the flange they screw into with 5 mm intervals (figure 2.9b). The spacers are covered with a piece of Armaflex insulation as shown in figure 2.10c. Table A.2 list the different nozzle dimensions. The nozzle throat diameters varied from 1.5 mm to 3.5 mm.

Figure 2.10: a,b) The nozzle and spacer
c) The nozzle and spacers screwed together and covered with insulation

A 99 mm diameter 2 mm thick stainless steel locator (figure 2.11a) is used to align the primary nozzle with the secondary nozzle. The spacer fits tightly over the nozzle, as shown in figure 2.11b.

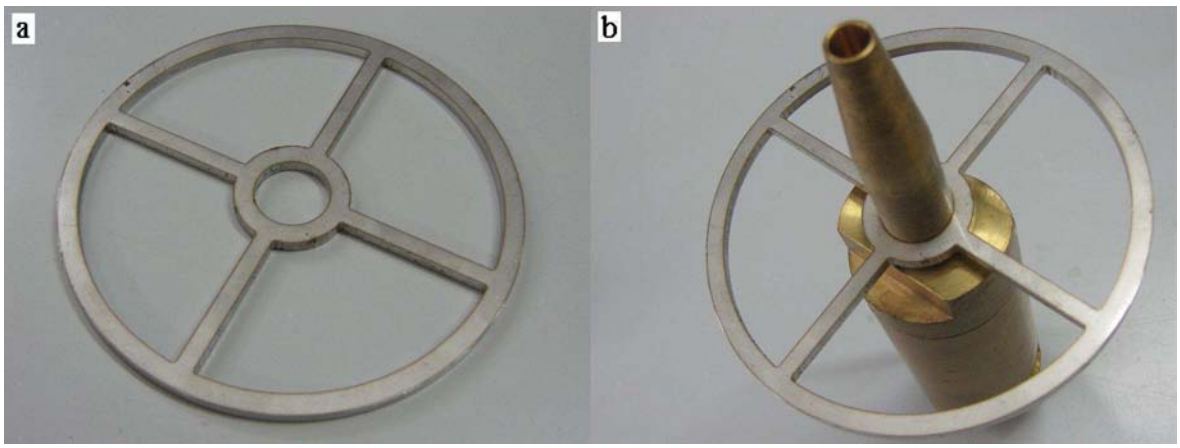

Figure 2.11: a) Stainless steel locator
b) Locator and nozzle

2.2.5 Other components

A 40 mm ID, 2 mm wall thickness stainless steel pipe connects the boiler and ejector assembly. This pipe is tilted at an angle of 15 ° from the horizon. Condensate that forms inside the pipe can run back to the boiler (figure 2.4). The pipe is covered with 10 mm thick Armaflex insulation.

A data logger connected to a PC is used to log the temperatures from the T-type thermocouples. The voltage to each electric element is also recorded. The serial numbers of the equipment used can be found in table A.3.

The test facility has no pump between the condenser and boiler and no expansion valve between the condenser and evaporator. Such a system is termed an open loop system.

2.3 The Experimental Test Procedure

Experiments are executed in batches. Before each test run the boiler and evaporator are filled with municipal tap water up to a predetermined level near the top of the sight glass. The boiler valve is closed and air is evacuated from the boiler by using a water-jet vacuum pump connected to the top of the boiler. The next step is to switch the boiler electric elements on.

While the boiler heats up to its operating temperature, the vacuum pump is used to evacuate air from the rest of the system. The steam pipe, ejector assembly, evaporator and condenser are all connected to each other without any valves. The vacuum pump is connected to the top of the ejector T-piece. When the boiler is at its operating temperature the boiler valve is opened. This allows the connection pipe between the boiler and ejector to be heated. It also serves to drives out the air still trapped in the connection pipe. The boiler valve is only opened for about five seconds at a time. The boiler valve is opened and closed for a few times while the vacuum pump is running. This is done until the air is removed from the connection pipe and the rest of the system.

Next, the boiler valve is closed and the boiler water level is refilled to the predetermined level. The boiler is reheated to its operating temperature. The cooling water supply to the condenser is turned on and the data logger is switched on. To start a test run, the boiler valve is opened. An immediate rise in condenser pressure is observed while the evaporator temperature falls rapidly. The boiler and evaporator temperatures are controlled with a variac. The thermostat on each boiler element acts as an over-temperature and thus an over-pressure protection. The boiler and evaporator mass flow rate is determined by measuring the total amount of liquid that was converted into steam over the entire time interval of the test run.

3 EJECTOR THEORY

3.1 Ejector Theory

The primary and secondary nozzles are concentric. This allows one-dimensional compressible flow theory to be applied. Some of the first ejector models were presented by Keenan and Neuman (1942) and was used to analyse air ejectors. Their first one-dimensional model was based on ideal gas dynamics as well as the principles of conservation of mass, momentum and energy. Heat and friction losses were not considered. Their approach excluded the diffuser section and only provided solutions for ejectors with constant-area mixing chambers as opposed to a conical mixing section (constant pressure) as described in this thesis.

Later the theoretical model was extended to include a constant pressure mixing chamber and a diffuser (Keenan et al. (1950)). This model did not include friction nor heat losses. Eames et al. (1995a) extended the latter model to include irreversibilities associated with the primary nozzle, mixing chamber and diffuser. Their analysis is based on the well-known steady-state and steady flow equations of energy, momentum and continuity as follow:

Energy equation for an adiabatic process:

$$\sum \dot{m}_i (h_i + V_i^2/2) = \sum \dot{m}_o (h_o + V_o^2/2) \tag{3.1}$$

Momentum equation:

$$P_i A_i + \sum \dot{m}_i V_i = P_o A_o + \sum \dot{m}_o V_o \tag{3.2}$$

Continuity equation:

$$\sum \rho_i V_i A_i = \sum \rho_o V_o A_o \tag{3.3}$$

The following assumptions were made. Refer to figure 3.1:

1. Isentropic efficiencies were introduced to the primary nozzle, diffuser and mixing chamber to account for friction losses.
2. The primary and secondary flows enter the ejector at zero velocity.
3. At the primary nozzle plane (1), where the primary and secondary streams first meet, the static pressure is assumed to be uniform.

4. Mixing of the primary and secondary flows is complete before a normal shock wave occurs at the end of the mixing chamber.

The entrainment ratio of an ejector is defined as the ratio between the ejector (secondary) and boiler (primary) fluid mass flow rates:

$$R_m = \frac{\dot{m}_e}{\dot{m}_b} \tag{3.4}$$

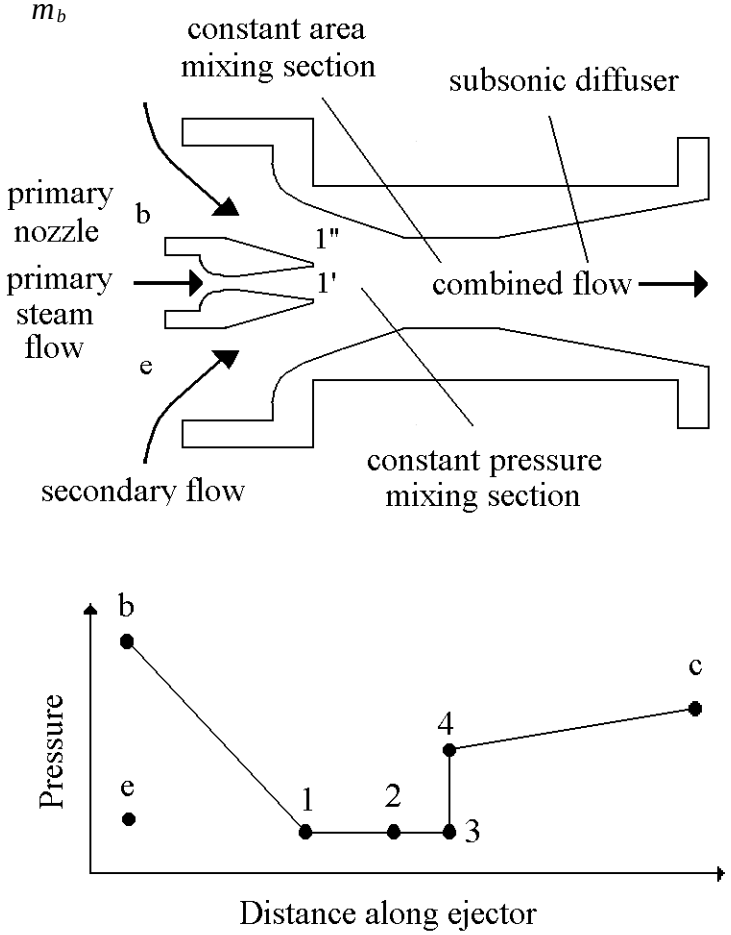

Figure 3.1: Schematic representation of an ejector (Eames et al., 1995a)

Mach number of the primary fluid at the nozzle exit plane

The high-pressure primary fluid at b expands through the nozzle and exits at 1' with supersonic speed. If the energy equation is applied between b and 1' and then simplified, the result is:

$$V_{1'}^{\,2} = 2\eta_b (h_b - h_{1'}) \tag{3.5}$$

where η_P is an isentropic efficiency of the primary nozzle.
The relation between the pressure ratio across the nozzle and Mach number at the exit of the nozzle is given as:

$$M_{1'} = \sqrt{\frac{2\eta_p}{k-1}\left[\left(\frac{P_b}{P_1}\right)^{\frac{k-1}{k}} - 1\right]} \tag{3.6}$$

Mach number of the secondary fluid at the nozzle exit plane

The secondary flow expands from e to 1". The Mach number for the secondary flow at the nozzle exit plane is derived in a similar fashion:

$$M_{1''} = \sqrt{\frac{2}{k-1}\left[\left(\frac{P_e}{P_1}\right)^{\frac{k-1}{k}} - 1\right]} \tag{3.7}$$

The mixing process

The momentum equation for ideal mixing is applied between 1 and 3:

$$P_1 A_1 + \dot{m}_b V_{1'} + \dot{m}_e V_{1''} = P_3 A_3 + (\dot{m}_b + \dot{m}_e) V_3 \tag{3.8}$$

Two assumptions are made. The entire mixing process between primary and secondary flows occur between 1 and 3 at constant static pressure ($P_1 = P_3$). The cross-sectional areas at the inlet and exit of the mixing chamber are equal ($A_1 = A_3$). Therefore:

$$\dot{m}_b V_{1'} + \dot{m}_e V_{1''} = (\dot{m}_b + \dot{m}_e) V_3 \tag{3.9}$$

The above relation describes fully idealized mixing and η_m is included as an efficiency for the entire mixing chamber:

$$\eta_m (\dot{m}_b V_{1'} + \dot{m}_e V_{1''}) = (\dot{m}_b + \dot{m}_e) V_3 \tag{3.10}$$

The velocity of the mixed fluid at 3 can be explicitly expressed as:

$$V_3 = \eta_m \left[\frac{\dot{m}_b V_{1'} + \dot{m}_e V_{1''}}{\dot{m}_b + \dot{m}_e} \right] \tag{3.11}$$

Equation (3.11) can be rewritten in terms of the Mach number:

$$M_3^* = \frac{M_{1'}^* + R_m M_{1''}^* \sqrt{T_e / T_b}}{\sqrt{(1+R_m)(1+R_m T_e / T_b)}} \tag{3.12}$$

where the relationship between M and M* is given as:

$$M^* = \sqrt{\frac{(k+1)M^2/2}{1+(k-1)M^2/2}} \tag{3.13}$$

Pressure ratio across a normal shock wave

A normal shock wave occurs within the constant-area mixing section if the velocity of the mixed flow entering this section is supersonic. During the shock process the flow experiences a sudden change in the flow velocity and pressure. Theoretically the shock wave has an infinitesimal thickness. The shock occurring between 3 and 4 would therefore be an irreversible compression process in which the Mach number suddenly falls to less than unity. The Mach number of the mixed flow after the shock is:

$$M_4 = \sqrt{\frac{M_3^2 + 2/(k-1)}{[2k/(k-1)]M_3^2 - 1}} \tag{3.14}$$

The pressure lift ration across the shock wave is:

$$\frac{P_4}{P_3} = \frac{1+kM_3^2}{1+kM_4^2} \tag{3.15}$$

Pressure lift ratio across the subsonic diffuser

The mixed flow is further compressed as it passes through the subsonic diffuser. In an additional assumption, the mixed flow velocity reduces to zero at the diffuser exit (c). The pressure lift ratio across the diffuser is:

$$\frac{P_c}{P_4} = \left[\frac{\eta_d (k-1)}{2} M_4{}^2 + 1 \right]^{\frac{k}{k-1}} \qquad (3.16)$$

Solution of Equations (3.5) – (3.16)

The temperature, pressure and mass flow rate of the primary and secondary fluids are all known. Temperatures and pressures are taken from the thermocouples and pressure gauges. Mass flow rate is calculated from the volume flow over a certain time period. The following procedure was used to obtain the ejector exhaust pressure.

1 The pressure at the nozzle exit plane is unknown and determined by an iterative process. An initial value for P_1/P_e is guessed.
2 From equations (3.6) and (3.7) the Mach numbers of the primary and secondary fluids at the nozzle exit plane (M_1' and M_1") are calculated.
3 Equation (3.12) is used to calculate the Mach number of the mixed fluid M_3.
4 Equation (3.14) is used to calculate the Mach number of the mixed fluid after the shock wave M_4.
5 Equation (3.15) is used the calculate the pressure lift ratio across the shock wave P_4/P_3.
6 Equation (3.16) is used to calculate the pressure lift ratio across the diffuser P_c/P_4.
7 P_4/P_3, P_c/P_4 and P_1/P_e are all known and the exhaust pressure P_c can be calculated.
8 Steps 1 to 7 are repeated with new values of P_1/P_e until the maximum P_c is obtained.

Eames et al. (1995a) suggested values of 0.85, 0.85 and 0.95 for the primary nozzle, diffuser and mixing chamber efficiencies respectively. According to these authors, these values were found to give acceptable correlation with experimental data provided by ESDU (1986).

3.2 Ejector Performance

The thermodynamic performance of a steam ejector is evaluated by the coefficient of performance. This is the ratio of the evaporator heat load and the sum of the boiler energy input and pump work. The COP is calculated as follows:

$$COP = \frac{\dot{Q}_{evap}}{\dot{Q}_{boiler} + \dot{W}_{pump}} \approx \frac{P_{evap(elec)}}{P_{boiler(elec)}} = \frac{(VI)_{evap}}{(VI)_{boiler}} \tag{3.17}$$

The pump work can be omitted since it is typically less than 1% of the boiler heat input (Aphornratana and Eames, 1997). Note that $P_{evap(elec)}$ and $P_{boiler(elec)}$ represent electric power input and not pressure and V represents electric volts and not volume.

The COP can also be calculated as:

$$COP = R_m \frac{h_{g-evap} - h_{f-cond}}{h_{g-boiler} - h_{f-cond}} \tag{3.18}$$

where R_m was defined earlier as:

$$R_m = \frac{\dot{m}_e}{\dot{m}_b} \tag{3.19}$$

Certain authors, however, use the terms electric and water COP when referring to the COP and entrainment ratio. These terms are defined as follow:

$$COP_{elec} = COP = COP_{water} \frac{h_{g-evap} - h_{f-cond}}{h_{g-boiler} - h_{f-cond}} \tag{3.20}$$

and:

$$COP_{water} = R_m = \frac{\dot{m}_e}{\dot{m}_b} \tag{3.21}$$

From equations 3.18 and 3.19 it can be observed that COP_{elec} and COP_{water} differ with a value of:

$$\frac{h_{g-evap} - h_{f-cond}}{h_{g-boiler} - h_{f-cond}} \tag{3.22}$$

The magnitude of term (3.20) is typically 0.931 to 0.946 for the temperature ranges of T_e = 5 °C to 10 °C, T_c = 15 °C to 25 °C and T_b = 90 °C to 110 °C. This results in a COP_{water} value which is 5.7 % to 7.4 % higher than the COP_{elec} value.

The COP_{water} value is usually calculated by measuring the change in the water level in the boiler and evaporator sight glass. The density of water in the evaporator and boiler differ between 95.2 % to 96.5 % (T_e = 5 °C to 10 °C and T_b = 90 °C to 110 °C). The effect of this

phenomenon is that the measured COP_{water} is 3.5 % to 4.8 % lower than the actual COP_{water} value.

The combined effect of the two cases above results in the measured COP_{water} value being 2.0 % to 2.1 % higher that the COP_{elec} value.

If an experimental setup has no condensate return system and batches are run during experiments, the system becomes an open loop system. The open loop COP_{elec} is:

$$COP_{elec(ol)} = \frac{P_{evap\_elec}}{P_{boiler\_elec}} = R_m \frac{h_{fg-evap}}{h_{fg-boiler}} \tag{3.23}$$

where, as before, the closed loop COP is:

$$COP_{elec(cl)} = \frac{P_{evap\_elec}}{P_{boiler\_elec}} = R_m \frac{h_{g-evap} - h_{f-cond}}{h_{g-boiler} - h_{f-cond}}$$

$$= R_m \frac{h_{fg-evap} + h_{f-evap} - h_{f-cond}}{h_{fg-boiler} + h_{f-boiler} - h_{f-cond}} \tag{3.24}$$

The $COP_{elec(ol)}$ and $COP_{elec(cl)}$ differ from each other with less than 0.5 % in the following temperature ranges T_e = 5 °C to 10 °C, T_c = 15 °C to 25 °C and T_b = 95 °C to 105 °C. The experimental setup used in this project is an open loop system similar to that of Eames et al. (1999). The published experimental data, however, is relevant to a closed loop system unless otherwise stated.

In this thesis, when a graph of experimental data is plotted, the terms COP_{water} and COP_{elec} are used. The term COP is used as a collective term when referring to the system performance in general. This term is further used on the axis of a graph when both COP_{elec} and COP_{water} are plotted. The terms COP and R_m are used on graphs taken from published data and represent COP_{elec} and COP_{water}.

4. LITERATURE REVIEW

4.1 General

This chapter discusses experimental results found in literature. The aim is to explain the operation of a steam jet ejector in more detail.

Note that steam in the system is saturated unless otherwise stated. The result of this is that there is a direct relationship between the steam temperature and pressure. Temperature is used when referring to the boiler and evaporator and pressure is used when referring to the condenser.

For an ejector to operate properly the flow through the primary nozzle must be choked. This is usually the case since the pressure ratio (nozzle outlet/inlet pressure) is only required to be below 0.57 for saturated steam as working fluid (Çengel and Boles, 2002). When this pressure ratio is maintained, the choked flow results in a Mach number of unity in the nozzle throat. The mass flow rate through the nozzle is then entirely dependent on the upstream conditions (boiler temperature).

In addition to the choking of the primary nozzle, the ejector is characterised by another choking phenomenon in the secondary nozzle. As pointed out by Huang et al. (1985), the choking of the secondary ejector results from the acceleration of the entrained flow from a stagnant state at the evaporator inlet to a supersonic flow in the mixing chamber.

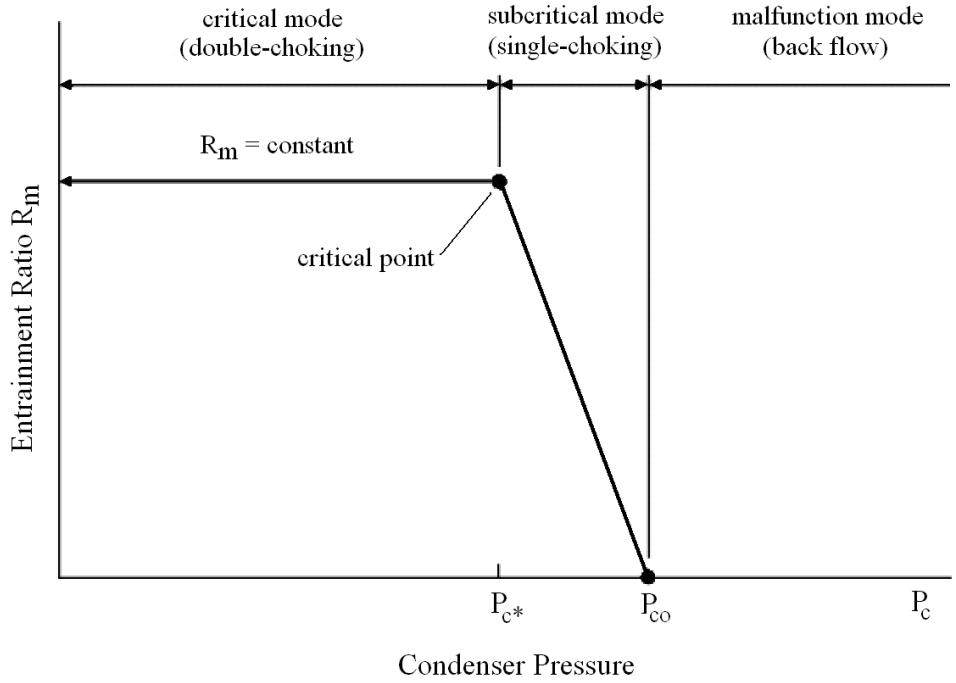

Figure 4.1: Operational modes of an ejector (Huang and Chang, 1999)

Figure 4.1 shows the variation of entrainment ratio R_m with discharge or condenser pressure P_c at fixed boiler and evaporator temperatures. The ejector performance can be divided into three operational modes, based on the condenser pressure P_c:

(a) Critical (double-choking) mode when $P_c \leq P_{c*}$ where the primary and the entrained flows are both choked and the entrainment ratio is constant

(b) Subcritical (single-choking) mode when $P_{c*} < P_c < P_{co}$ where only the primary flow is choked and R_m changes with the back pressure P_c

(c) Malfunction (back-flow) mode when $P_c \geq P_{co}$ where both the primary and the secondary flows are not choking and the entrained flow is reversed

This ejector behaviour is confirmed by experiments. Refer to figure 4.2 for work done by Eames et al. (1995).

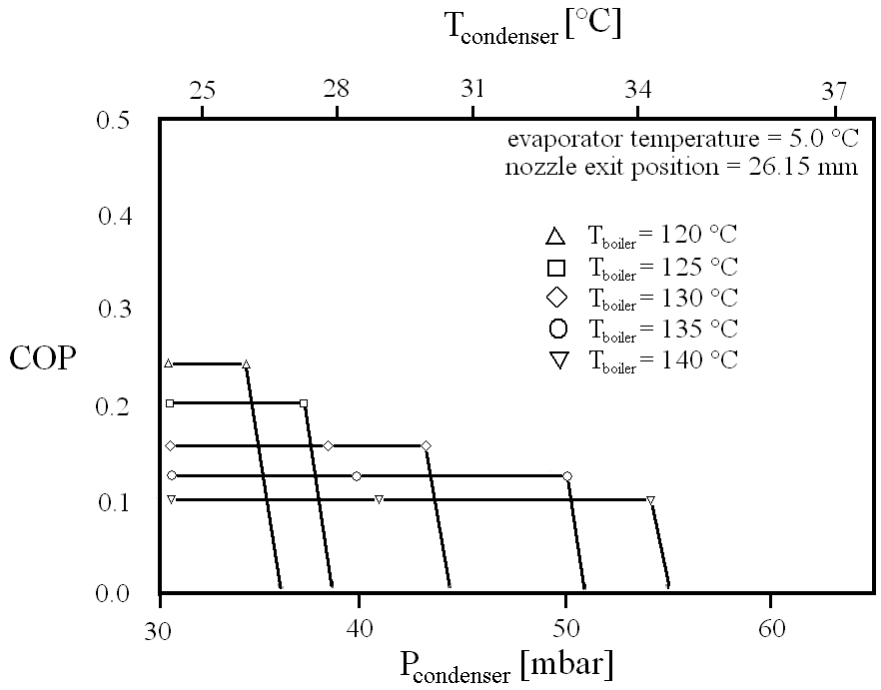

Figure 4.2: Measured COP versus condenser pressure and boiler temperature for a constant evaporator temperature (Eames et al., 1995)

When the flow through the primary nozzle is choked, the mass flow rate of steam does not increase when lowering the condenser pressure. This attribute of the nozzle is the reason for the constant entrainment lines as can be seen in figure 4.1 and 4.2. From this it is noted that the most economical point to operate the ejector is at the critical point. The critical points for various boiler and evaporator temperatures are plotted on a graph showing COP versus the

condenser pressure in figure 4.3. The critical points are connected to form isotherms.

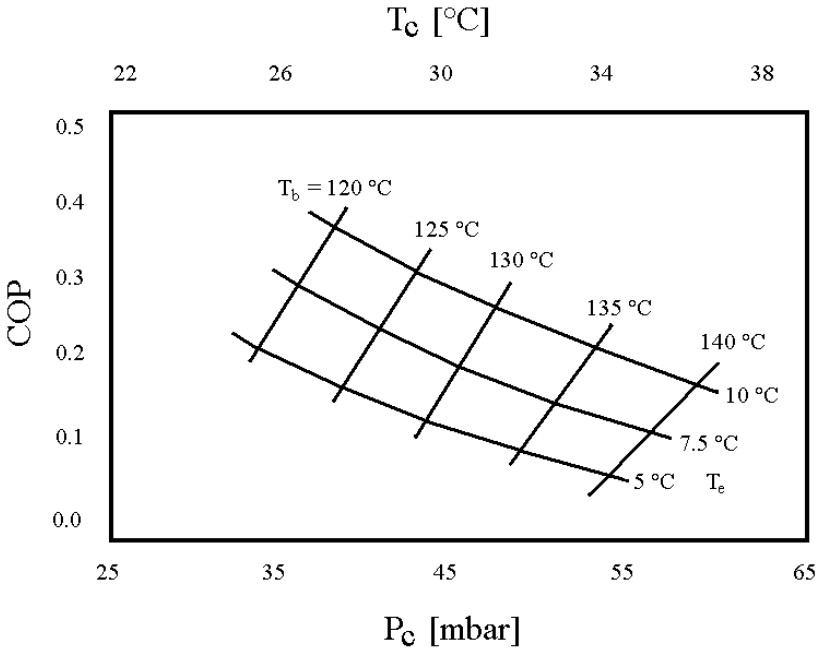

Figure 4.3: Measured COP versus condenser pressure, boiler and evaporator temperatures (Eames et al., 1995)

4.2 Effect of Condenser Pressure

Chunnanond and Aphornratana (2004b) conducted experiments to measure the pressure profile along the secondary nozzle as shown in figure 4.4.

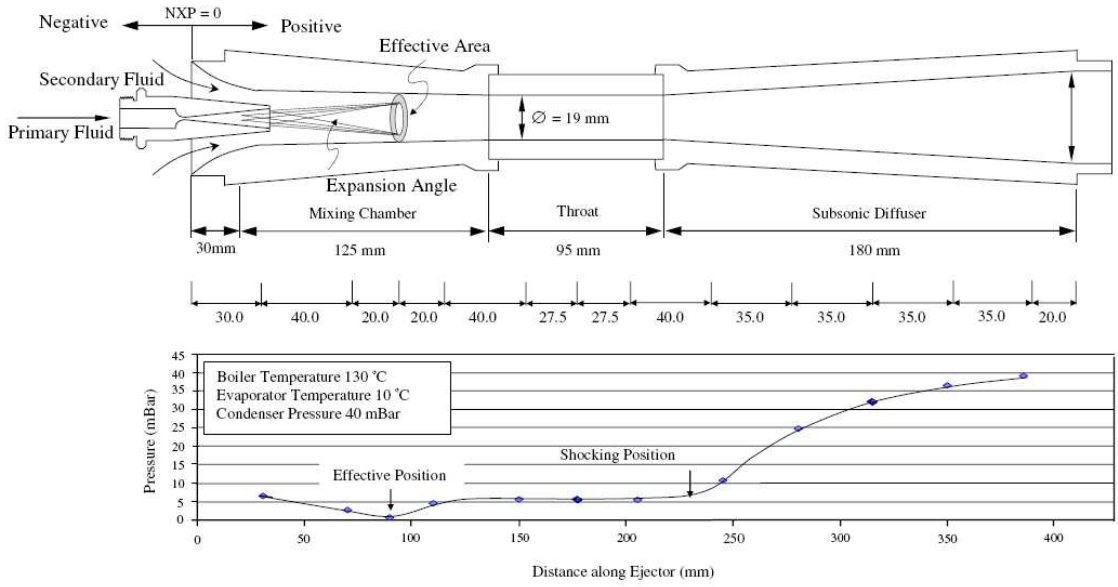

Figure 4.4: Typical pressure profile along an ejector (Chunnanond and Aphornratana, 2004b)

The mixing characteristics of the primary and secondary flows can be explained with the aid of figure 4.4. The top figure indicates the primary flow that fans out into the mixing chamber without mixing with the secondary flow. This flow results in a converging duct with a certain expansion angle for the entrained secondary flow.

The secondary flow is accelerated to sonic speed at the expense of static pressure. The position where the secondary flow reaches sonic velocity is referred to as the effective position. This is the position where the secondary flow chokes and the cross section was defined by Munday and Bagster (1977) as the effective area. They suggested that the mixing of the primary and secondary flows only starts after the effective position and that this causes the rise in static pressure beyond the effective area (figure 4.4 bottom). Note that the converging mixing chamber acts as a diffuser to a supersonic flow.

The velocity and pressure of the mixed flow remains constant while it passes through the constant area throat section of the secondary ejector. At a certain position in either the throat or diffuser section, a transverse shock wave is induced creating a compression effect. This position is referred to as the shocking position. After this position the velocity of the mixed flow drops to sonic values. The subsonic diffuser compresses the flow further and the flow exits the diffuser with low velocity.

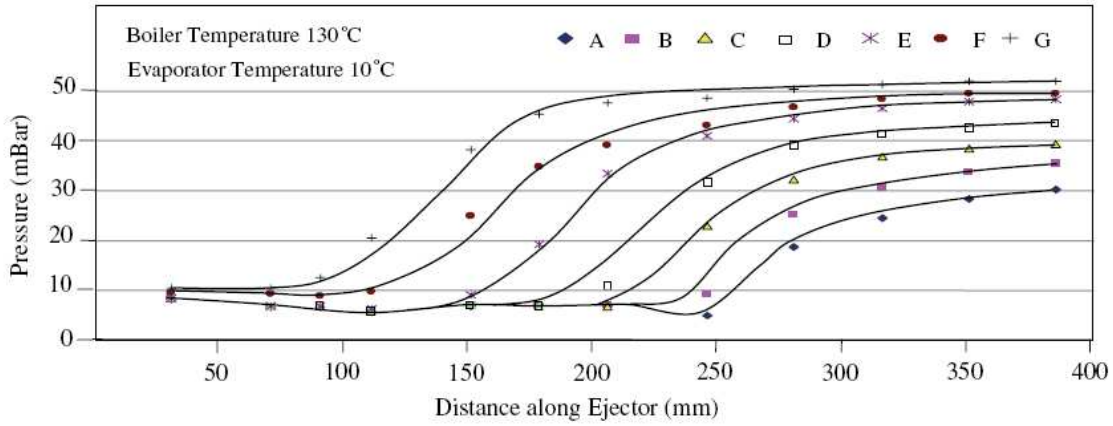

Figure 4.5: Steam ejector static pressure profile along an ejector at various condenser pressures (Chunnanond and Aphornratana, 2004b)

Figure 4.5 shows the pressure profile along an ejector for seven different condenser pressures. Pressures A – E represent the critical mode and F and G represent the subcritical mode. It can be seen from the figure that the shocking position moves towards the primary nozzle as the condenser pressure increases. If the condenser pressure is higher than the critical pressure, the shock wave is moved so close to the primary nozzle that the entrainment and mixing process is influenced. If the condenser pressure is increased further, the ejector loses its function completely as explained above.

4.3 Effect of Boiler Temperature

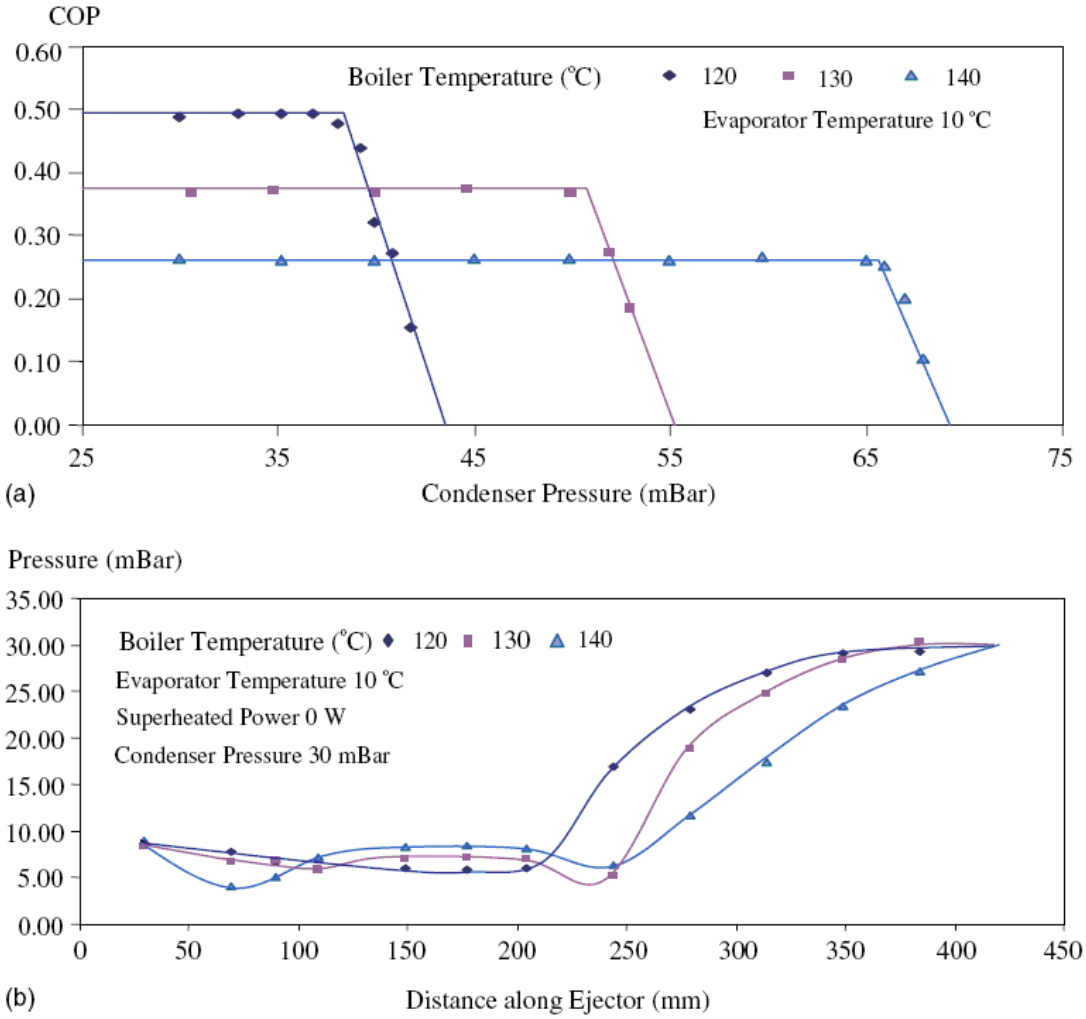

Figure 4.6: Steam ejector at different boiler temperatures (a) COP versus condenser pressure (b) Pressure profile (Chunnanond and Aphornratana, 2004b)

Figure 4.6 shows that decreasing the boiler temperature increases the COP at the expense of critical condenser pressure. The entrainment and mixing through the primary nozzle can be explained with the aid of figure 4.6 and figure 4.7. When the boiler temperature decreases the mass flow rate through the primary nozzle is reduced. This causes the expanded wave at the nozzle outlet to exit with reduced momentum and results in a smaller expansion angle. This new longer entrained duct allows higher secondary mass to be entrained through the mixing chamber and results in the effective position to move towards the condenser (downstream). The downstream movement of the effective position results in the critical condenser pressure to increase.

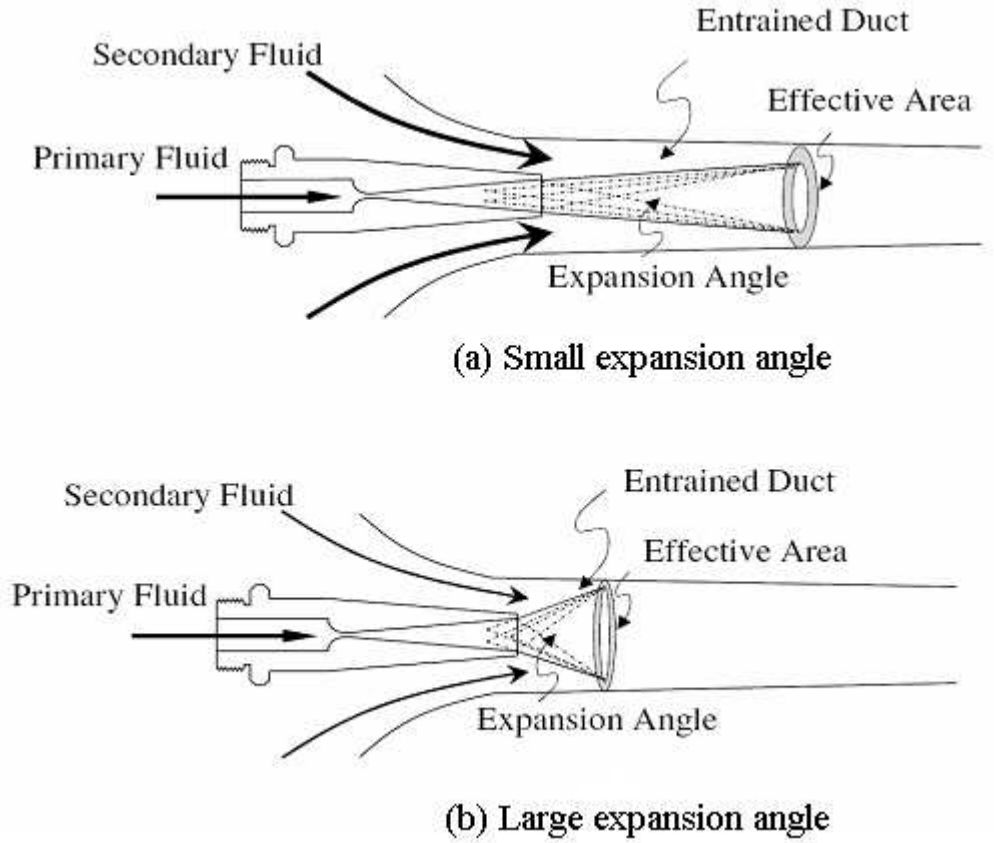

Figure 4.7: Effect of operating conditions on the entrainment and mixing process in the mixing chamber (Chunnanond and Aphornratana, 2004b)

4.4 Effect of Evaporator Temperature

When the evaporator temperature is increased, the COP and critical condenser pressure increases as can be seen from figure 4.8. The higher evaporator temperature and thus mixing chamber pressure result in a longer entrained duct as shown in figure 4.7 a. The primary flow exits the primary nozzle into an area with a higher pressure and the fanning out is reduced. The longer entrained duct can entrain higher amounts of secondary flow and therefore the COP increases. The momentum of the mixed flow increases with a larger portion of secondary flow entrained. The result is a critical condenser pressure that increases.

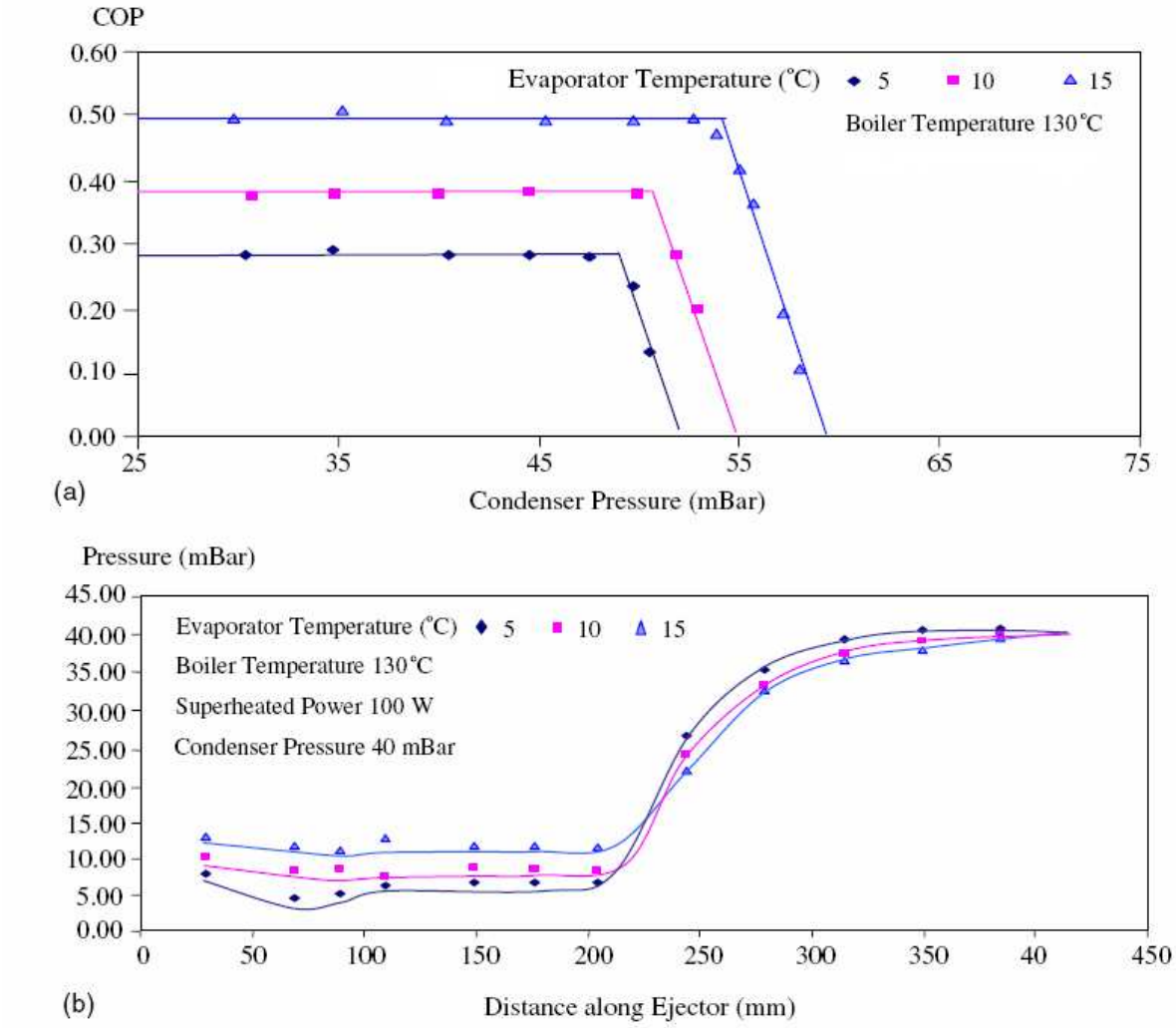

Figure 4.8: Steam jet ejector at different evaporator temperatures (a) COP versus condenser pressure (b) Pressure profile (Chunnanond and Aphornratana, 2004b)

4.5 Effect of Primary Nozzle Exit Position

The primary nozzle exit position (NXP) is defined as the distance from the primary nozzle exit to the bell-mouth inlet of the mixing chamber. NXP is positive when the primary nozzle exit is down-stream of the mixing chamber inlet (figure 4.9).

Tests were conducted by Aphornratana and Eames (1997), Eames et al. (1999) and Chunnanond and Aphornratana (2004b) to investigate the effect of the primary nozzle exit position on the system performance.

Figure 4.10 shows the results when the evaporator heat load is kept constant and NXP is varied (Aphornratana and Eames 1997). The entrained flow and condenser pressure is fixed during the test. The ejector performance improves if the evaporator temperature reduces. The optimum primary nozzle position is therefore where the evaporator temperature is a minimum.

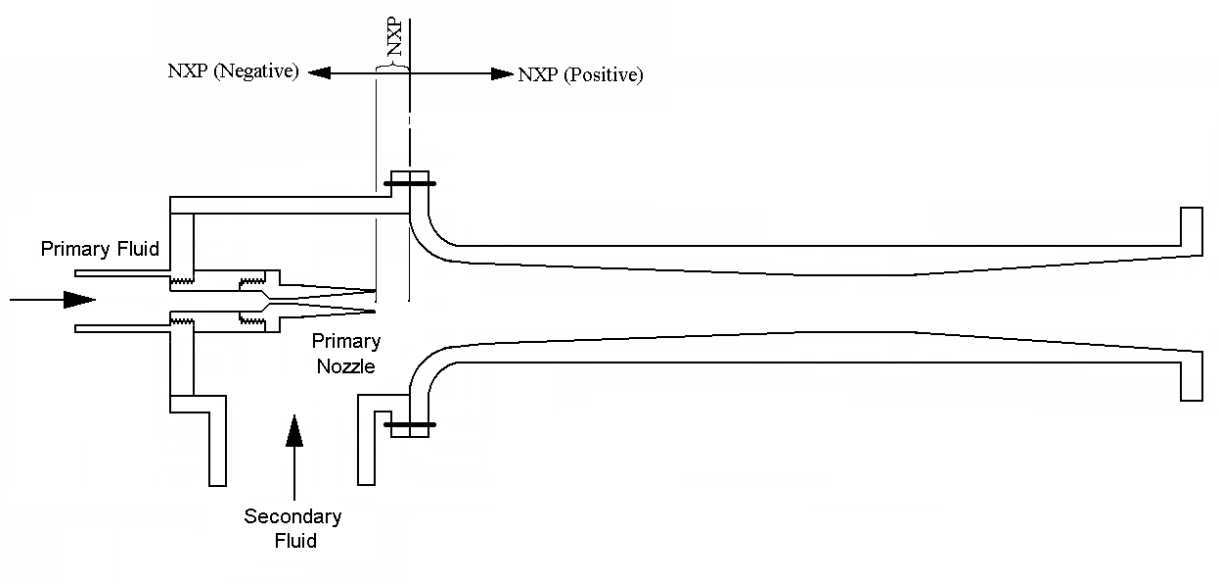

Figure 4.9: Primary nozzle exit position

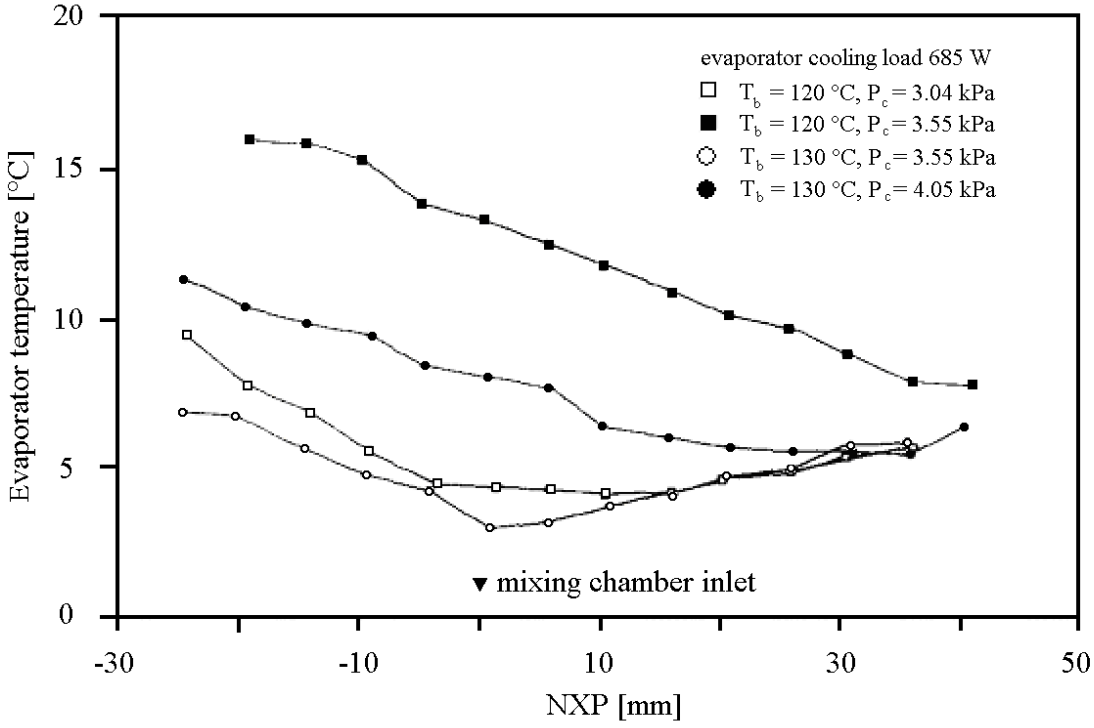

Figure 4.10: Measured evaporator temperature versus primary nozzle exit position (NXP), boiler temperature and condenser pressure (Aphornratana and Eames, 1997)

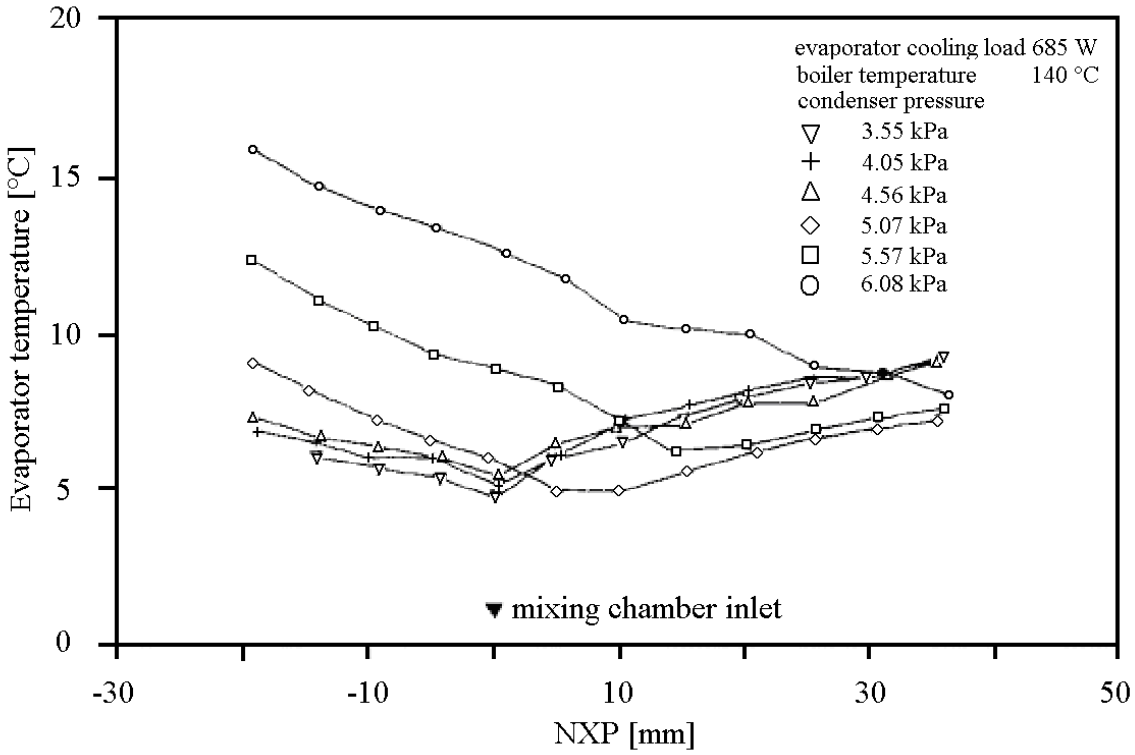

Figure 4.11: Measured evaporator temperature versus primary nozzle exit position (NXP) and condenser pressure (Aphornratana and Eames, 1997)

The results from figure 4.10 and 4.11 are:

- With the boiler and condenser pressures fixed, the evaporator temperature decreases as the primary nozzle exit position moves towards the mixing chamber inlet. The evaporator temperature reaches a minimum temperature at a certain position. Further increasing the nozzle exit position towards the mixing chamber inlet increases the evaporator temperature.

- For a fixed primary nozzle position and cooling load, the evaporator temperature decreases when the boiler temperature increases or the condenser pressure reduces. The effect of the boiler temperature and condenser pressure reduces when the value of the primary nozzle exit position is large (primary nozzle is well into the mixing chamber).

- The optimum primary nozzle exit position was found near the mixing chamber inlet. ESDU (1986) suggests placing the primary nozzle exit 0.5 to 1.0 times the mixing chamber diameter upstream of the mixing chamber inlet (equivalent to -9 mm to –18 mm in figure 4.10 and figure 4.11). The primary steam pressure commonly used in industry, however, is in the

range of 500 kPa to 2000 kPa. The pressure range referred to in figure 4.10 and figure 4.11 is 200 kPa to 350 kPa.

- A single optimum primary nozzle exit position cannot be found and depends on the boiler, condenser and evaporator temperatures and pressures.

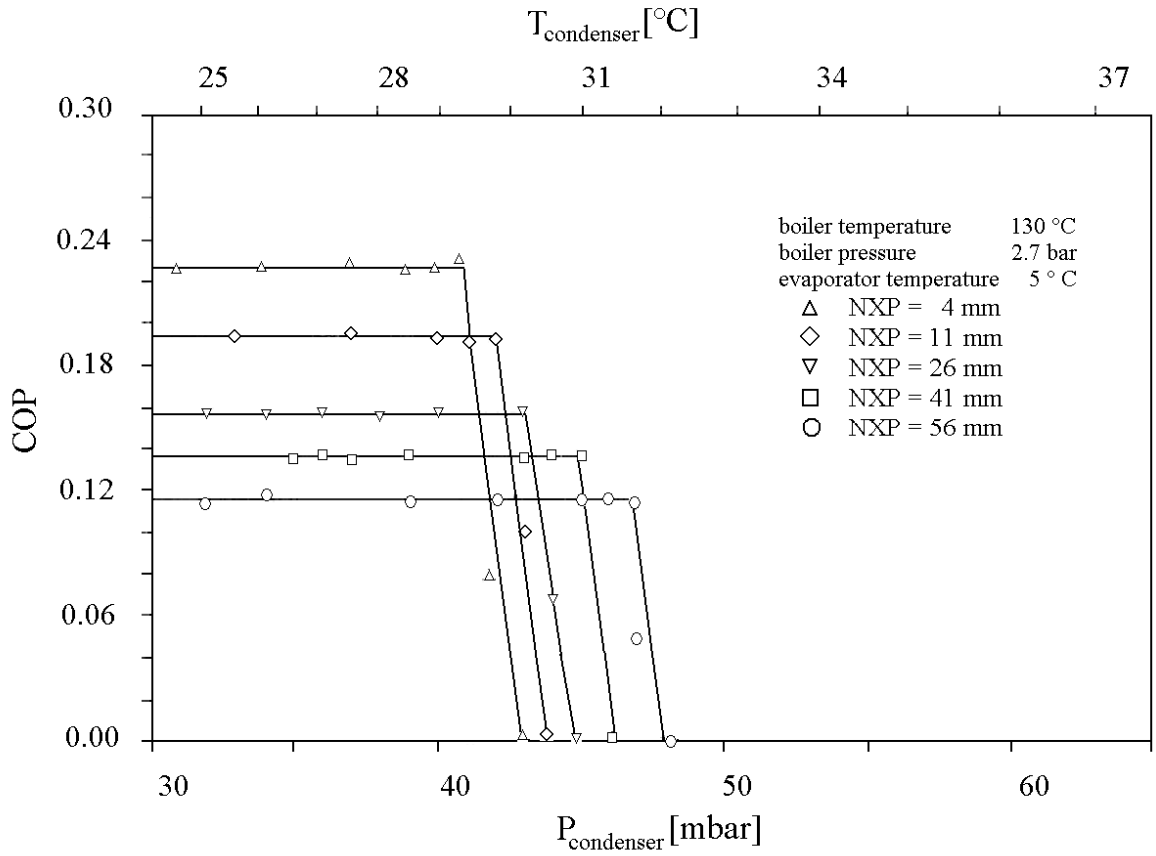

Figure 4.12: Measured COP at different primary nozzle exit positions (NXP) (Aphornratana and Eames, 1997)

Figure 4.12 shows the effect of the primary nozzle position on the system COP. Moving the primary nozzle exit position into the mixing chamber reduces the COP but increases the critical condenser pressure.

Chunnanond and Aphornratana (2004b) obtained similar results (figure 4.13a, top) and suggests that moving the primary nozzle out of the mixing chamber results in a larger entrainment duct and therefore larger entrainment and COP. This is verified by the pressure at the primary nozzle exit position being higher for a nozzle further away (upstream) of the mixing chamber (figure 4.13b).

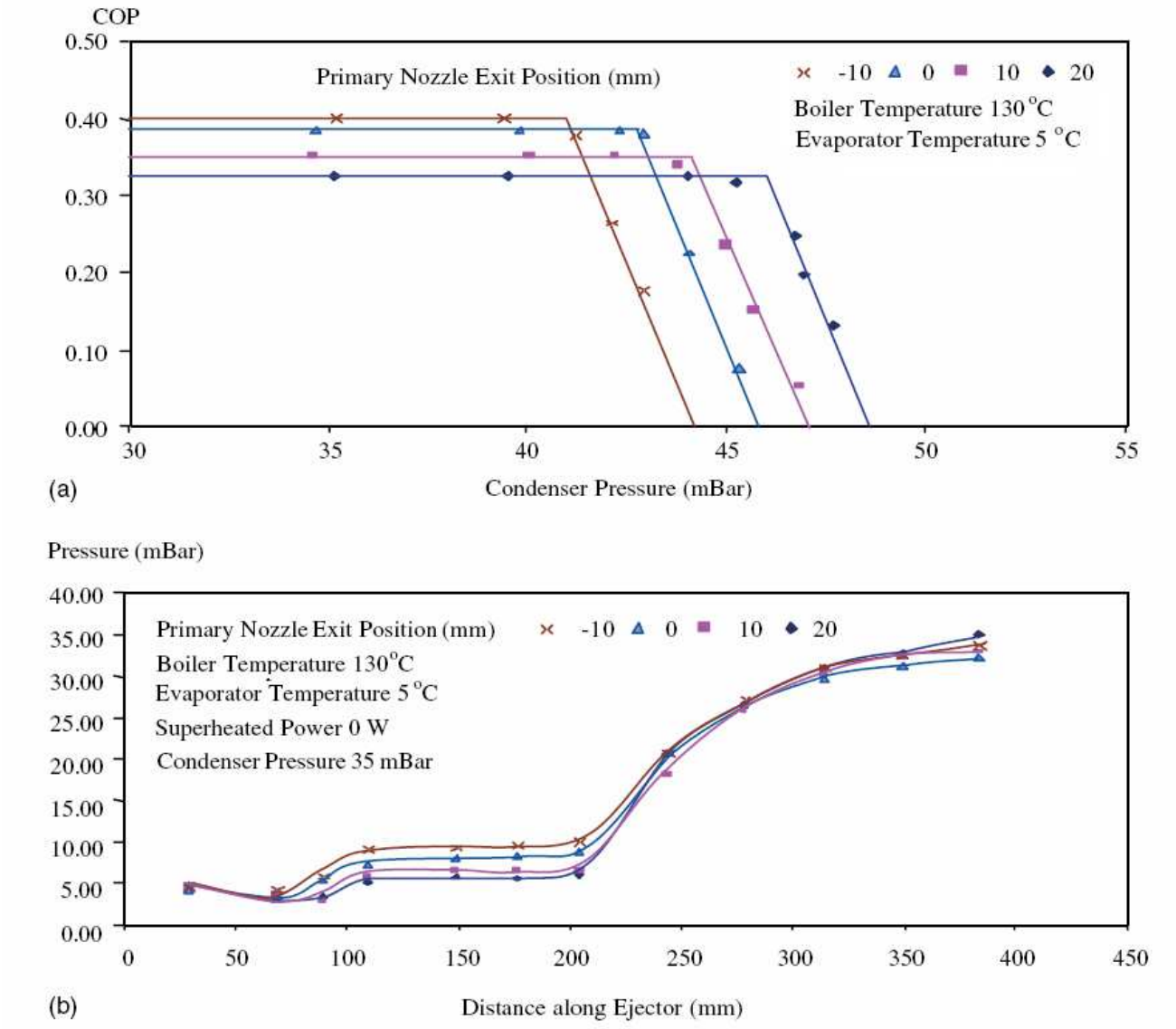

Figure 4.13: Steam ejector with varying primary nozzle exit position
(a) COP versus nozzle exit position
(b) Pressure profile for various nozzle exit positions
(Chunnanond and Aphornratana, 2004b)

4.6 Primary Nozzle Outlet Area Effect

Eames et al. (1999) investigated the effect of A_T (ratio of primary nozzle exit and throat area, $A_T = A_{exit}/A_t$) on system performance. Two nozzles with A_T values equal to 16 and 36 respectively were tested. Both nozzles had a throat diameter of 2 mm and a divergent angle of 8°. The nozzle with A_T = 16 performed about 10 % better than the nozzle with A_T = 36. Eames et al. (1999) concluded that a poorer entrainment performance was the result of increasing the degree of overexpansion by designing the primary nozzle to have a larger than critical exit area.

4.7 Primary Nozzle Throat Area

A_R is defined as the primary nozzle throat area divided by the secondary nozzle throat area. $A_R = A_t/A_4$. Chunnanond and Aphornratana (2004b) found that reducing A_R (reducing A_t and keeping A_4 constant) increases the COP at the expense of the critical condenser pressure. A smaller primary nozzle throat results in a smaller mass of primary steam that expands. This results in higher static pressures at the primary nozzle outlet and the downstream movement of the effective position.

Eames et al. (1999) obtained similar results. In their experiments the primary nozzle throat area was kept constant while the secondary nozzle throat area was varied. Lowering A_R, the boiler pressure could be reduced without changing the evaporator temperature or critical condenser pressure. Alternatively lowering A_R resulted in increasing the critical condenser pressure without altering the evaporator temperature or boiler pressure. In both cases the decreasing of A_R were at the expense of the entrainment ratio and therefore COP.

4.8 Superheating of Primary Steam

Chunnanond and Aphornratana (2004b) investigated the effect of superheating the primary steam. The steam from an 8 kW boiler could be superheated by adding up to 180 W of additional heat to the primary steam in their experimental setup. Their results indicated that the superheated level had very little impact on either the COP or critical condenser pressure. Thus, according to the recommendation of ESDU (1986), the superheating of steam has no advantage other than to prevent the damage of the ejector caused by wet steam.

4.9 Operating Conditions

In summary, when designing a steam jet ejector, the critical condenser pressure can be increased by:

- increasing the primary nozzle throat or decreasing the secondary ejector throat
- increasing the boiler temperature
- advancing the primary nozzle exit position towards the mixing chamber inlet (up to a optimum point where after it has the opposite effect)
- increasing the evaporator temperature

The COP can be increased by:

- decreasing the boiler temperature and pressure (up to a optimum point for a specified critical condenser pressure after which the COP falls rapidly)
- decreasing the primary nozzle throat area

- advancing the primary nozzle exit position towards the mixing chamber inlet
- increasing the evaporator temperature

After the boiler and evaporator temperatures and condenser pressures are selected and the optimum primary nozzle position is found, the ejector operation can be described with the help of figure 4.14. This figure was obtained from work done by Aphornratana and Eames (1997) with an experimental steam ejector with a movable primary nozzle.

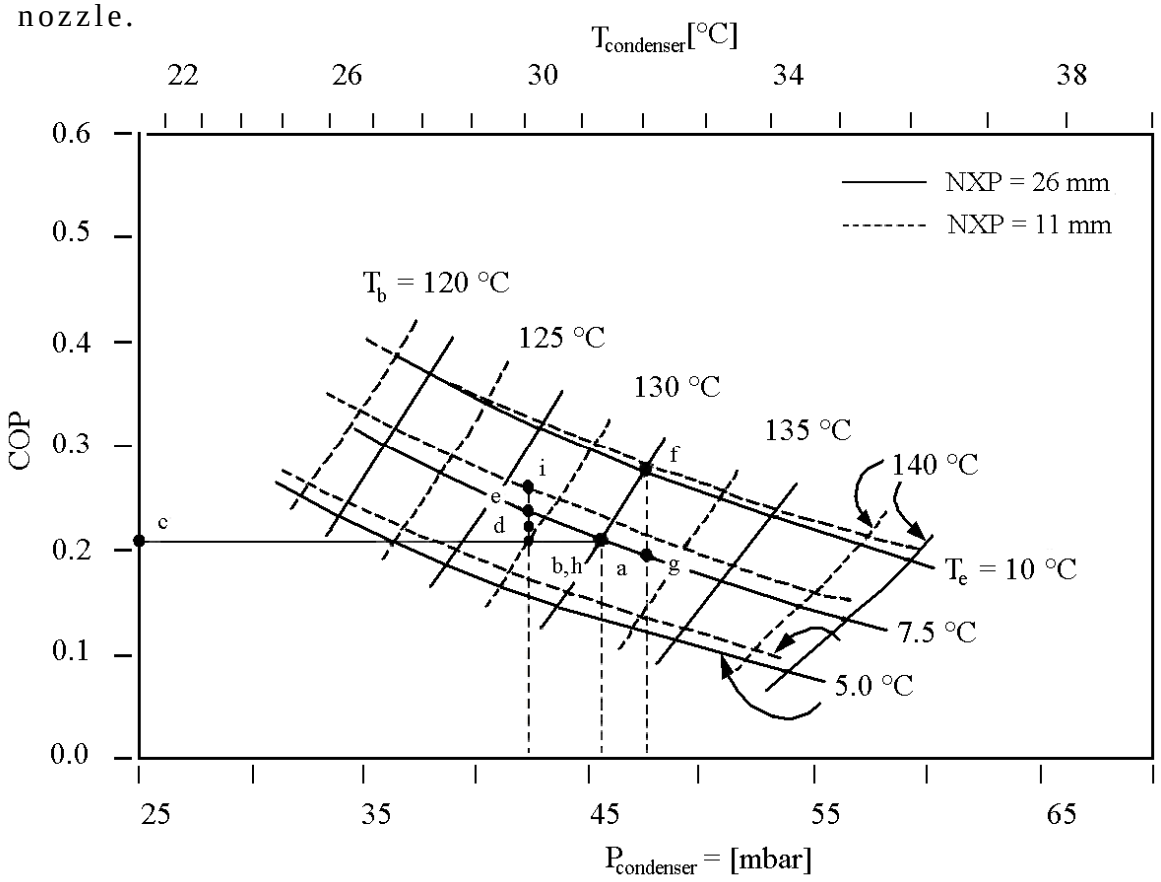

Figure 4.14: Performance characteristics of an experimental steam ejector (Aphornratana and Eames, 1997)

Note that the isotherms represent operation at critical condenser pressures as explained in paragraph 4.1. Point a on figure 4.14 represents a normal operating point with T_b = 130 °C, T_e = 7.5 °C and P_c = P_{crit} = 4.6 kPa (31.4 °C) and the primary nozzle exit position at 26 mm.

If, in a first scenario, the condenser pressure drops to 4.3 kPa (30.2 °C) with the boiler and evaporator temperature remaining the same, the cycle will operate at point b. Note that the cycle is not operating at its critical condenser pressure any more. The reason the evaporator and boiler temperature as well as the COP remain unchanged (line a-b-c) was explained earlier with the help of figure 4.1 and 4.2.

The cycle performance can be increased by operating the system at a new critical condenser pressure. This can be done using one of the following methods:

Reduce the boiler temperature

- If T_b is reduced from 130 °C to 127.5 °C while the condenser pressure remains at the new value of 4.3 kPa, the new operating point would still be point b but the cycle will operate at its critical condenser pressure. The COP and the cooling capacity are unchanged but T_e reduces to 6.5 °C.

- If T_b is reduced from 130 °C to 127.2 °C and the condenser pressure remains the same, the cycle will operate at a critical condenser pressure which is point d. The COP improves slightly and the evaporator temperature drops to 7 °C. The cooling capacity, however, stays the same.

- If T_b is reduced from 130 °C to 126.9 °C and the condenser pressure remains the same, the cycle will operate at its critical condenser pressure at point e. The COP and cooling capacity rises but the evaporator temperature remains at its original value of 7.5 °C.

Change the primary nozzle exit position.

- If the primary nozzle exit position is varied from 26 mm to 11 mm (closer to the mixing chamber) while T_b remains 130 °C and P_c stays at 4.3 kPa, the new operating point will be point h. Note that although point h and b are the same on figure 4.14, point h operates at critical condenser pressure and refers to the dotted line isotherms. The COP and cooling capacity remains unchanged while T_e reduces to 6 °C.

- If the primary nozzle exit position is varied from 26 mm to 11 mm and T_b reduces from 130 °C to 128.5 °C while P_c remains at 4.3 kPa, the new operating point will be point i. Note that point i refers to the dotted line isotherms. The COP and cooling capacity increases while T_e remains at its initial value of 7.5 °C.

In a second scenario let the condenser pressure now increase to 4.82 kPa (32.1 °C). This value is higher than the design point critical condenser pressure. Optimal operating can be restored by increasing T_b and keeping T_e constant. This results in point g. The COP and cooling capacity is reduced. Alternatively the evaporator temperature can be increased while the boiler temperature remains the same. The COP and cooling capacity are increased and result in point f.

5. EXPERIMENTAL RESULTS

This chapter discusses the experimental results obtained during system testing. The system was first tested at a documented temperature of T_b = 130 °C and compared to published data. The focus of the experiments, however, was to operate the boiler temperature below T_b = 100 °C. Primary nozzles with different throat areas as well as different nozzle positions were investigated. The effect of boiler temperature and condenser pressure on the system performance is discussed.

5.1 Familiar Boiler Temperatures

Steam ejectors in the boiler temperature range of T_b = 120 °C to 140 °C and T_e = 5 °C to 15 °C are well documented in literature. Experiments were done and compared to this documented data to verify the operation of the experimental setup.

An experiment was conducted on a nozzle with a throat diameter of d_t = 2 mm (nozzle 3) at T_b = 130 °C. This was done at a primary nozzle exit position (NXP) of 25 mm and T_e = 10 °C. The experimental results are compared to various published data in table 5.1. The experimental results compare well to results obtained by other authors, especially Sun (1996).

Table 5.1: Comparison of experimental results for a steam ejector operating at T_b = 130 °C and T_e = 10 °C

T_e [°C]	T_b [°C]	T_c [°C]	P_c [kPa]	COP_{elec}	COP_{water}	NXP [mm]	A_t	Author
5	130	30.8	4.47	0.167	0.276	26.16	90	1
7.5	130	31.5	4.66	0.207	0.356	26.16	90	1
10	130	31.9	4.77	0.288	0.473	26.16	90	1
5	130	30.5	4.38	0.160	-	26	81	2
7.5	130	31.3	4.59	0.210	-	26	81	2
10	130	32.0	4.80	0.266	-	26	81	2
10	130	32.2	4.86	-	0.299	-	81	3
10	130	30.0	4.25	0.284	0.308	25	81	4

1) Chunnanond & Aphornratana (2004)
2) Aphornratana & Eames (1997)
3) Sun (1996)
4) Author - Nozzle 3

There are two thermocouples in the evaporator. There is a thermo-couple in the evaporator top that measures the evaporator vapour temperature. The second thermocouple measures the evaporator liquid temperature at the bottom of the evaporator tank. When referred to the evaporator temperature in this document, the evaporator liquid temperature is implied unless otherwise stated. It was observed that

the evaporator vapour temperature is lower than the liquid temperature while the system is running.

5.2 Boiler Temperature and Primary Nozzle Throat Diameter

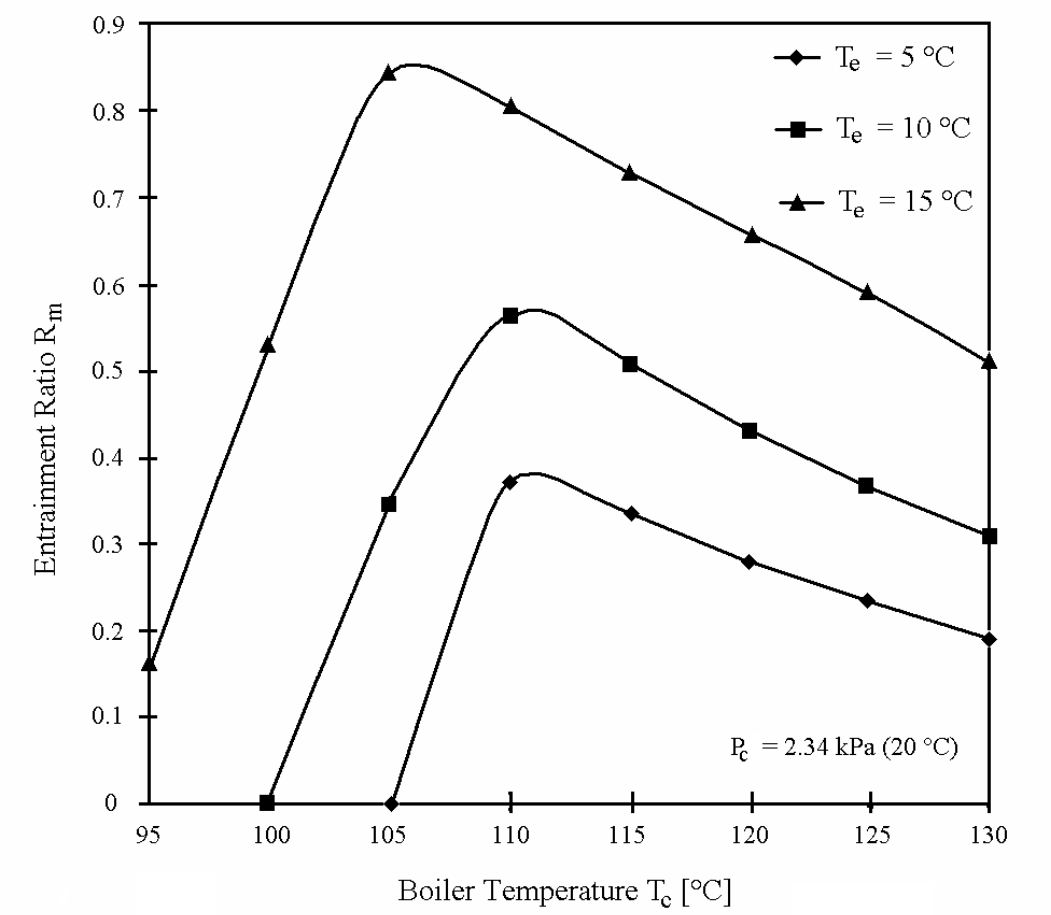

Figure 5.1: Effect of boiler temperature on entrainment ratio (Sun, 1996)

It can be seen in figure 5.1 that the system has an optimum boiler temperature. This optimum is dependent on the evaporator temperature and condenser pressure. Note that these results may seem to differ from figure 4.2 where the COP increases when lowering the boiler temperature. The reason the R_m in figure 5.1 drops towards the left (decrease of boiler temperature) is due to the condenser pressure that is held constant at 2.34 kPa (20 °C) during the experiment. As the boiler temperature is decreased, the critical condenser pressure of the specific operating point decreases accordingly. The sudden drop in COP observed in figure 5.1 is due to the critical condenser pressure that drops below the constant condenser pressure of 2.34 kPa.

The curves in figure 5.1 must be shifted towards the left in order to find the optimum entrainment ratio (and COP) at a lower boiler temperature value. In order to achieve this, the secondary to primary nozzle throat area ratio A_R must be decreased. This method is docu-

mented by various authors (Sun, 1996, Eames et al., 1995, Chunnanond and Aphornratana, 2002b). Figure 5.2 represents results obtained by Sun (1996). Here the condenser pressure, evaporator temperature and R_m are held constant while the boiler temperature varies to result in the corresponding primary and secondary nozzle throat diameters. The value of A_R decreases from 65.2 down to 29.7 as T_b decreases from 130 °C down to 100 °C.

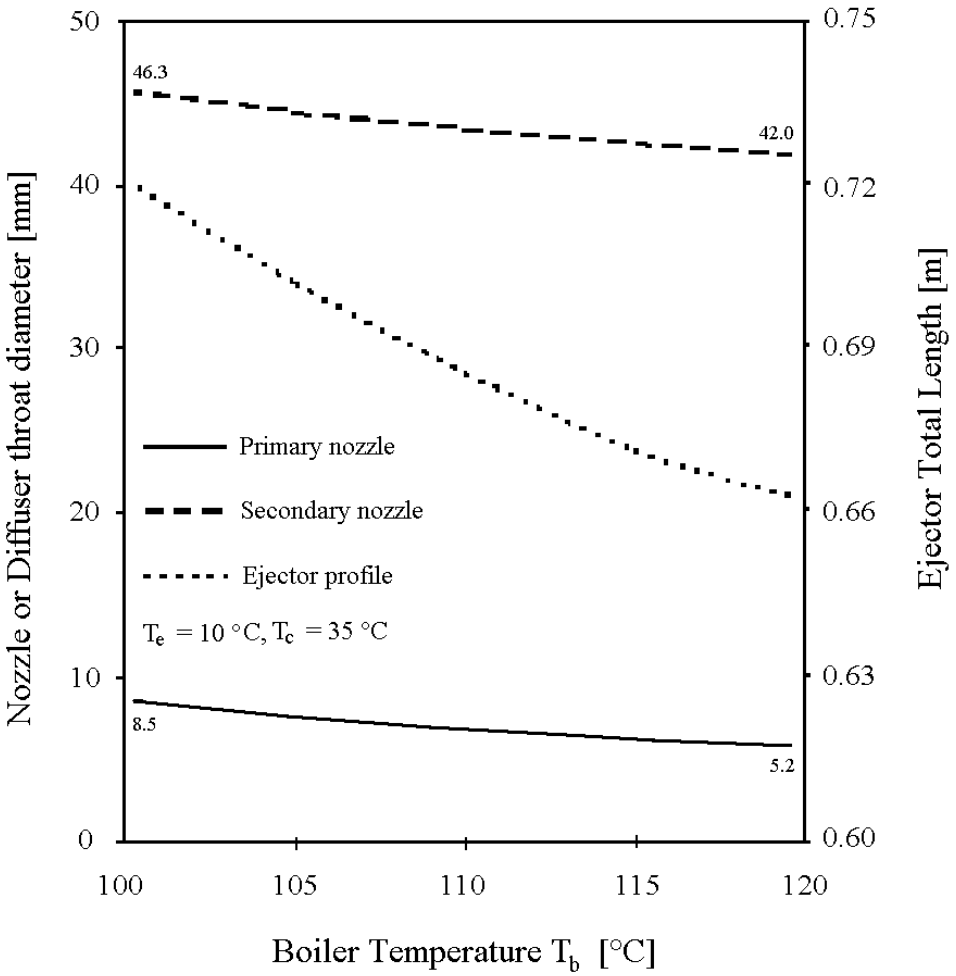

Figure 5.2: Theoretical operation of a steam ejector. Primary nozzle throat diameter, diffuser length and total length versus boiler temperature (Sun, 1996)

No published data on primary nozzle throat diameters and ejector profiles could be found for experimental systems that operate below 110 °C. In order to find the nozzle throat diameter that corresponds to an optimum boiler temperature in the range T_b = 95 °C to 105 °C and evaporator temperature of T_e = 10 °C, primary nozzles with different throat sizes were tested for a constant secondary nozzle throat diameter of 18 mm. Since a 2 mm diameter primary nozzle operated at a T_b = 130 °C, primary nozzles with throat diameters of 2.5 mm, 3.0 mm and 3.5 mm were tested. The results of these experiments are included in figure 5.3. The specifications of each nozzle is listed in Table 5.2.

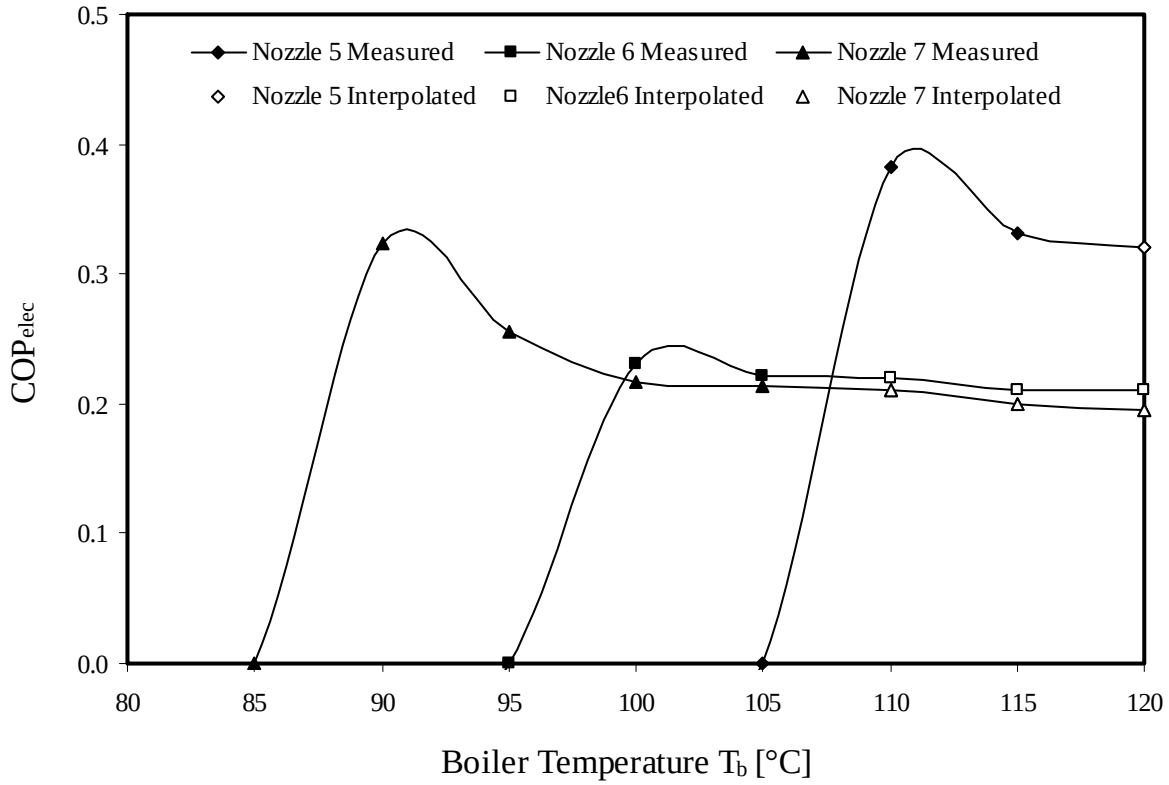

Figure 5.3: COP versus boiler temperature for different primary nozzles ($P_c \geq 2.0$ kPa, $T_c \geq 18.3$ °C, $T_e = 10$ °C, NXP = -5 mm)

Table 5.2: Primary nozzle geometries (mm)

Nozzle number	A	B	C	D	E	A_T	A_R*
5	2.5	10	42.85	8	52.15	16	51.8
6	3	12	51.50	8	43.50	16	36.0
7	3.5	14	60.00	8	35.00	16	26.4

*A_R corresponds to a secondary nozzle throat diameter of $d_t = 18.0$ mm

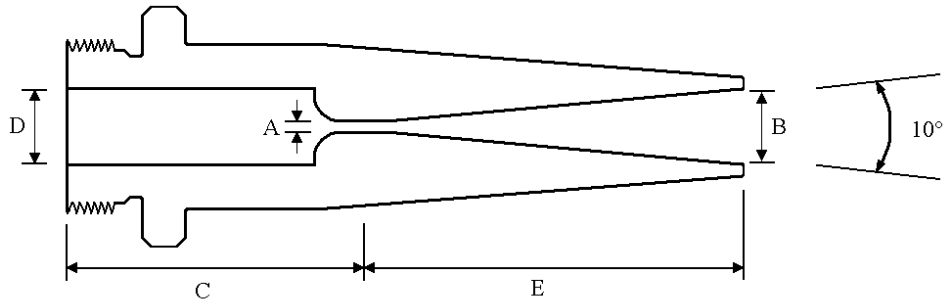

It can be observed from figure 5.3 that the optimum boiler temperature can be lowered to 90 °C at the expense of COP. As explained earlier, the reason for the drop in COP values as the boiler pressure decreases is due to the condenser pressure of the experimental setup that was limited to 2.0 kPa (18.3 °C).

If P_c is increased to 2.34 kPa (20 °C) the results would differ from those shown in figure 5.3. The result of increasing the condenser pressure is an increase of the optimum boiler temperature and a decrease in COP values. It is therefore advantageous to have a condenser pressure as low as possible.

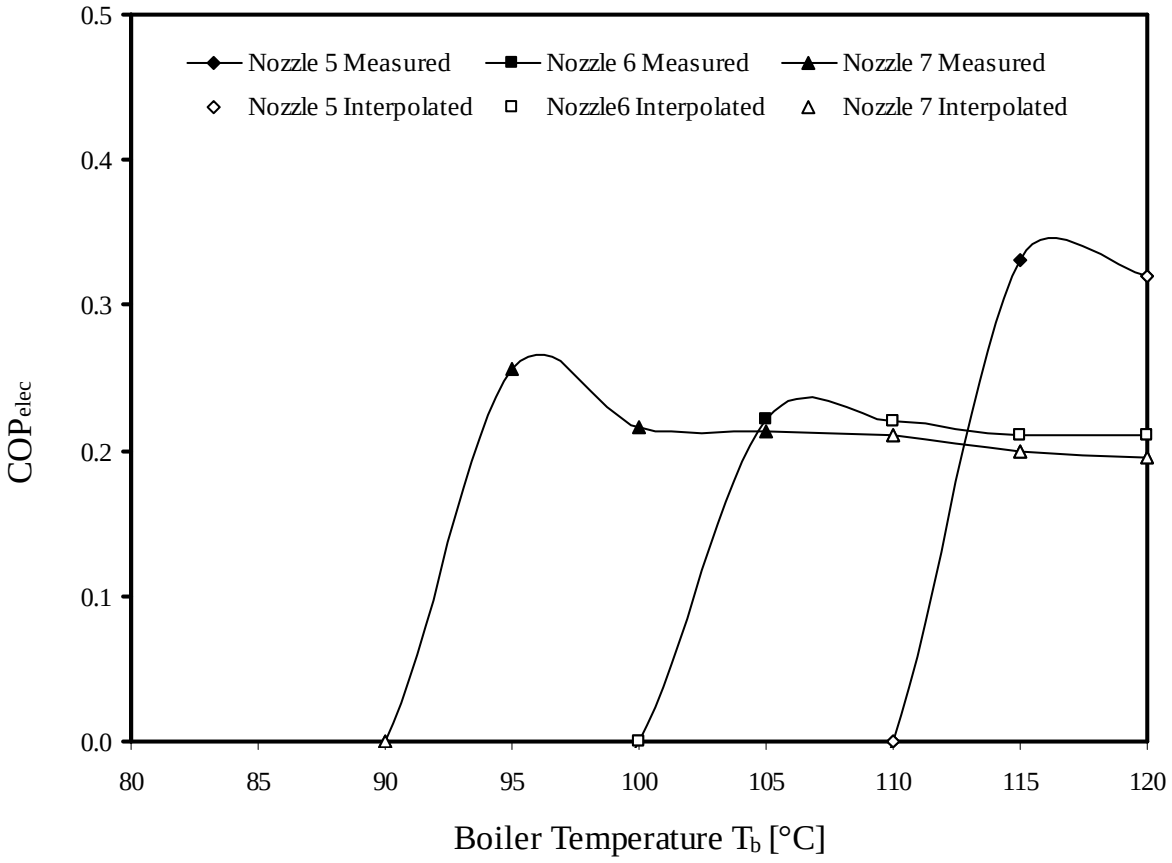

Figure 5.4: COP versus boiler temperature for different primary nozzles ($P_c \geq 2.34$ kPa, $T_c \geq 20$°C, $T_e = 10$°C, NXP = -5 mm)

5.3 Primary Nozzle Exit Position

The effect of the primary nozzle position on the system performance is given in figures 5.5 and 5.6. The nozzle exit position, NXP, is defined as the distance from the primary nozzle tip to the start of the bell mouth inlet of the secondary nozzle (figure 4.9). The NXP value is measured in mm and is positive if the nozzle tip is downstream of the bell mouth inlet.

It is clear from figure 5.6 that NXP = -5 mm is the optimum operating point for Nozzle 7. If the primary nozzle is too far upstream from the bell-mouth inlet, the COP drops. In a similar manner, the COP drops if NXP is too large (inside the secondary nozzle).

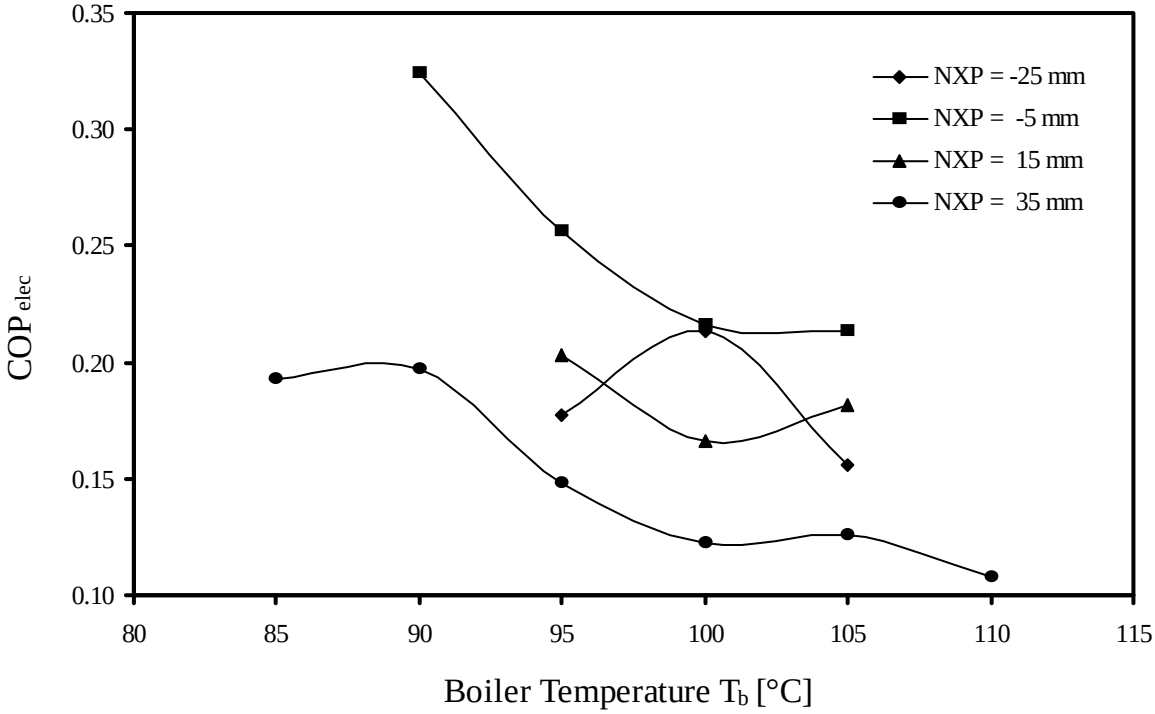

Figure 5.5: The effect of primary nozzle exit position on system performance for Nozzle 7

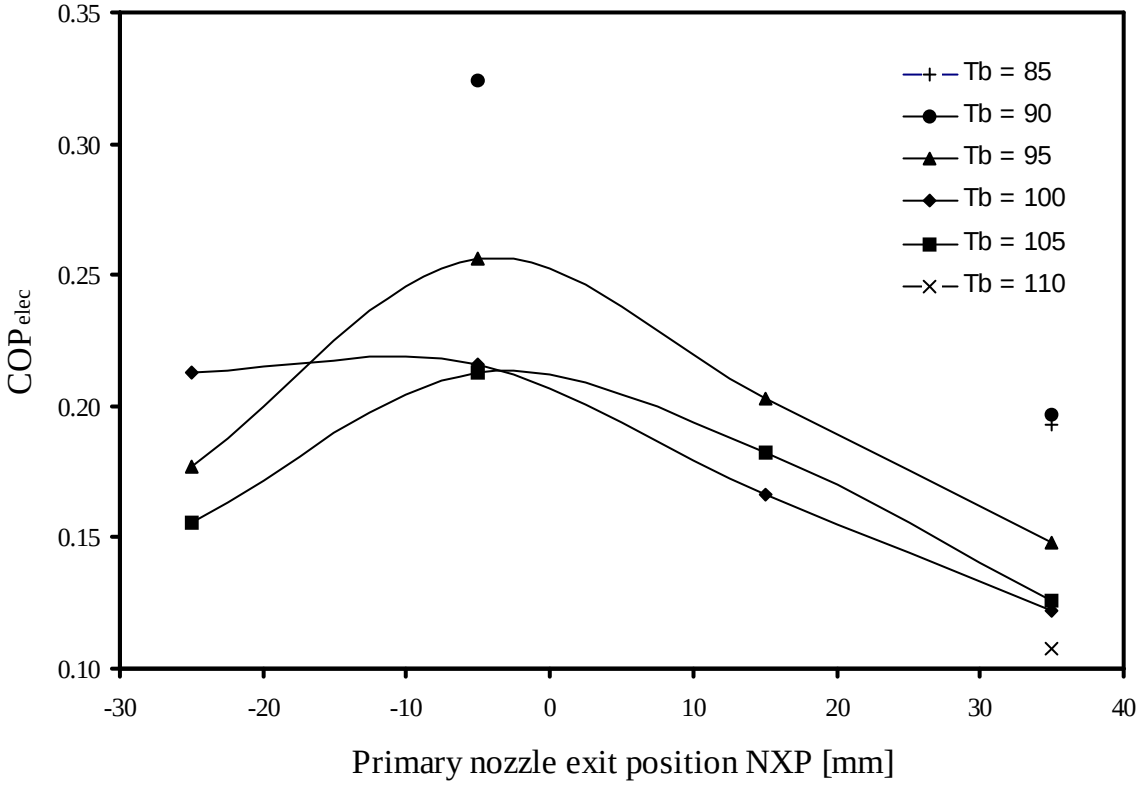

Figure 5.6: The effect of primary nozzle exit position on system performance for Nozzle 7

5.4 Subzero Temperatures

The question whether a steam jet ejector can produce ice often arises. When the steam tables are examined, it is noticed that saturated water freezes at a pressure below 0.612 kPa (figure 5.7). As can be seen from figure 5.7, saturated water is at its triple point when the pressure equals 0.612 kPa. If the pressure is reduced below 0.612 kPa, either ice or vapour would exist depending on the temperature.

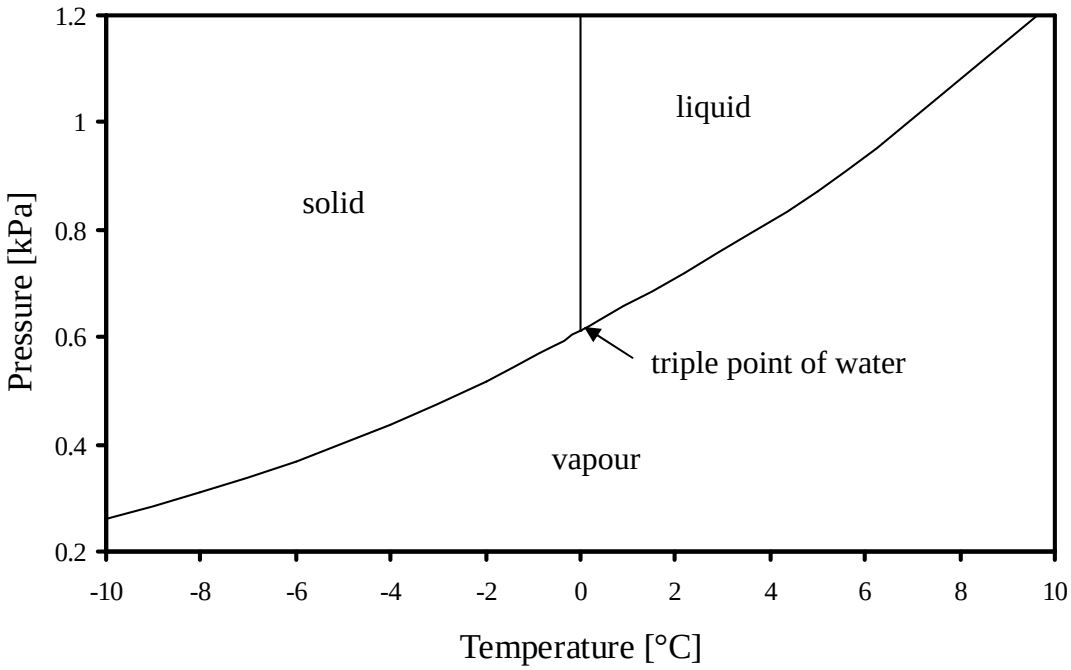

Figure 5.7: The characteristics of water in the vicinity of its triple point (Çengel and Boles, 2002)

Subzero evaporator temperatures were investigated using nozzle 7 and T_b = 105 °C. The results of this experiment are shown in figure 5.8.

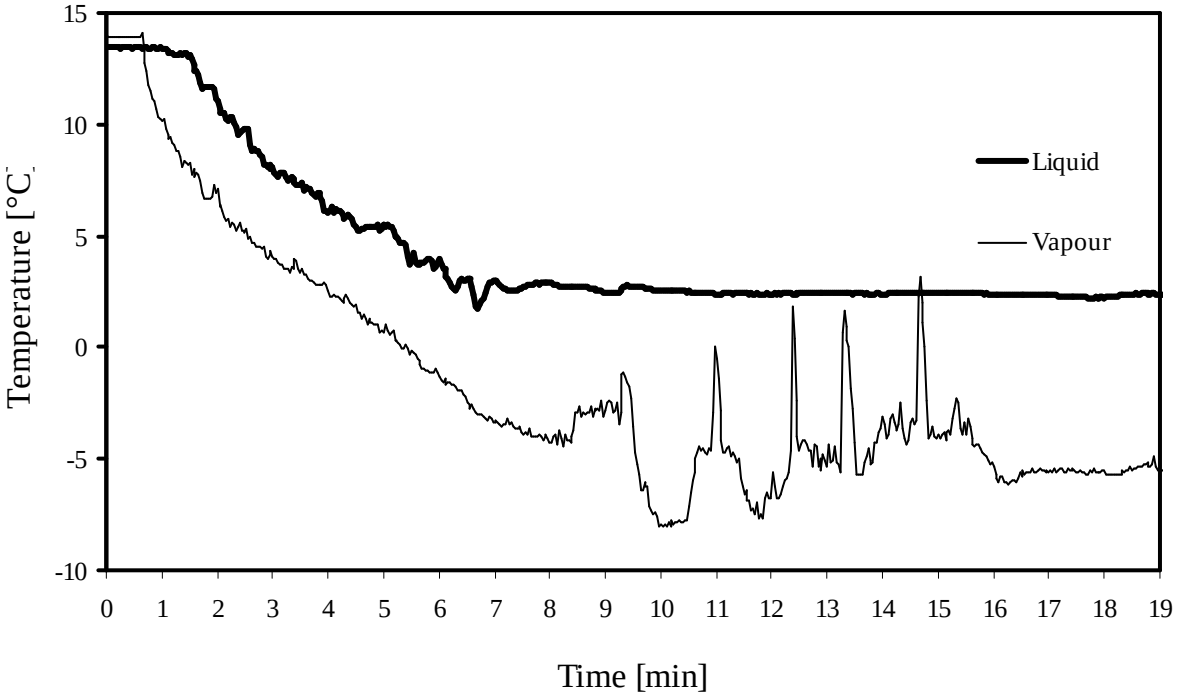

Figure 5.8: Evaporator temperatures versus time

After 5.5 min the evaporator vapour temperature was below 0 °C. The minimum vapour temperature of –8 °C was reached after about 10 min. Some instability is observed for the time 8 min to 7 min. After this the evaporator vapour temperature settled just below -5 °C.

Note that the evaporator liquid temperature settled around 2.4 °C. The evaporator water is cooled from the top and natural convection in the water enables the liquid at the bottom of the evaporator to cool down. The density of water increases as it is cooled down. When the water reaches a temperature of 4 °C its density, however, starts to decrease (figure 5.9) and its volume increases. Due to this phenomenon, natural convection in water that is cooled from the top does not occur below 4 °C. The liquid at the bottom of the evaporator is cooled from 4 °C to 2.4 °C due to conduction through the water itself as well as through the stainless steel walls of the evaporator.

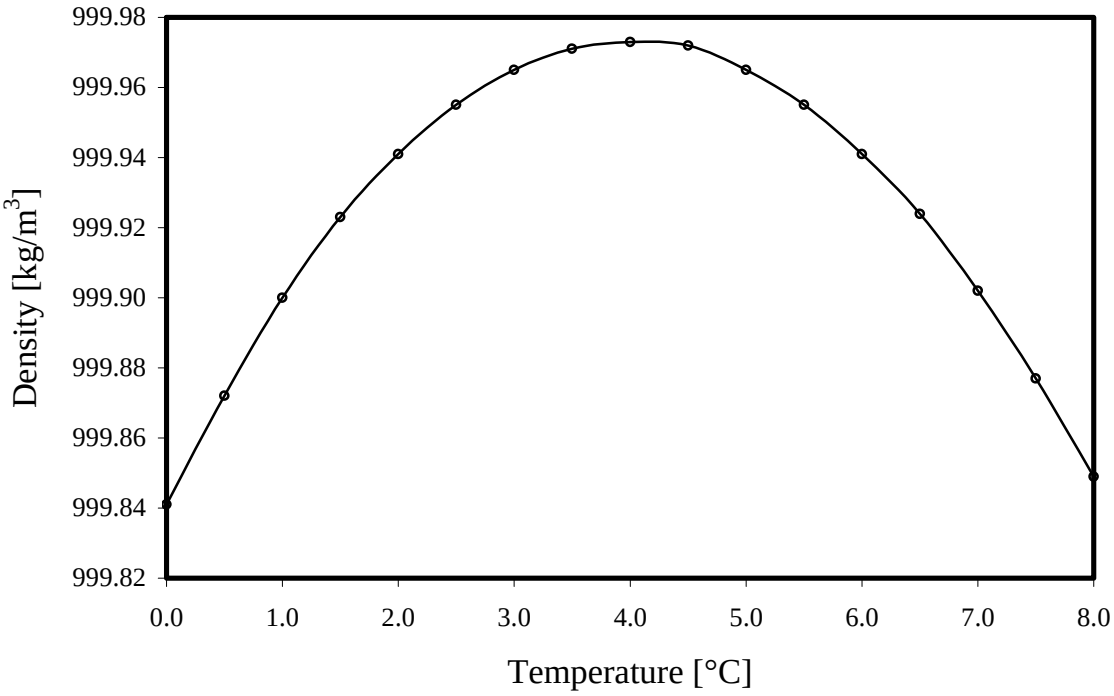

Figure 5.9: Water density in the vicinity of 4 °C (Çengel and Boles, 2002)

It is suspected that the evaporator liquid froze at the surface. The suspicion is supported by the water level in the sight glass that rose. In a test that was conducted, the sight glass level (distance from the bottom of the evaporator to the water level in the sight glass) rose from 272 mm to 468 mm. The volume of water liquid only increases marginally (0.002 %) from 4 °C down to 2.4 °C. The effect of the water expanding in the evaporator would only be noticed if the water surface inside the evaporator was frozen and the only place for the cold water under the ice to expand was up the sight glass (figure 5.10).

The documentation of the operation of a steam jet ejector with evaporator temperatures below 5 °C could not be found in literature. Most authors, e.g. Sun and Eames (1995b), stated the following: “One problem with steam-jet systems is that the cooling temperature can only be above the freezing point of water.”

Water is often used as a refrigerant in an adsorbtion refrigerator with zeolite as adsorbent. Cooling is achieved by lowering the pressure in the evaporator and causing forced evaporation of water. Dupont et al. (1982) tested such an experimental unit. The unit was powered by solar thermal heat and used an air-cooled condenser. The unit had a COP of 0.1 and could produce 7.0 kg of ice per square meter of collector area. This proofs that ice can be produced by the forced evaporation of water.

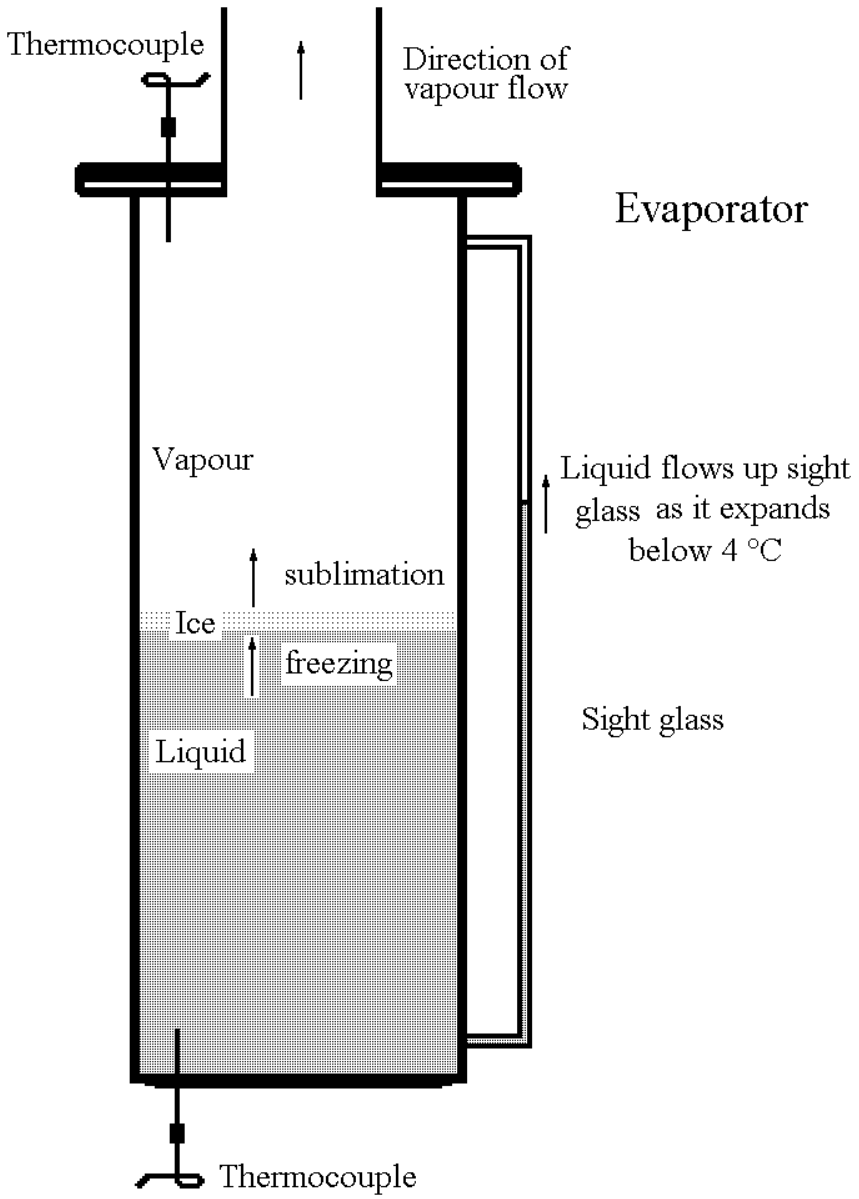

Figure 5.10: The evaporator during subzero vapour temperatures

Another test was conducted in order to investigate the subzero evaporator capabilities of the ejector system. Nozzle 6 was used and the evaporator vapour reached a temperature as low as – 8.5 °C. The suspicion that ice formed in the evaporator was confirmed by ice forming at the water level in the evaporator sight glass. This is shown in figure 5.11.

Figure 5.11: Ice in the evaporator sight glass

5.5 Comparing Theory and Experimental Results

The theoretical model explained in chapter 3 was put into an Excel spread sheet. The theoretical model is used to predict a critical condenser pressure. The boiler and evaporator temperatures as well as entrainment ratio values are used to compute the critical condenser pressure.

In this text, three different theoretical models are used. Each model has different values for η_p, η_d and η_m. The efficiency values for "theory 1" are $\eta_p = 0.85$, $\eta_d = 0.85$ and $\eta_m = 0.95$ as suggested by Eames et al. (1995). The values for "theory 2" are $\eta_p = 0.8$, $\eta_d = 0.8$ and $\eta_m = 0.8$ and for "theory 3" they are $\eta_p = 0.75$, $\eta_d = 0.75$ and $\eta_m = 0.75$.

The effect of η_d is relatively small on the critical condenser pressure. A 10% change in η_d only has a 0.2 % effect on P_c. η_m has the largest influence on P_c. A 10 % change in η_m changes P_c by 14.1 %. A 10 % change in η_p has a 3.4 % effect on P_c. It is clear from this information that the mixing efficiency between the primary and secondary streams dominates the performance of the ejector.

Figure 5.12 compares the experimental results of Eames et al. (1995b) with the three theory scenarios. Note that there are two experimental COP values (COP_{elec} and COP_{water}). The same data of figure 5.12 is plotted COP versus condenser temperature in figure B.6.

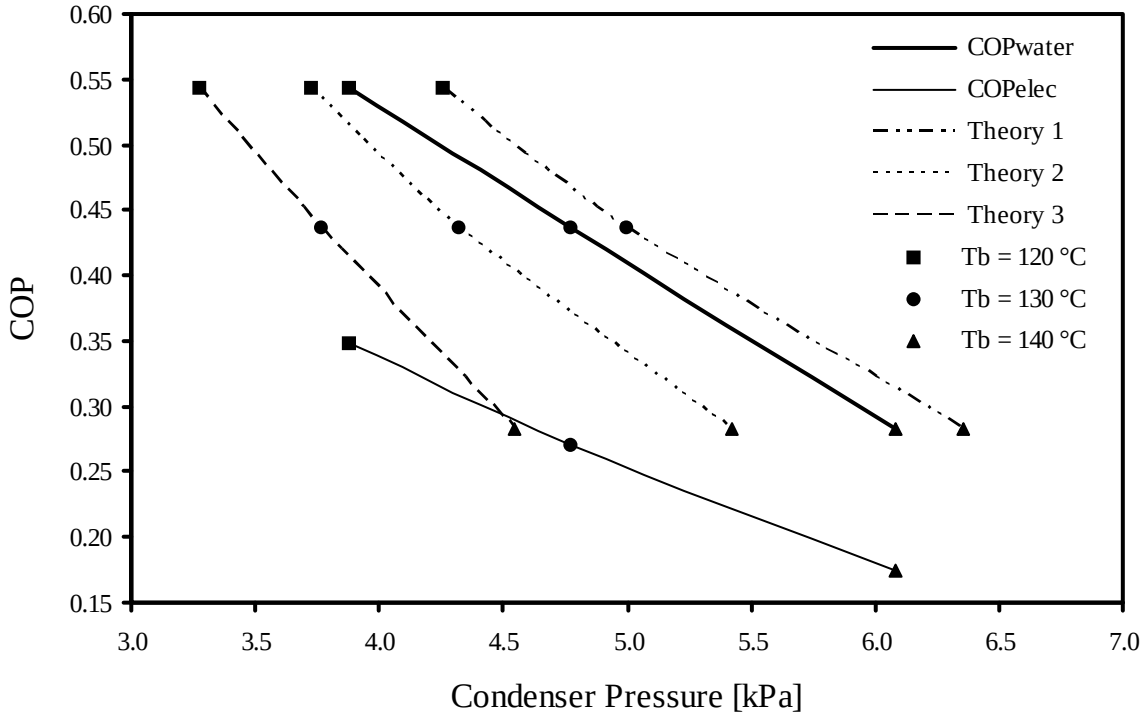

Figure 5.12: Water and electric COP compared to three theoretical models. T_e = 10 °C, A_R = 81, NXP = 26 mm (Eames et al., 1995b)

The experimental results of Eames et al. (1995) show that the electrical COP is on average 60% lower than the water COP value. This difference is due to the unwanted heat losses from the boiler and heat gains to the evaporator from the environment. The water COP compares well to theory 1 and on average only differs by 3.5 %. The complete range of experimental data from Eames et al. (1995b) is tabulated in table A.1.

Since the theory does not make provision for the primary nozzle exit position, the best COP values obtained for Nozzle 7 were used to compare to the theory. The best COP results were obtained at NXP = -5 mm. Nozzle 7, with T_e = 10 °C and T_b = 95 °C to 105 °C was compared to the three different theory scenarios in Figure 5.13.

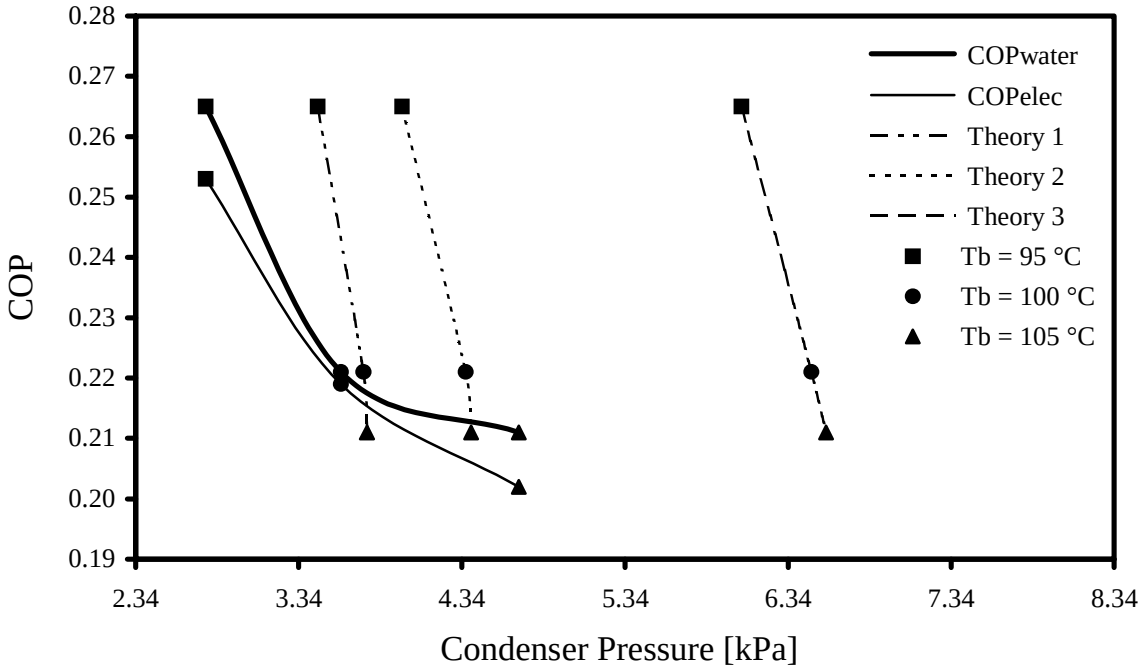

Figure 5.13: Electric and water COP compared to three theoretical models. T_b = 95 °C to 105 °C, T_e = 10 °C, A_R = 26.5

As expected and can be seen from figure 5.13, the water and electric COP differ. The electric COP differs in the range of 85.3 % to 99.1 % in comparison with the water COP value. This value is considerably higher than the value recorded by Eames et al. (1995b) of 60%. The main reasons for this could be that the apparatus used in this thesis was reasonably well insulated and was operated at lower boiler temperatures.

The experimental water COP compares the best with theoretical model three. The water COP correlates on average within 39.4 % with theoretical model one, within 14.8 % with theoretical model two and within 10.4 % with theoretical model three.

The apparatus used by Eames et al. (1995b) used a water circulation pump and spray nozzle system in the evaporator. The lack of such a system in the apparatus that was tested could be the reason for the large deviation from theoretical model one. Another reason could be the lower boiler to condenser pressure ratio at which the tests were conducted which can lead to higher inefficiencies that will reduce the system performance.

5.6 Comparison to Published Data

Figure 5.14 and table 5.3 show the experimental results of various authors. These differ due to the differences in equipment, primary nozzle exit position and area ratios. Note that E2, E3 and E6 represent electricity input ratios (COP_{elec}). The other data (E1, E4 and E5) represent entrainment ratios (COP_{water}).

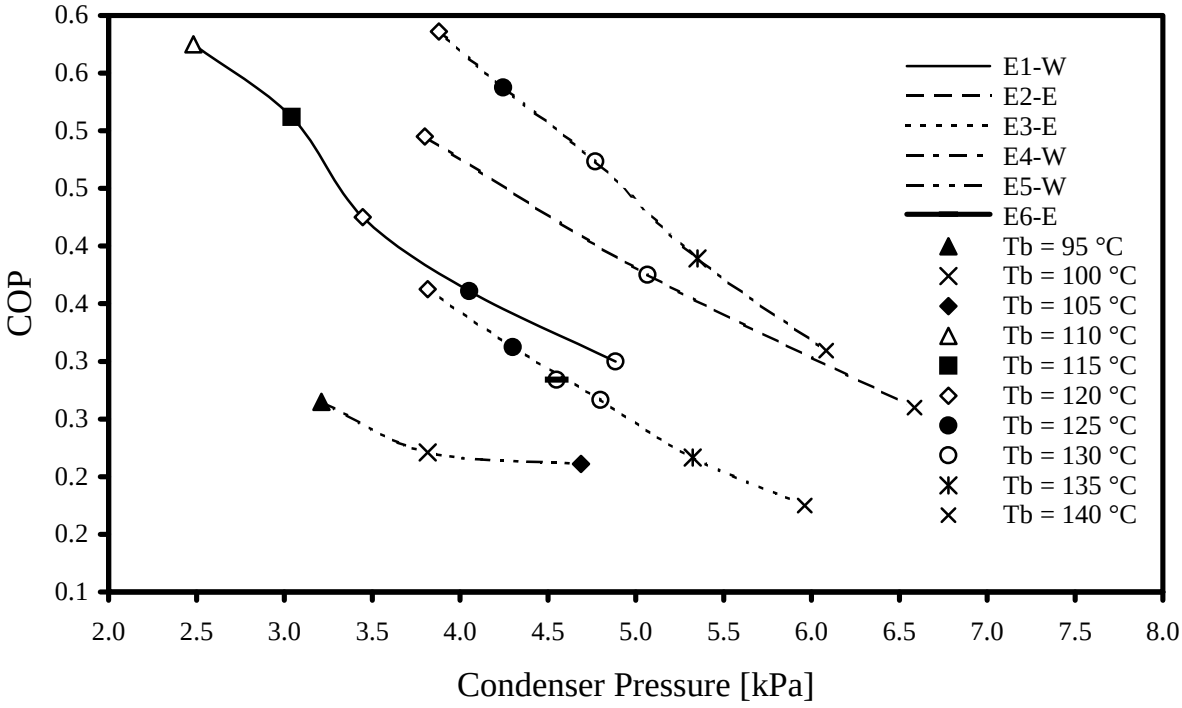

Figure 5.14: Comparison of different published data for T_b = 95 °C to 140 °C and T_c = 10 °C

The purpose of this comparison is to form a general idea of work done until present on steam jet ejectors. From figure 5.14, it could be concluded that higher COP and lower T_{crit} values would be expected from the experiments. The A_R value for E5, however, is significant lower than E1 – E4.

Table 5.3: Comparison of different published data

Data Series	Author*	Measured Data	System	A_R	NXP [mm]	T_e [°C]
E1-W	1	COP_{water}	Closed	81	-	10
E2-E	2	COP_{elec}	Closed	90	26.16	10
E3-E	3	COP_{elec}	Closed	81	26	10
E4-W	4	COP_{water}	Closed	90	26.16	10
E5-W	5	COP_{water}	Open	36	16	10
E6-E	6	COP_{elec}	Open	81	25	10

*1) Sun (1996)
2) Chunnanond & Aphornratana (2004)
3) Aphornratana & Eames (1997)
4) Eames et al. (1995)
5) Author – Nozzle 7
6) Author – Nozzle 3

5.7 Electric Power Input

The electric voltage to each element is recorded by the data logger. The voltage value is used to calculate the electric power input into the boiler and evaporator as follows:

$$P_{elec} = VI = V^2 / R \qquad (5.9)$$

Only one of the 4 kW elements on the boiler was used during the tests. The second 4 kW boiler element was only used when the boiler was heated to its working temperature. In an experiment, the resistance of the 4 kW boiler element that was used during the tests varied in the range of R_{4kW} = 14.144 Ω to 14.185 Ω as the temperature varies from 85 – 115 °C (figure 5.15). The total change in resistance over the mentioned temperature span is 0.041 Ω. This value is 0.32% of the average resistance of 14.161 Ω. A boiler resistance value of 14.16 Ω was used for all calculations in this text unless otherwise stated.

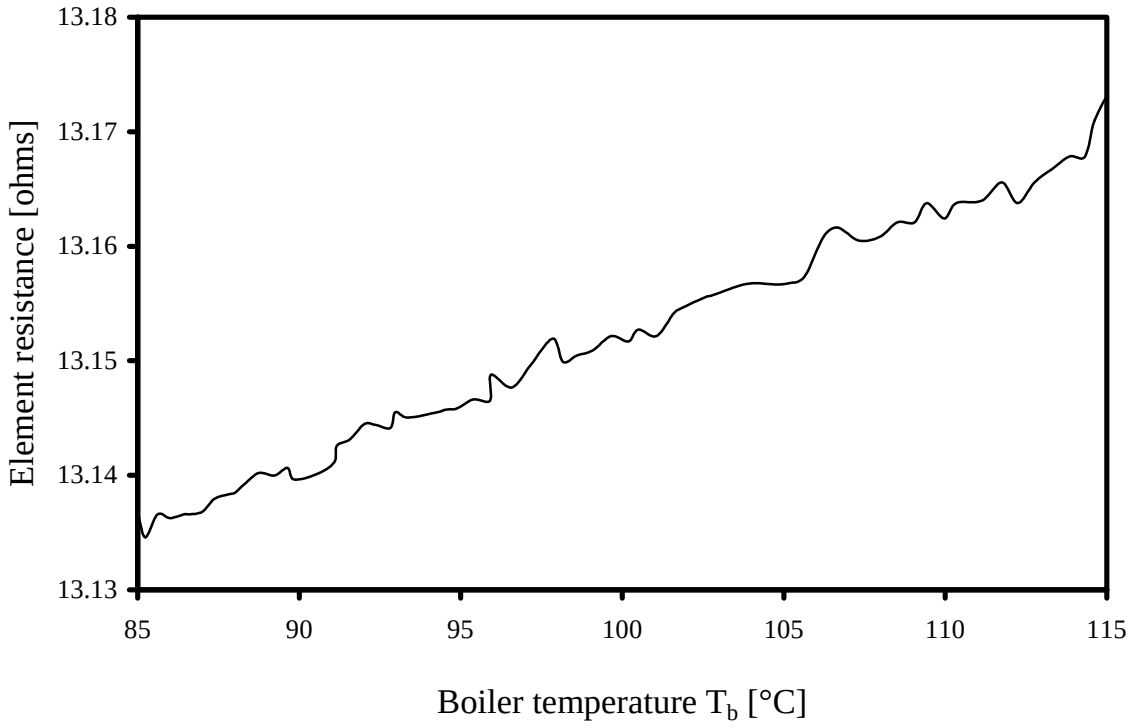

Figure 5.15: Boiler element resistance

The 3 kW evaporator element resistance stayed relatively constant at R_{3kW} = 17.7 Ω over the temperature range of 4 °C to 13 °C. This can be seen in figure 5.16.

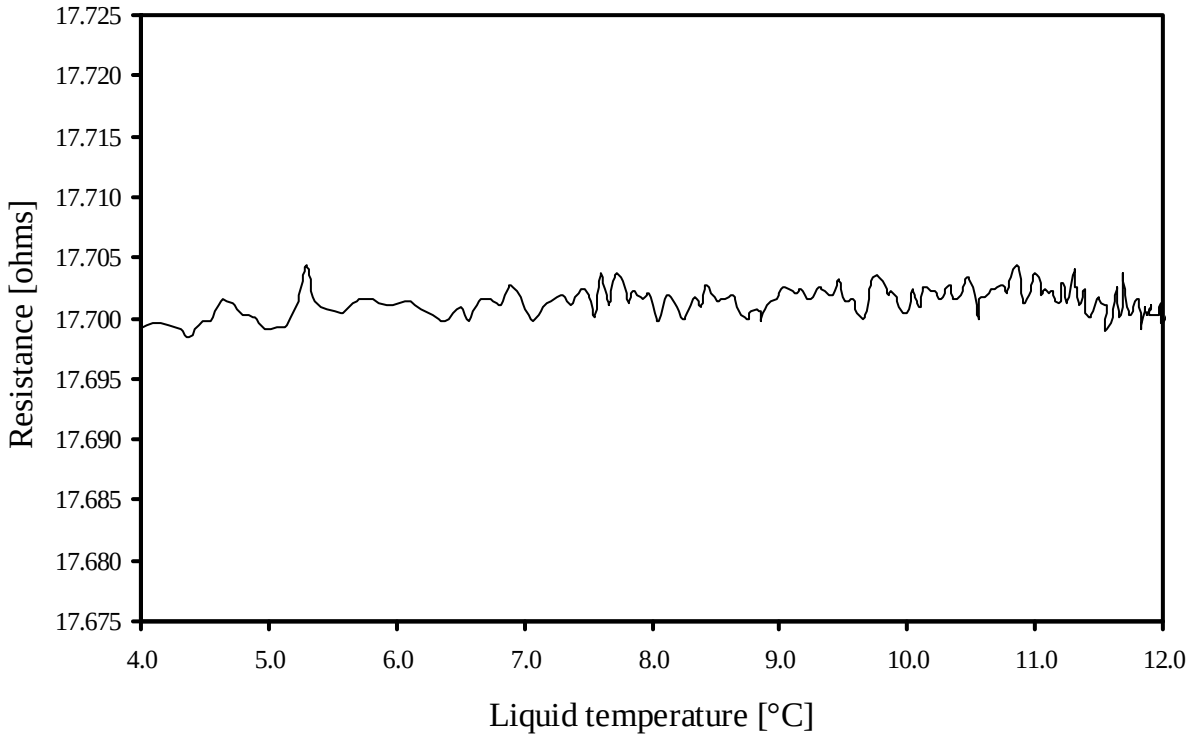

Figure 5.16: Evaporator element resistance

5.8 Energy Balance

An energy balance is performed in order to determine the losses in the system:

$$Energy_{in} = Energy_{out} \quad (5.10)$$

Since no work is done by or on the open loop system this becomes:

$$heat_{in} = heat_{out} \quad (5.11)$$

The total energy balance is represented by:

Boiler heat in + Evaporator heat in + Evaporator heat gain = Condenser heat out + Boiler heat losses + Other heat losses

or

$$P_{b\_elec} + P_{e\_elec} + Q_e = Q_c + Q_b + Q_{other} \quad (5.12)$$

A sample calculation is presented below:

Nozzle 7

T_b = 95 °C
V_b = 208.13 V
P_{b_elec} = V^2/R
= 208.13/14.16
= 3059.2 W
Q_b = 272.2 W*

T_{cw_in} = 15.2 °C
T_{cw_out} = 18.2 °C
h_{cw_in} = 38.5 kJ/kg
h_{cw_out} = 55.2 kJ/kg
m' = 0.205 kg/s
$Q_c = m'(h_i - h_o)$ = 0.205 x (55.2 – 38.5) = 3426.3 kW

T_e = 9.3 °C
Q_e = 2.7 W*
$P_{e\_elec} = V^2/R$ = 132.13/17.7 = 986.3 W

$Q_{other} = P_{b\_elec} + P_{e\_elec} + Q_e - Q_c - Q_b$

Q_{other} = 3059.2 + 986.3 + 2.7 – 3426.3 – 272.2 = 349.7 W

*These values were obtained experimentally and explained later in this chapter

The heat losses relevant to the uninsulated boiler top and bottom, as well as all the other heat losses amount to 349.7 W. This is 11.4 % of the boiler electrical input. Figure 5.17 shows an infrared photo of the boiler top and bottom. From the photo, it can be clearly seen that the major heat losses from the boiler is from the top and bottom flange. Additional IR images can be found in figure B.3 – B.5.

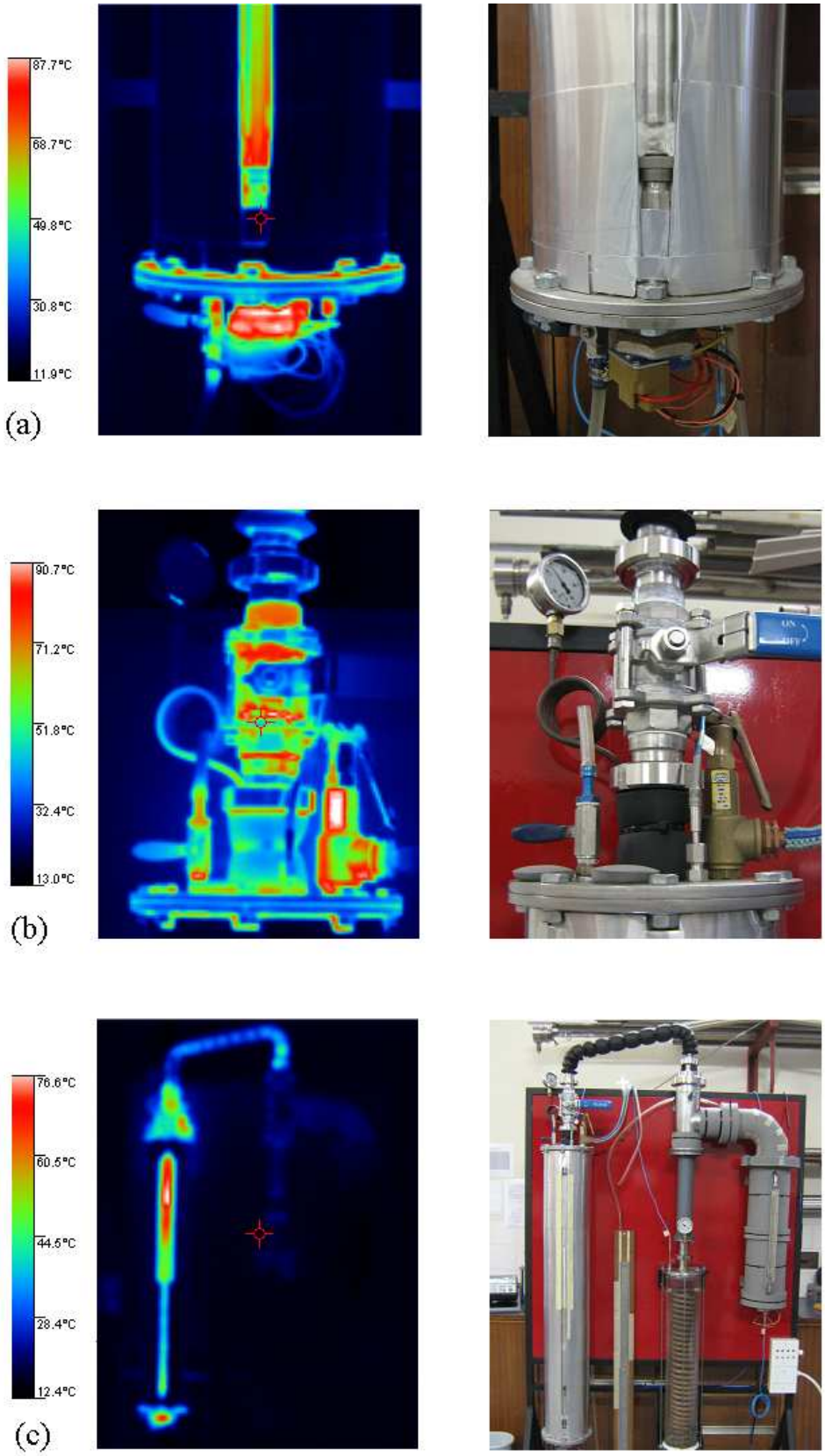

Figure 5.17: Infrared images pertaining to boiler heat losses
(a) The boiler bottom
(b) The boiler top
(c) The complete system

5.9 Boiler and Evaporator Heat Losses and Gains

5.9.1 Boiler heat losses

Tests were conducted to determine the boiler heat losses. In a typical test, the thermostat on the boiler elements was set to 100 °C. The test was conducted over a time span of 32 hours. Boiler temperatures were maintained near 100 °C and recorded every 15 s. The boiler heat losses are equal to the boiler energy input. Typical test results can be seen in figure 5.18.

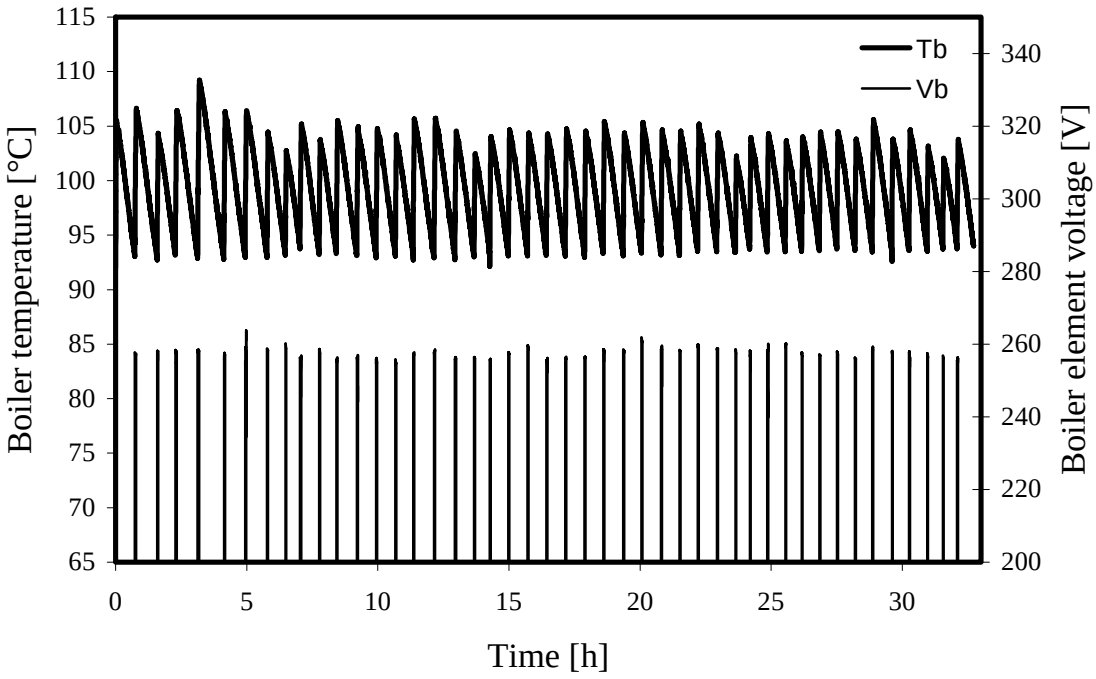

Figure 5.18: Boiler temperatures and voltages during a boiler insulation test at T_b = 100 °C

The total boiler heat loss versus ambient temperature of the same test is shown in figure 5.19. The ambient temperature varied in the range T_a = 12.3 °C to 14.0 °C. The boiler heat losses stayed relatively constant at 260 W throughout the duration of the test. From figure 5.19, it can be observed that the variation of the ambient temperature in the recorded temperature range has a minimal effect on the boiler heat losses.

Similar tests at different boiler temperatures and boiler liquid volumes were conducted. The results of these tests can be interpolated to predict the boiler heat losses for a particular boiler operating temperature and liquid volume.

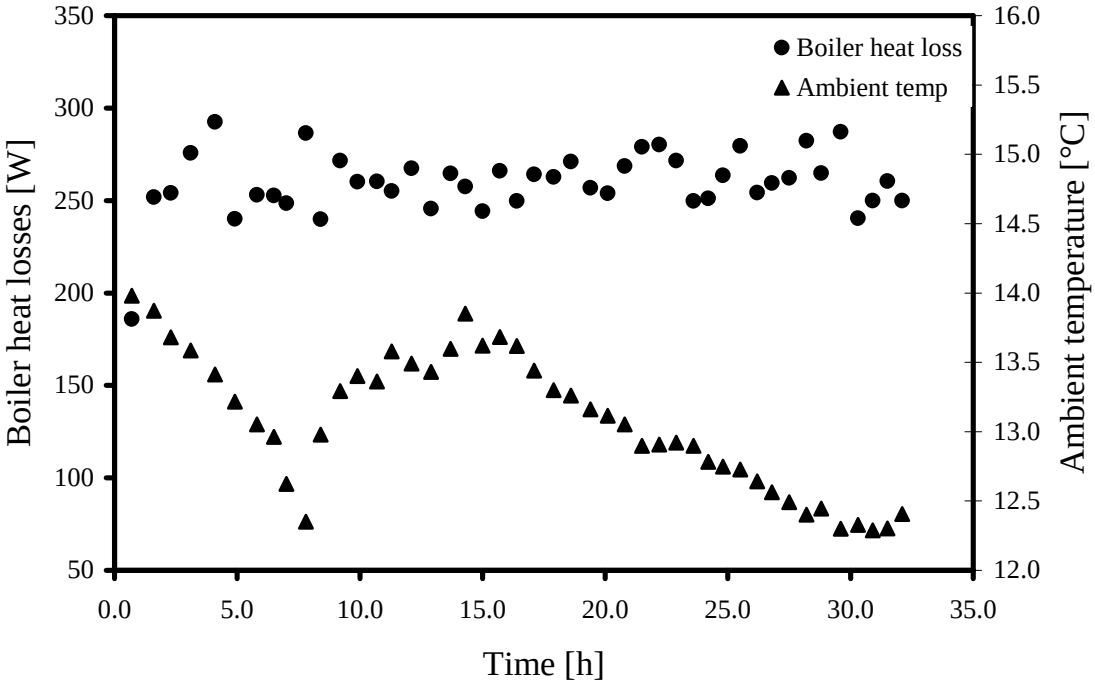

Figure 5.19: Boiler heat losses and ambient temperatures during a boiler insulation test at T_b = 100 °C

5.9.2 Evaporator heat gains

An evaporator insulation test was conducted by cooling the evaporator liquid down to 4 °C. The evaporator heat gain can be calculated if the evaporator liquid volume and rate of temperature increase is known.

Figure 5.20 present the results of a test done on 5.6 L of evaporator water. The evaporator liquid and ambient temperatures were recorded. From this data it is calculated that the heat gain to the evaporator is 2.7 W at T_e = 10 °C. From this it can be concluded that the evaporator is well insulated. With a typical evaporator cooling load of 1 kW, the evaporator unwanted heat gain can be neglected.

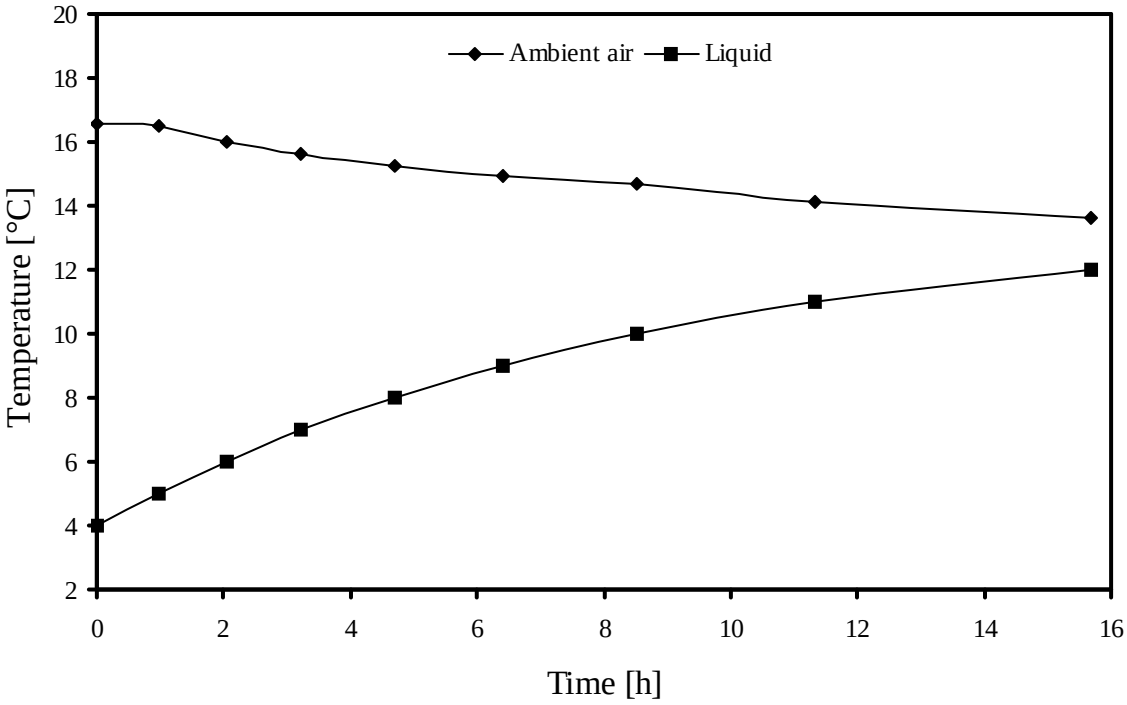

Figure 5.20: Evaporator liquid and ambient temperatures

5.10 Additional Data

The reader should note that a data CD is located on the last page of this thesis. A complete set of all the experimental data can be found on this CD. This includes the raw data as well as the processed data.

6. SOLAR POWERED COOLING

6.1 General

The use of solar energy for the boiler of a jet ejector system is not a novel idea and can be tracked back to the 1960's (Kakabaev and Davletov 1966). Various articles have been published suggesting different working fluids e.g. R113 (Al-Khalidy, 1998), R134a (Alexis and Karayiannis, 2005 and Selvaraju and Mani, 2006), R141b (Huang et al., 1998 and Vidal et al., 2006), ammonia (Sankarlal and Mani, 2006), water, methanol and ethanol (Riffat and Holt, 1998). It can be noticed from the dates of these articles that there is a renewed focus worldwide into solar powered ejector refrigeration and cooling.

6.2 Practical Solar Powered System Using Steam

Water as working fluid in ejector systems is by far the most environmentally friendly. Other working fluids e.g. ammonia and methanol have an inherent safety and health risk and is generally more expensive.

Up to date, the only published work that could be found on a practical system that uses steam below 100 °C is Nguyen et al. (2001). These authors further have the only practical solar powered steam jet ejector system on which information have been published. Their solar ejector cooling system was installed in an office building in Loughborough, UK. It uses heat from an evacuated tube heat-pipe solar collector array to drive the boiler. Evacuated tube collectors operate the best in locations as the UK where there are predominately diffused solar radiation. The solar collector was used for space heating and domestic purposes during the winter months. The system was backed by a gas burner that could be used during summer or winter.

The unit was installed in a single storey building with the condenser and ejector assembly installed in the roof space. Condenser cooling water was sourced from an existing pond and was pumped to the condenser via a strainer using a small submersible pump. The system utilised a direct expansion evaporator that was installed in the existing air handling unit. This system has a cooling capacity of 6.7 kW based on a COP of up to 0.3. The condenser pressure is 4.25 kPa (30 °C). The boiler and evaporator temperatures are 85 °C and 8 °C respectively. The system operated without a mechanical pump as will be explained later. This system can be seen in figure 6.1.

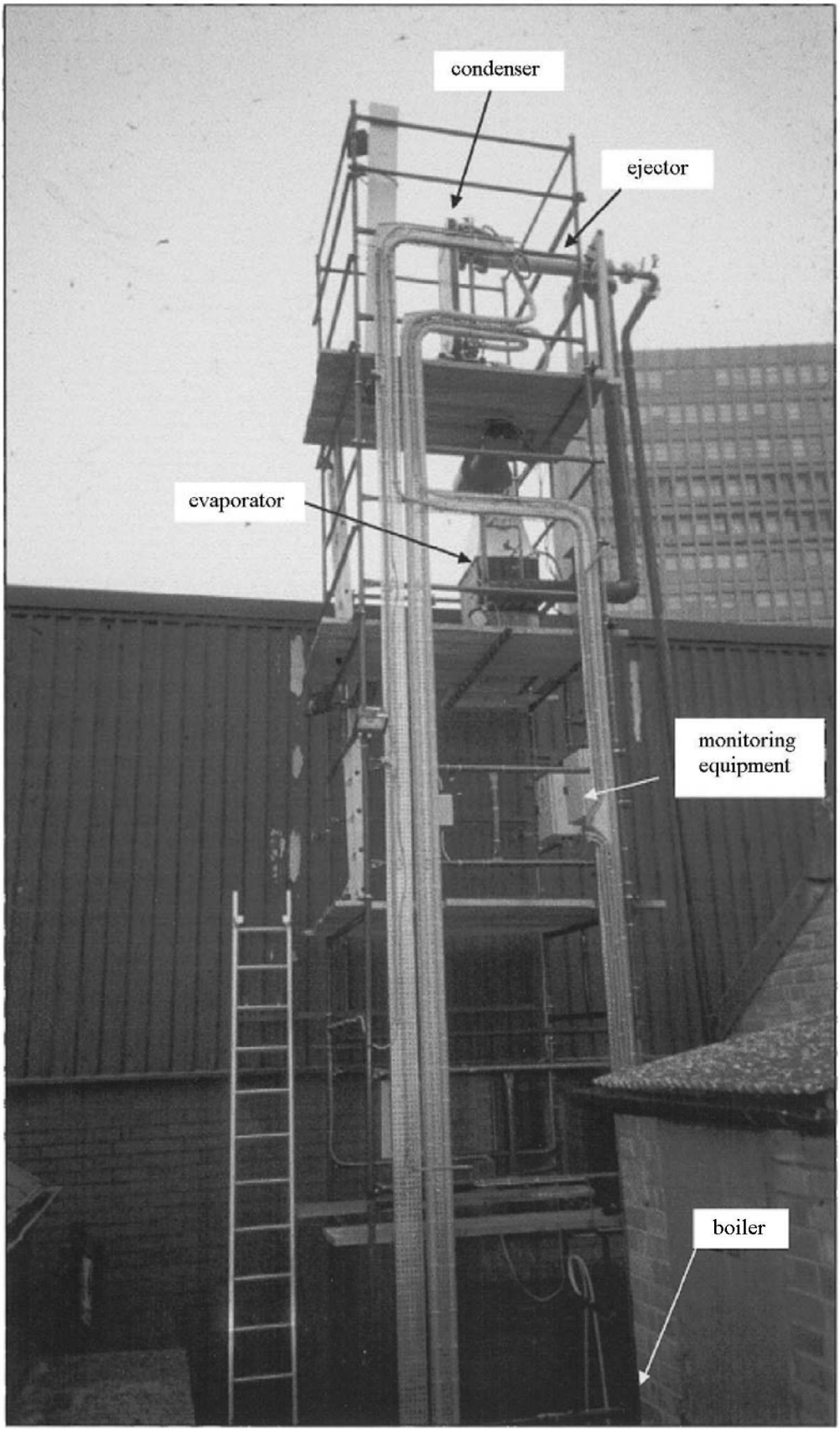

Figure 6.1: Solar powered ejector system in the UK, laboratory setup (Nguyen et al., 2001)

Nguyen et al. (2001) failed to specify any critical design data e.g. primary nozzle throat size, ejector profile and secondary nozzle throat size, etc. Some experimental data was obtained from the authors through personal communication. An example of their experimental results can be seen in figure 6.2. It can be noted from the figure (additional symbols were added for the ease of the reader) that the system operates at a boiler temperature near T_b = 80 °C. The condenser pressure varied between P_c = 2.66 kPa to 3.21 kPa (T_c = 23.1 °C to 25.2 °C). The usable evaporator cooled water output was in the range T_{ew_out} = 4 °C to 5 °C.

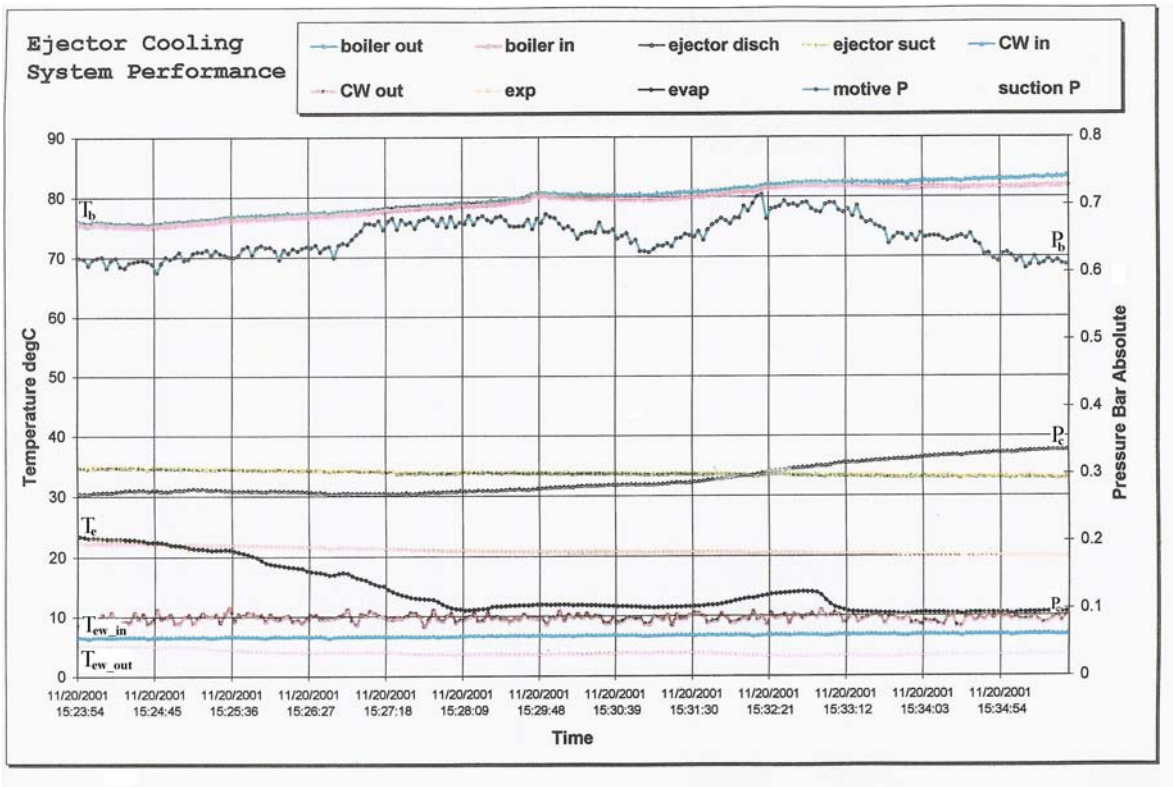

Figure 6.2: Experimental data from a steam jet ejector cooling system installed in the UK (Tony, 2005)

6.3 Practical Implications

6.3.1 Night time cooling

The question of how to cool or refrigerate during the night using solar energy is quite popular. The use of phase change materials (PCM) is a simple and passive method of achieving night-time cooling. A PCM is a chemical mixture that changes phase between liquid and solid at a predetermined temperature. Ice is the best example of a natural PCM.

If solar thermal cooling is used to refrigerate, the inner walls of a fridge could be lined with a PCM of a preferred temperature. PCM

has been successfully used in the development of a battery free photovoltaic powered fridge, as reported by Ewert and Bergeron (2000). The same techniques can be used for a solar thermal powered fridge.

Research on using phase change materials in buildings in order to reduce the cooling load is receiving active research worldwide (Fang and Zhang, 2006, Arkar et al., 2006 and Nagano et al., 2006).

6.3.2 Part load operation

The main problem with the usage of solar energy lies in part load conditions. One method to overcome this problem is to use a multiple ejector system. An array of similar ejectors that are all connected in parallel and disconnected via valves during the night at each ejector inlet. As the sun rises and the boiler reaches a certain temperature, the first ejector is selected by means of a thermostat or similar device. As more solar energy becomes available, more steam is produced and thus more ejectors are brought into operation. When the sun sets in the evening or during cloudy periods in the day, some of the ejectors are switched off. Using this method, one standard ejector can be manufactured and used for any size of cooling system. This method has economically advantages due to lower design and manufacturing cost. This configuration compensates for the fluctuations in primary mass flow.

In a similar fashion, a multiple ejector system consists of a range of different ejectors (different NXP and A_R values). Using this configuration, a single ejector is selected by means of a thermostat or other device in order to sustain an optimal working condition at the current boiler temperature and condenser pressure. This configuration compensates for the fluctuations in boiler temperatures and condenser pressures.

Finally, a combination of the two configurations mentioned can be utilised to compensate for fluctuations in mass flow as well as T_b and P_c. These suggested methods are only conceptual and should be investigated in further studies.

6.4 The Pump

There are two methods to replace the condensate feed pump. By doing this, the use of electricity is eliminated and the system is purely powered by thermal energy.

6.4.1 Gravity feed pump

If the condenser condensate outlet is situated 10 m above the feed water inlet of the boiler, a hydrostatic pressure drop of about 100 kPa will result. A 10 m height difference would be adequate for a

boiler operating at 101.35 kPa (100 °C) and a condenser at 2.34 kPa (20 °C).

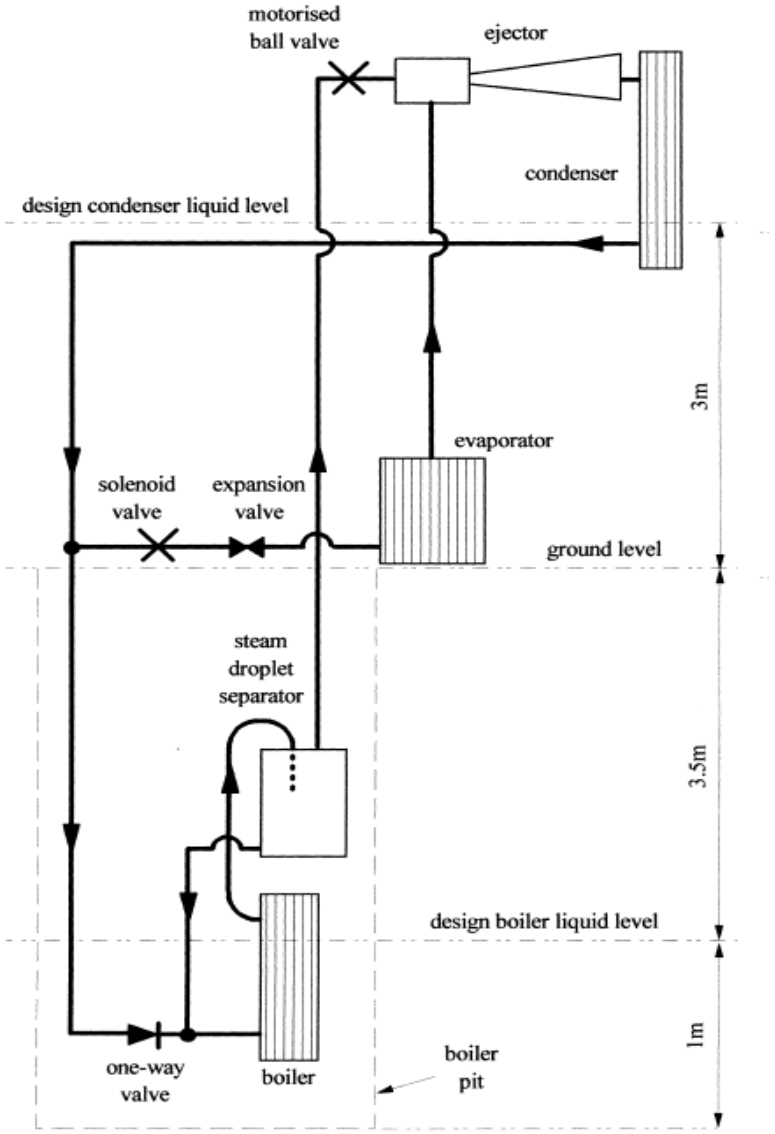

Figure 6.3: Solar powered steam jet ejector system in the UK, installation layout (Nguyen et al., 2001)

The cooling system described in chapter 6.3 (Nguyen et al. 2001) utilised this method as shown in figure 6.3. Here the height difference between the condenser outlet and boiler inlet is only 7 m. A one-way valve is located at the boiler inlet. The relatively long vertical steam pipe that runs from the boiler to the ejector causes steam condensation to occur. A steam droplet separator is added at the boiler outlet to ensure dry steam to the ejector.

For more detailed technical information on gravity feed systems used for steam jet ejectors, the reader is referred to recent work done by Srisastra and Aphornratana (2005) on this topic. They concluded that

the addition of a gravity feed system to an existing ejector system results in no loss of performance.

6.4.2 Duel ejector system

Shen et al. (2005) proposed the use of a second ejector in an ejector system. The purpose of the second ejector (vapour-liquid) is to pump condensate from the condenser to the boiler (figure 6.4).

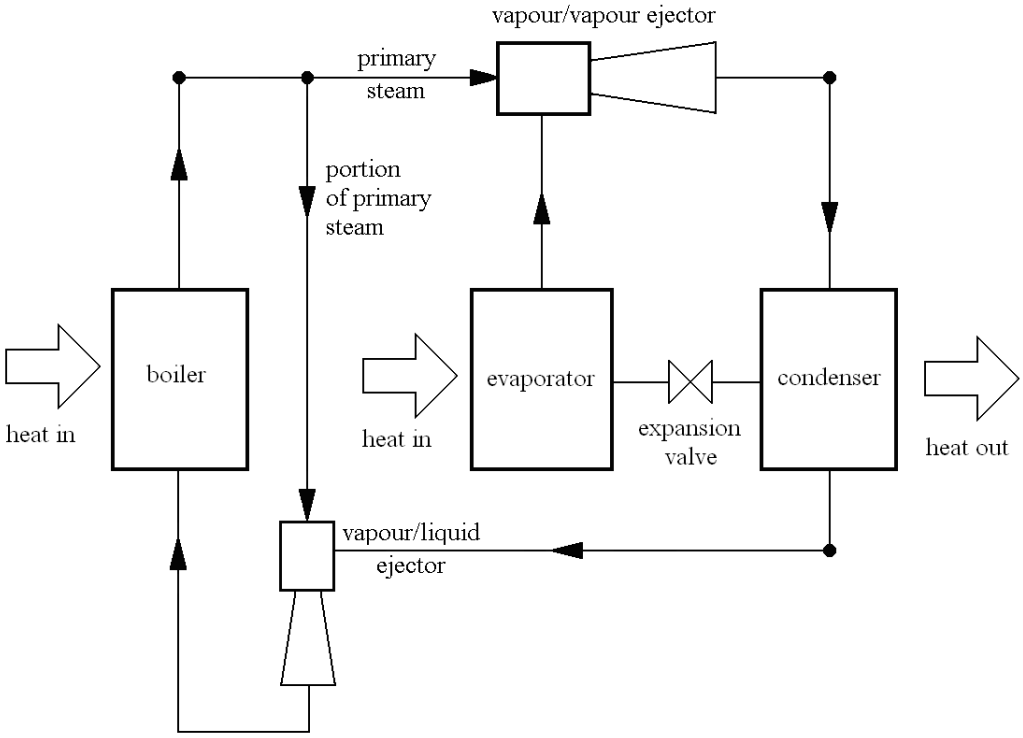

Figure 6.4: Dual ejector system, general layout (Shen et al., 2005)

In their work, a numerical model was used to predict the performance of the vapour-liquid ejector as well as the complete refrigeration cycle. The entrainment ratio of the gas-liquid ejector with water as fluent is superior above any other refrigerant as shown in figure 6.5. No experimental work was done by Shen at al. (2005). It is predicted that the performance of this system would not significantly differ from an ejector system with a mechanical pump. The efficiency of the vapour-liquid ejector is of the same order as for a small condensate pump. Additionally, the pump work is typically only 1 % of the heat input into the boiler and does not have a significant effect on the COP.

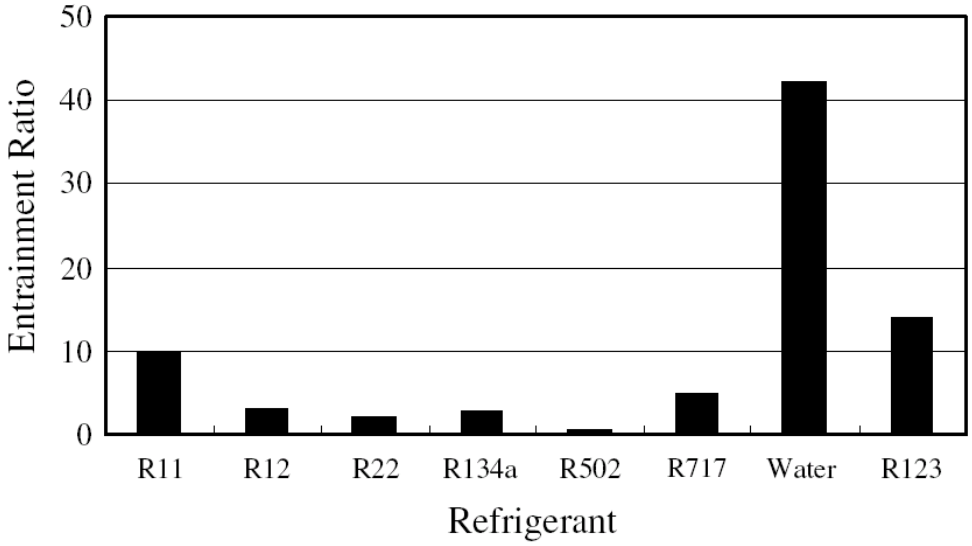

Figure 6.5: Entrainment ratio for vapour-liquid ejector for different working fluids (Shen et al., 2005)

6.5 Solar Collectors

The type of solar radiation (direct or diffused) for each location would determine the kind of solar collector that can be used. Evacuated tube collectors are superior when compared to flat plate solar collectors in terms of diffused solar radiation conditions. The operating temperatures of these collectors are listed in table 6.1.

Table 6.1: Typical operating temperatures of different solar collectors (Rona 2004 and Assilzadeh et al., 2005)

Type of collector	Typical operating temperature
Flat plate collector	< 70
High efficiency flat plate collector	60 – 120
Evacuated tube collector	60 – 130

In a study, Huang et al. (2001) compared three different solar collectors as listed in Table 6.2.

Table 6.2: Three different solar collectors (Huang et al., 2001)

Collector Type	Description	C_{sc} [W/°Cm^2]
A	low-cost specially designed single-glazed flat-plate collector with a selective surface	3.5
B	a conventional single-glazed solar collector with a selective surface	5.7
C	a vacuum-tube solar collector with tube-in-sheet fin	2

The efficiency of each collector is given by

$$\eta_{sc} = 0.8 - C_{sc}\frac{T_m - T_a}{G} \qquad (6.1)$$

where:

T_m = mean fluid temperature in the panel [°C]
T_a = ambient temperature [°C]
G = solar irradiance [W/m^2]
C_{sc} = collector constant [W/°Cm^2] (Refer to table 6.2)

According to figure 6.6, the evacuated tube collectors are more efficient than flat plate solar collectors. Flat plate collectors, however, are less expensive compared to evacuated tube collectors. Other advantages of flat plate collectors are ease of installation, durability and that they can be produced locally with simple tools. This makes flat plate collectors more attractive for developing countries. The disadvantage of flat plate collectors is that they take up more space than evacuated tube collectors. Currently no concentrating collectors, including evacuated tube collectors, are commercially produced in South Africa.

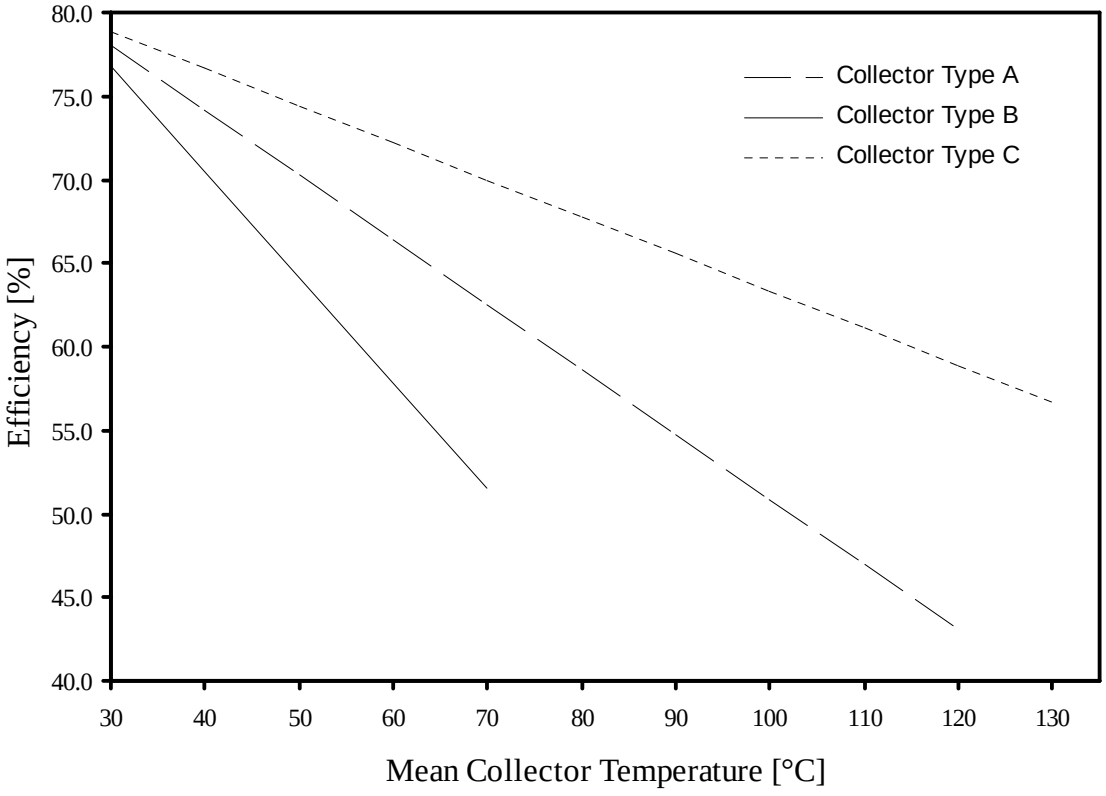

Figure 6.6: Efficiency comparison of three types of solar collectors with $T_{ambient}$ = 25 °C and G = 900 W/m^2 (Huang et al., 2001)

Figure 6.7: Solar thermal collectors
a) Flat plat solar collector (CEI, 2006)
b) Evacuated tube collector (Norfolksolar, 2006)

Figure 6.7 shows a photo of a plat plate solar collector and an evacuated tube array typically used for domestic water heating.

6.6 Collector Configurations

Three methods exist for incorporating a solar collector into an ejector system. They are shown in figure 6.8. Figure 6.8 (a) shows a direct heating setup. Here the solar collector acts as the boiler. One disadvantage of this system is that the pump should be sized according to the required flow rate and system pressure. This makes controlling the boiler pressure more difficult (Al-Khalidy, 1998).

Figure 6.8 (b) shows a closed-loop system. An intermediate heat transfer fluid is used to transport heat from the solar collector to the boiler. For boiler temperatures below 100 °C, water with a corrosion inhibitor is typically used. Transformer oil is best suited when the boiler temperature exceeds 100 °C (Al-Khalidy, 1998).

Figure 6.8 (c) shows an open loop ejector system. This system was experimentally compared to the other two systems mentioned above by Shchetinina et al. (1987). They found that the open loop system gave increased efficiency due to the mean collector temperature that could be reduced. The condensing temperature could be reduced by the use of municipal tap water. This raises the COP of the system.

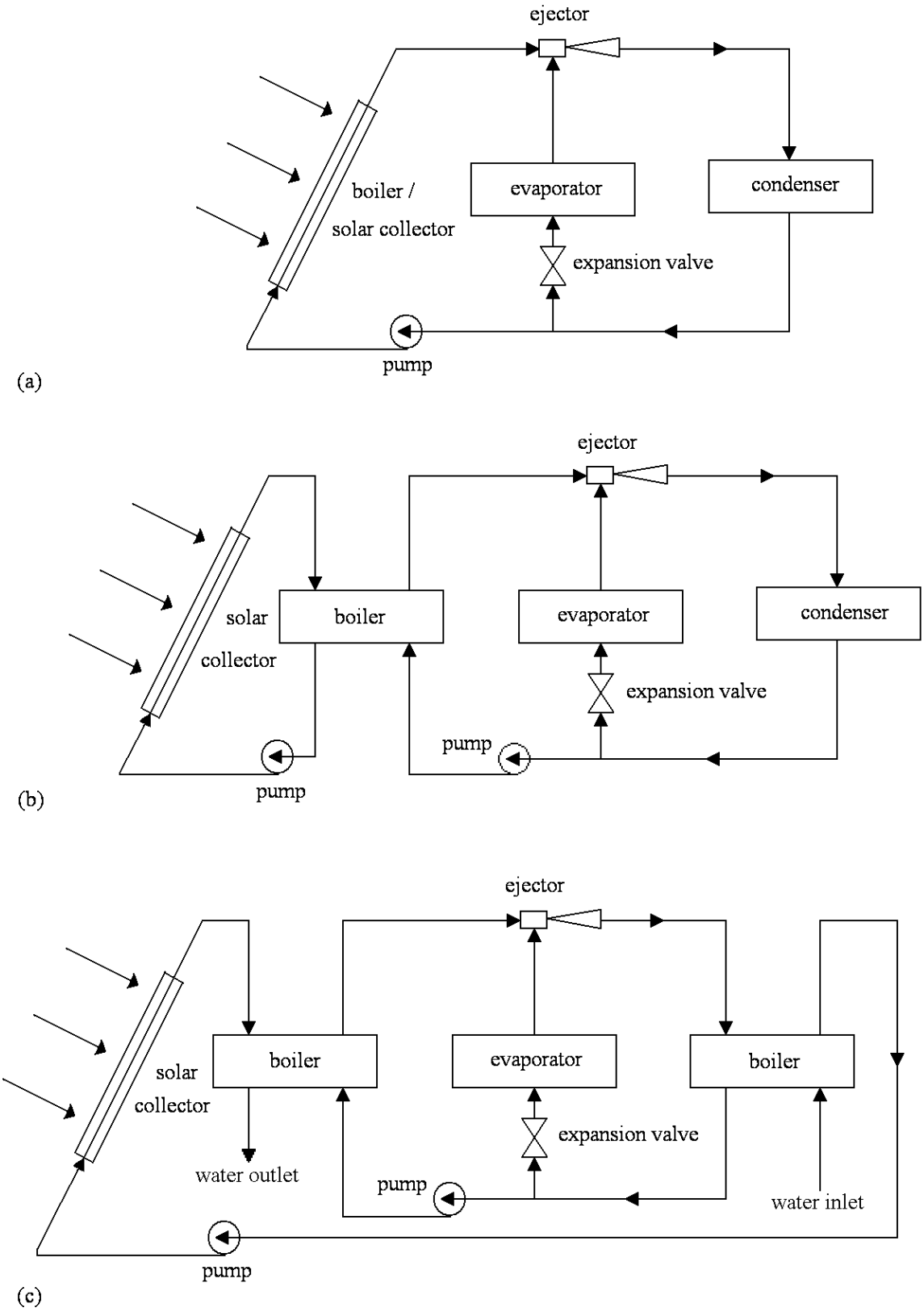

Figure 6.8: Solar powered ejector configurations
(Sun and Eames, 1995)
(a) direct heating
(b) closed-loop
(c) open-loop

6.7 Economic Aspects

6.7.1 Ejector system

Nguyen et al. (2001) compared their solar powered ejector cooling system to a conventional vapour compression air conditioner. The systems were compared over a period of 30 years, which is the expected lifetime of a typical ejector cooling system. The lifetime of a vapour compression system is estimated at 15 years. The required start-up capital calculations was based on an annual interest rate of 6 %. A 600-hour per year running time is assumed. It is assumed that the ejector system has no maintenance cost while two services per year are required for the vapour compression system. These amounts are summarised in table 6.3.

Table 6.3: Equipment purchase cost over a 30-year period (Nguyen et al., 2001)

	Vapour compression	Ejector refrigeration
Expected lifetime (years)	15	30
Initial purchase price (£)	5500	19600
Interest rate (% pa)	6	6
Loan period	15	30
Inflation rate (% pa)	3	3
Replacement required	Yes	No
Replacement cost (£)	8569	-

Table 6.4: Annual running costs (Nguyen et al., 2001)

	Vapour compression	Ejector refrigeration
Total electricity consumption (kW)	2.5	0.3
Cost of electricity (£/kW h)	0.07	0.07
Energy cost (£/h)	0.18	0.021
Running time (h/year)	600	600
Annual energy cost (£)	108	12.6
Service interval (year)	0.5	-
Estimated service cost (£)	120	-
Annual service cost (£)	240	-
Annual running cost (£)	348	12.6

The equipment and running costs for both systems are given in Table 6.4, including the cost incurred over the first 15 years (the assumed vapour compression system lifetime). Over the 30 years, the ejector cooling system is slightly more expensive than the vapour

compression system. The payback period for an ejector cooling system is approximately 33 years.

A similar economic analysis was performed as part of a proposed solar powered ejector air-conditioner for a hospital in Mexico. The system would have a boiler temperature of 160 °C, a condenser temperature of 30 °C and an evaporator temperature of 10 °C. The system would have a 13 kW cooling capacity and a predicted COP of 0.62. The economic analysis predicted a payback period of 5 years (Wolpert et al., 2000 and Wolpert et al., 2003).

In conclusion, the two case studies represented proofed that a solar driven steam jet ejector air conditioning system is economic feasible. In general, the viability of a solar powered ejector air conditioner does depend on the location where the system is installed, which in turn determines the available sunlight, electricity cost and equipment prices.

6.7.2 Solar collectors

The solar ejector system of Nguyen et al. (2001) in the UK used evacuated tube collectors to drive the boiler. A study executed by Meyer (2005) investigated the use of flat plate solar collectors. It was concluded that flat plate solar collectors could be used to drive a steam jet ejector cooling device in locations like Southern Africa where there is an abundance of direct solar radiation. These systems could even operate effectively in the winter months, especially in areas that do not receive winter rain. It was further concluded that the cost of flat plate solar collectors is about 30 % of the cost of evacuated tube collectors. The comparison was based on collectors that produce steam at the same temperature and mass flow rate. Since the solar collector array is a significant cost component of a solar driven ejector system, this could dramatically contribute to the reduction of the total system cost.

6.7.3 Vacuum cooling

Another area where an ejector system has economical advantage is in the cold food storage industry. The vacuum cooling method becomes impractical with conventional systems since the large specific volume of the evaporated gas at low pressures requires compressors with high pressure ratios and large displacement volumes. Sun and Eames (1995) concluded that the steam jet refrigeration systems compete strongly with mechanical compressor systems in these applications. The practical ability of an ejector system to produce rapid cooling was discussed in chapter 5.3.

7. SUMMARY, CONCLUSIONS AND RECOMMENDATIONS

A working prototype of a steam jet ejector was manufactured and successfully operated at boiler temperatures below 100 °C. From the work presented in the previous chapters, it can be further concluded that the steam jet ejector is a viable system on a practical and economical basis.

7.1 Summary

A summary of the objectives and their outcomes are:

7.1.1 Design and build a small scale steam jet ejector experimental setup.

In chapter 2 a small scale steam jet ejector experimental setup was designed and build. The setup is of an open loop configura-tion and it can operate at boiler temperatures in the range of T_b = 85 °C to 140 °C. Typical evaporator liquid temperatures range from T_e = 5 °C to 10 °C while the water-cooled condenser temperatures range from T_c = 15 °C to 35 °C. The boiler is powered by two 4 kW electric element. The cooling load is simulated by a 3 kW electric element. The electric elements are controlled by the use of a variac. Primary nozzles with throat diameters of 1.5 mm, 1.75 mm, 2.0 mm, 2.5 mm, 3.0 mm and 3.5 mm were manufactured. The position of the primary nozzle can be varied relative to the bell mouth inlet of the secondary nozzle. This is accomplished by using spacers of different lengths. Only one secondary nozzle was constructed with a throat diameter of 18 mm. The start-up and operational procedure of the system is explained in chapter 2.

7.1.2 Explain the fluid dynamic theory relevant to the steam jet ejector.

The theory based on published work by Eames et al. (1995a) is explained in chapter 3. The theory accounted for the efficiencies of the primary nozzle, mixing chamber and diffuser. Out of these three efficiencies, the diffuser efficiency has the smallest contribution to the system performance. The efficiency of the mixing chamber is more dominant than the other two efficiencies. The theory lacks in defining the effect of variations in the primary nozzle exit position.

The comparison of the theoretical model to experimental results proofed that the theoretical model is liable to some extend. That is for boiler temperatures in the range T_b = 110 °C to 140 °C. At boiler temperatures in the range T_b = 90 °C to 110 °C the theo-

retical model seems to be less accurate in prediction of the system performance.

7.1.3 Explain the function and fluid dynamics of a steam jet ejector in the context of a literature study.

The work of various authors on small scale steam ejectors were represented in chapter 4. The parameters that govern the functionning of a steam jet ejector are: boiler temperature, evaporator temperature, critical condenser pressure, primary nozzle exit position and the primary and secondary nozzle throat ratio A_R. A condenser pressure below the critical condenser pressure and the super heating of the primary steam has a negligible or no effect on the system's operation.

7.1.4 Verify the operation of a small scale steam ejector system at familiar boiler temperatures.

The operation of a steam ejector is well documented in the boiler temperature range of T_b = 110 °C to 140 °C. Chapter 5 compared experimental results that relate to a boiler temperature of T_b = 130 °C and an evaporator temperature of T_e = 10 °C to that of data published in literature. The experimental data compare well to various published experimental data at similar operating conditions.

7.1.5 As the main aim of this thesis, investigate and document the proposed operation of the system at boiler temperatures below 100 °C.

In chapter 5 primary nozzles with throat diameters of 2.5 mm, 3.0 mm and 3.5 mm are tested while the secondary ejector throat diameter is held constant at 18 mm. The corresponding A_R values for these nozzles are 51.8, 36.0 and 26.4. The different nozzles allow the boiler to operate in the temperature range of 85 °C to 110 °C.

E.g. the system operated at a boiler temperature T_b = 95 °C, a corresponding evaporator temperature of T_e = 10 °C and a critical condenser pressure of P_{crit} = 3.00 kPa (25.2 °C) to yield an electrical COP of 0.253.

7.1.6 Investigate the possibility of a solar thermal driven system

Chapter 6 explained by means of a case study that it is possible to run a steam ejector on solar energy. Although ample work is published on solar powered ejectors with other working fluids, very little data could be found on solar powered steam ejectors.

7.1.7 Through the above lay the foundation for further research in this field of research and comment on any new applications thereof or insight gained into steam jet ejectors powered by low grade waste heat.

The experiments documented in chapter 5 demonstrated that 7 L of water could be cooled from room temperature to 2.4 °C in less than 10 min. The evaporator vapour temperature reached temperatures as low as –8.5 °C.

According to the author the work presented here should serve as an aid as well as a motivation for further research on steam ejectors powered by a low grade heat source including solar energy.

7.2 Conclusions

7.2.1 It can be concluded from the experimental work presented in chapter 5 that this small scale experimental test facility was successfully designed and constructed.

7.2.2 From this literature study in Chapter 4 it can be concluded that the parameters that govern the functioning of a steam jet ejector are: boiler temperature, evaporator temperature, critical condenser pressure, primary nozzle exit position and the primary and secondary nozzle throat ratio A_R. A condenser pressure below the critical condenser pressure and the super heating of the primary steam has a negligible or no effect on the system's operation.

7.2.3 From the experimental work presented in Chapter 5 it can be concluded that it is possible to operate a steam jet ejector at boiler temperatures below 100 °C.

7.2.4 From this experimental work presented it can be concluded that a steam ejector can be applied for rapid subzero vacuum cooling.

7.2.5 It is concluded from the case study that was presented in chapter 6 that solar powered steam jet air conditioning has practical and economically viability when compared to conventional vapour compression air conditioners.

7.3 Recommendations

7.3.1 In practice only closed loop ejector systems are utilised. It is recommended that a condensate pump be installed between the condenser and boiler as well as an expansion valve between the condenser and evaporator. This would reconfigure the experimental setup from an open loop to a closed loop system.

7.3.2 The theory makes no provision for the primary nozzle exit position. There exists a lot of uncertainty about the exact method of the mixing of the primary and secondary streams in the mixing chamber. It would be of great aid to the design of a steam ejector utilising low grade heat if the theory could clearly explain the effect of the primary and secondary nozzle throat diameter ratio on the optimum boiler temperature.

Further investigation into the theoretical model behind the ejectors operation is necessary. The theoretical model should be extended to accommodate the effect of the primary nozzle exit position.

It is technically challenging to measure the exact operation of the mixing chamber, especially the primary nozzle exit velocity and pressure. One method of obtaining a better insight into the functioning of the mixing chamber is by means of computational fluid dynamics (CFD). It is recommended that the use of CFD be incorporated in the research of ejectors.

7.3.3 Except for the authors mentioned in this text, no published data on experimental work done on steam ejectors with boiler temperatures below T_b = 110 °C could be sourced. It is recommended that more experimental tests be conducted on steam ejectors with boiler temperatures below 110 °C.

7.3.4 It is recommended that further theoretical and experimental work be conducted with the focus on solar powered ejector systems. E.g. investigate the possibilities to overcome the part load conditions, night-time cooling, correct solar collector selection and eliminating the condensate pump.

7.3.5 No published work or reference could be found to the application of a steam jet ejector to subzero vacuum cooling. It is recommended that the possibility to use steam ejectors for vacuum cooling in the food industry be investigated.

REFERENCES

Alexis GK and Karayiannis EK (2005) A solar ejector cooling system using refrigerant R134a in the Athens area, *Renewable Energy*, vol 30, pp 1457–1469

Al-Khalidy N (1998) An experimental study of an ejector cycle refrigeration machine operating on R113, *International Journal of Refrigeration*, vol 21(8), pp 617–625

Aphornratana S and Eames IW (1997) A small capacity steam-ejector refrigerator: experimental investigation of a system using ejector with movable primary nozzle, *International Journal of Refrigeration*, vol 20(5), pp 352–358

Arkar C, Vidrih B and Medved S (2006) Efficiency of free cooling using latent heat storage integrated into the ventilation system of a low energy building, *International Journal of Refrigeration*, (In press, corrected proof, available online, www.sciencedirect.com)

Assilzadeh F, Kalogiroub SA, Alia Y and Sopiana K (2005) Simulation and optimization of a LiBr solar absorption cooling system with evacuated tube collectors, *Renewable Energy*, vol 30, pp 1143–1159

ASHRAE (1969) "Steam-jet refrigeration equipment", ASHRAE Guide and Data Book, US, chapter 13

CEI – Clean Energy International (2006), available online, www.cleanenergyinternational.com/solar_water.htm, September 2006

Çengel YA and Boles MA (2002) "Thermodynamics - An Engineering Approach", chapter 16, fourth edition, McGRaw and Hill

Chunnanond K and Aphornratana S (2004a) Ejectors: applications in refrigeration technology, *Renewable and Sustainable Energy Reviews* vol 8, pp 129-155

Chunnanond K and Aphornratana S (2004b) An experimental investigation of a steam ejector refrigerator: the analysis of the pressure profile along the ejector, *Applied Thermal Engineering* vol 24, pp 311-322

Dupont M, Guilleminot JJ, Menuier F and Nguyen P (1982) Study of solar ice conservators using day night intermittent zeolite 13X-water cycle in temperate and tropical climates, *Proceedings of meetings of Commission E1-E2, Jerusalem, Issued by International Institute of Refrigeration*, pp 193-200

Eames IW, Aphornratana S and Haider H (1995a) A theoretical and experimental study of a small-scale steam jet refrigerator, *International Journal of Refrigeration*, vol 18(6), pp 378–386

Eames IW, Aphornratana S and Sun DW (1995b) The jet-pump cycle-a low cost refrigerator option powered by waste heat, *Heat Recovery Systems & CHP*, vol 15(8), pp 711–21

Eames IW, Wu S, Worall M and Aphornratana S (1999) An experimental investigation of steam ejectors for application in jet-pump refrigerators powered by low-grade heat, *Proceedings of the I MECH E Part A Journal of Power and Energy*, 1 October, vol 213(5), pp 351-361

ESDU - Engineering Sciences Data Unit (1986), "*Ejector and Jet Pump Design for Steam Driven Flow*", Engineering Sciences Data Unit, 251-259 Regent Street, London. Item No. 86030

Ewert MK and Bergeron DJ (2000) Development of battery-free solar refrigerator, *Solar Forum 2000 Proceedings*, ISES, Mexico City, September 2000

Fang X and Zhang Z (2006), A novel montmorillonite-based composite phase change material and its applications in thermal storage building materials, *Energy and Buildings*, vol 38(4), pp 377-380

Huang BJ, Jiang CB and Fu FL (1985), Ejector performance characteristics and design analysis of jet refrigeration system. ASME Journal of Engineering for Gas Turbines and Power, vol 107, pp 792–802

Huang BJ, Chang JM, Petrenko VA and Zhuk KB (1998) A solar ejector cooling system using refrigerant R141b, *Solar Energy*, vol 64, (4-6), pp 223–226

Huang BJ and Chang JM (1999) Empirical correlation of ejector design, *International Journal of Refrigeration*, vol 22, pp 379–388

Huang BJ, Petrenko VA, Samofatov IY and Shchetinina NA (2001) Collector selection for solar ejector cooling system, *Solar Energy*, vol 7(4), pp 269–274

Kakabaev A and Davletov A (1966) A Freon ejector solar cooler, *Geliotekhnika*, vol 2(5), pp 42-48

Keenan JH and Neuman E P (1942) A simple air ejector, *ASME Journal of Applied Mechanics*, June, A75-81

Keenan JH, Neuman EP and Lustwerk F (1950) An investigation of ejector design by analysis and experiment, *ASME Journal of Applied Mechanics*, September, pp 299-309

Meyer AJ (2005) Steam jet ejector cooling powered by low grade waste heat, A pre-study report for the thesis of MScEng, Energy Systems Laboratory, Department of Mechanical Engineering, University of Stellenbosch

Munday JT and Bagster DF (1977) A new theory applied to steam jet refrigeration, *Industrial and Engineering Chemistry Process Design and Development*, December, vol 16(4), pp 442–449

Nagano K, Takeda S, Mochida T, Shimakura K and Nakamura T (2006) Study of a floor supply air conditioning system using granular phase change material to augment building mass thermal storage-Heat response in small scale experiments, *Energy and Buildings*, vol 38(5), pp 436-446

Nguyen VN, Riffat SB and Doherty PS (2001) Development of a solar-powered passive ejector cooling system, *Applied Thermal Engineering*, vol 21, pp 157-168

Norfolksolar (2006) www.norfolksolar.co.uk/heatpipe.htm, September 2006

Pridasawas W (2003a) *Solar-driven ejector refrigeration system*, Division of Applied Thermodynamics and Refrigeration, Department of Energy Technology, Royal Institute of Technology, Stockholm, Sweden

Pridasawas W (2003b) *Solar Cooling and Sustainable Refrigeration*, Division of Applied Thermodynamics and Refrigeration, Department of Energy Technology, Royal Institute of Technology, Stockholm, Sweden,

Riffat SB and Holt A (1998) A novel heat pipe/ejector cooler, *Applied Thermal Engineering*, vol 18(3-4), pp 93–101

Rona N (2004) "*Solar Air-Conditioning Systems - Focus on components and their working principles*", eBook-edition, Building Services Engineering, Department of Building Technology, Chalmers University of Technology, Göteborg, Sweden 5765, Internserie: I2004:01, ISSN 1652-6007

Sankarlal T and Mani A (2006) Experimental studies on an ammonia ejector refrigeration system, *International Communications in Heat and Mass Transfer*, vol 33, pp 224–230

Selvaraju A and Mani A (2006) Experimental investigation on R134a vapour ejector refrigeration system, *International Journal of Refrigeration*, available on www.sciencedirect.com

Shchetinina, NA, Zhadan, SZ and Petrenko VA (1987) Comparison of the efficiency of various ways of heating the generator of a solar ejector Freon refrigeration machine, *Geliotekhnika*, vol 23(4), pp 71 – 74

Shen S, Qu X, Zhang B, Riffat S and Gillott M (2005) Study of a gas–liquid ejector and its application to a solar-powered bi-ejector refrigeration system, *Applied Thermal Engineering*, vol 25, pp 2891–2902

Srisastra P and Aphornratana S (2005) A circulating system for a steam jet refrigeration system, *Applied Thermal Engineering*, vol 25, pp 2247–2257

Stoecker WF (1959) *Refrigeration and Air Conditioning*, McGraw-Hill, New York

Sun D and Eames IW (1995) Recent developments in the design theories and applications of ejectors - a review. *Journal of the Institute of Energy*, June 1995, vol 68(475), pp 65-79

Sun D (1996) Variable geometry ejectors and their applications in ejector refrigeration systems. *Journal of Energy*, vol 21(10), pp 919 – 929

Tony (2005) Personal communication

Van Wyk PA (2000) Cooling agricultural produce using a vapour-jet ejector, Final Year Thesis, Department of Mechanical Engineering, University of Stellenbosch, Stellenbosch, South Africa

Vidal H, Colle, S and dos Santos Pereira G (2006) Modelling and hourly simulation of a solar ejector cooling system, *Applied Thermal Engineering*, vol 26, pp 663–672

Wolpert JL, Nguyen MV and Riffat SB (2000) Hybrid Solar/Gas Cooling Ejector unit for a Hospital in Mexico, Institute of Building Technology, School of the Built Environment; University of Nottingham; University Park, Nottingham, NG7 2RD,
ISES website: wire0.ises.org/wire/doclibs/SWC1999.nsf/id/793B72DDE2B79A75C1256920003D618F/$File/109.pdf, Nov 2004

Wolpert JL, Riffat SB and Redshaw S (2003) Prototype for a novel solar powered ejector air conditioning system in Mazunte Mexico,

University of Nottingham, Institute of Building Technology, Nottingham, United Kingdom, *Proceeding of the International Solar Energy Congress 2003*, Gothenburg

APPENDIX A – ADDITIONAL TABLES

Table A.1: Experimental results (Eames et al., 1995b)

T_e [°C]	T_b [°C]	T_c [°C]	P_c [kPa]	COP_{elec}	COP_{water}	COP_{theo}
5	120	26.5	3.45	0.239	0.404	0.508
5	125	27.8	3.75	0.197	0.344	0.466
5	130	30.8	4.46	0.157	0.276	0.365
5	135	33.4	5.17	0.127	0.251	0.316
5	140	34.4	5.47	0.102	0.178	0.277
7.5	120	27.3	3.65	0.306	0.500	0.597
7.5	125	29.5	4.16	0.250	0.419	0.505
7.5	130	31.5	4.66	0.207	0.355	0.436
7.5	135	33.4	5.17	0.173	0.297	0.379
7.5	140	35.3	5.78	0.138	0.233	0.328
10	120	28.3	3.85	0.369	0.586	0.685
10	125	30.0	4.26	0.328	0.537	0.607
10	130	31.9	4.76	0.288	0.473	0.530
10	135	34.0	5.37	0.237	0.389	0.454
10	140	36.3	6.08	0.188	0.309	0.382

Table A.2: Geometries of different nozzles

	Geometries[mm]				
Nozzle number	A	B	C	D	E
1	1.5	6	69.25	8	25.75
2	1.75	7	65.00	8	30.00
3	2.0	8	60.70	8	34.30
4	2.5	8	60.70	8	34.30
5	2.5	10	42.85	8	52.15
6	3.0	12	51.50	8	43.50
7	3.5	14	60.00	8	35.00

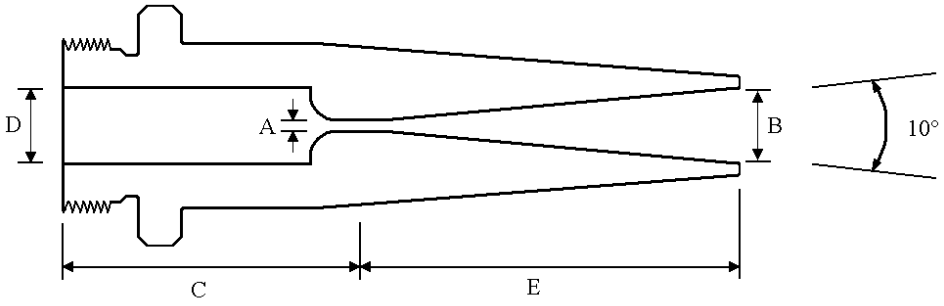

Table A.3: Serial numbers of devices used in experiments

Device	Serial number
IR Camera	2297380101-0001
Aligent data logger (34970A)	34970A MY44000670
Personal computer	20020227010

Table A.4: Summary of experimental results

T_{e_vapour} [℃]	T_{e_liquid} [℃]	T_b [℃]	NXP [mm]	Nozzle [number]	COP_{elec}	COP_{water}	T_{crit} [°C] [℃]	P_{crit} [kPa]
6.5	9.6	110.8	-5	5	0.383	0.399	>17.0*	1.96
6.1	8.6	115.9	-5	5	0.331	-	>19.6*	2.29
-	-	95	-5	6	-	-	-	
5.5	8.4	100.3	-5	6	0.231	0.210	18.2	2.11
5.6	8.6	105.3	-5	6	0.222	0.233	20.8	2.44
*	9.5	95	-25	7	0.177	-	19.1	2.22
5.1	8.1	100.5	-25	7	0.213	0.110	21.7	2.55
4.2	7.7	105	-25	7	0.156	0.129	27.3	3.26
7.0	9.0	91.1	-5	7	0.324	-	>16.9*	1.95
6.5	9.4	95.4	-5	7	0.253	0.265	22.6	2.67
7.3	9.8	100.3	-5	7	0.219	0.221	23.5	2.78
6.9	9.8	105.5	-5	7	0.202	0.211	31.6	3.81
6.3	9.1	95.2	15	7	0.203	0.209	21.4	2.52
6.9	9.7	100.3	15	7	0.166	0.151	25.1	2.98
7.1	9.9	105.2	15	7	0.182	0.183	30.1	3.62
6.6	9.1	85.3	35	7	0.193	-	>15.6*	1.78
8.1	10.0	90.2	35	7	0.197	-	>17.3*	2.00
7.4	9.9	95.2	35	7	0.148	-	>17.2*	1.98
7.3	9.7	100.2	35	7	0.122	-	>18.2*	2.11
7.4	10.0	105.5	35	7	0.126	-	>20.1*	2.35
7.4	10.0	110.9	35	7	0.108	-	>18.1*	2.10
7.2	9.8	129.8	25	3	0.284	0.308	30.0	4.25

* normal operating T_c value (below T_{crit})

APPENDIX B – ADDITIONAL PHOTOS/FIGURES

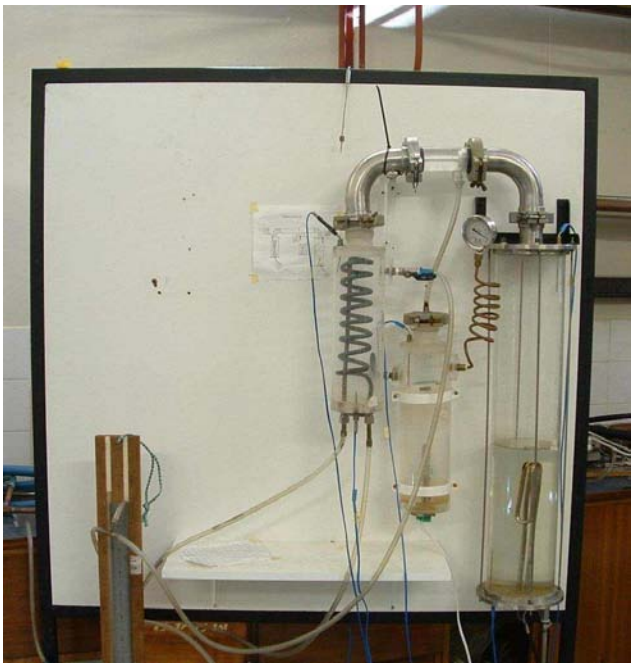

Figure B.1: Previous ejector setup at Stellenbosch University

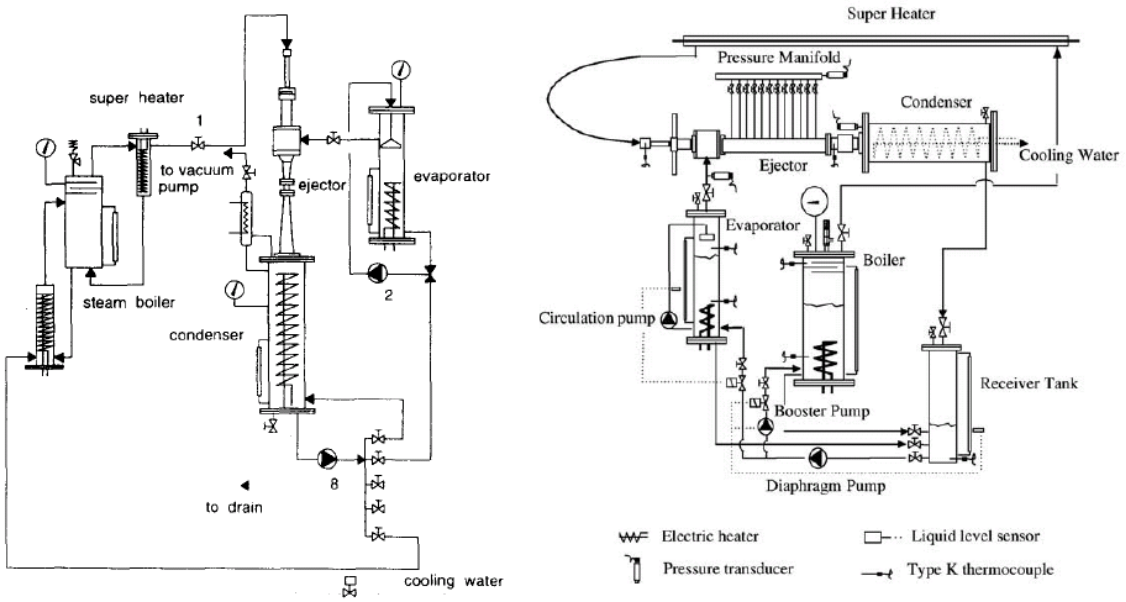

Figure B.2: Experimental setups from other authors (Aphornratana

and Eames, 1997, Left), (Chunnanond and Aphornratana, 2004, Right)

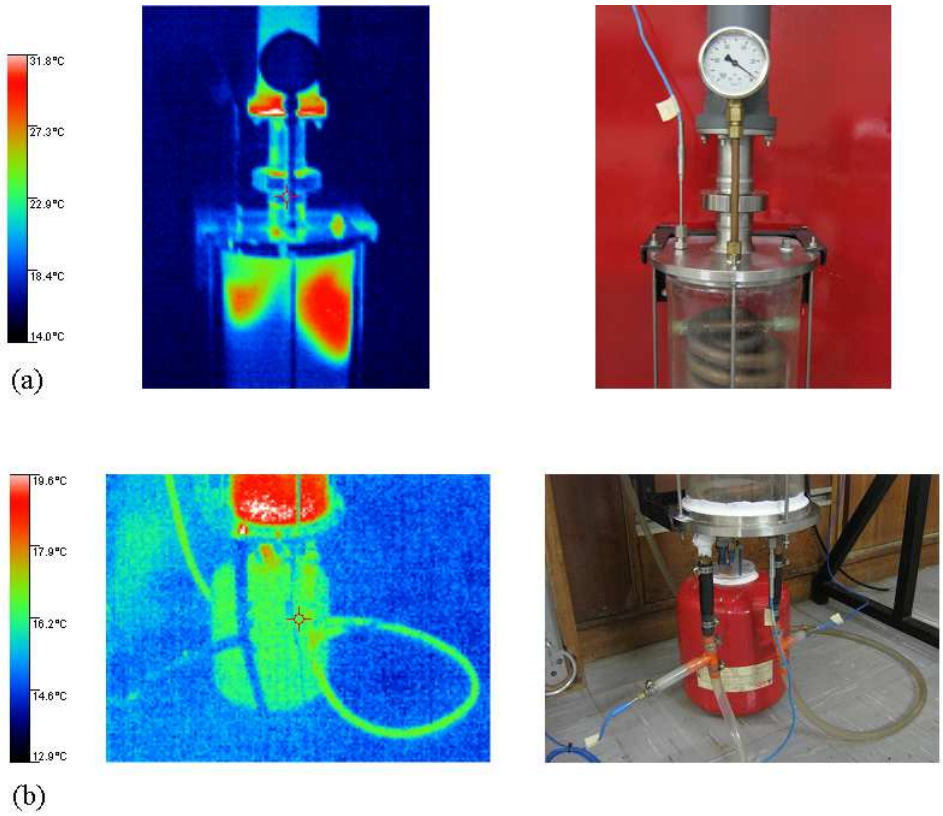

Figure B.3: IR and normal images of the condenser
(a) The condenser top (b) Reservoir and cooling water

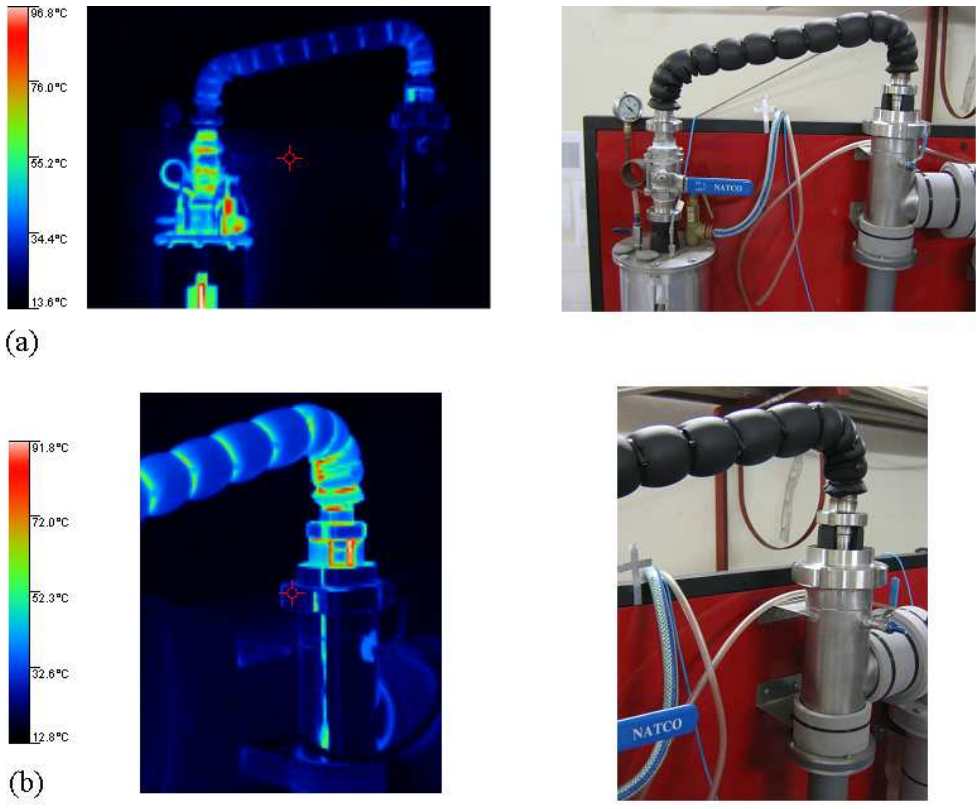

Figure B.4: IR and normal images of the steam pipe
(a) The boiler top and steam pipe
(b) The steam pipe inlet and ejector

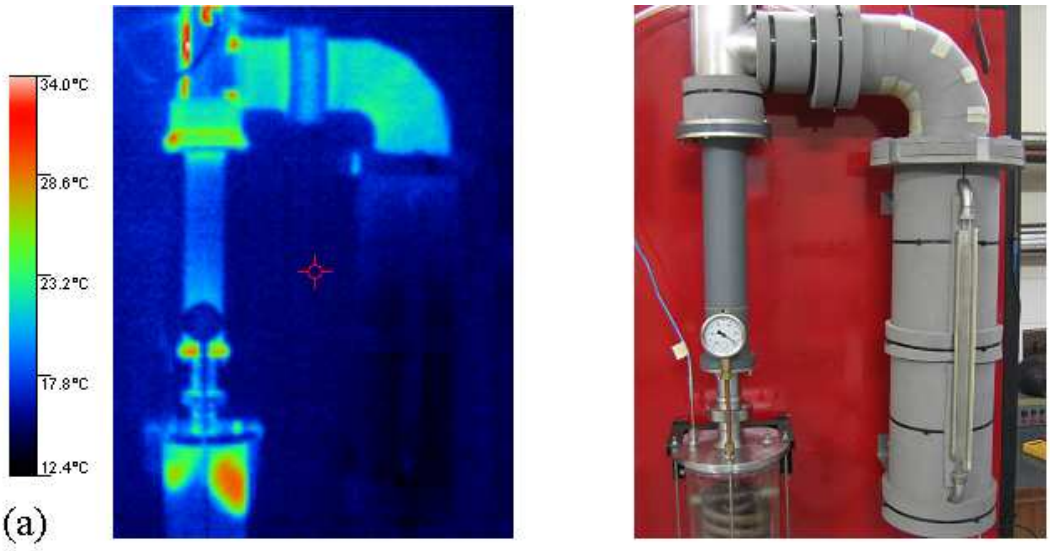

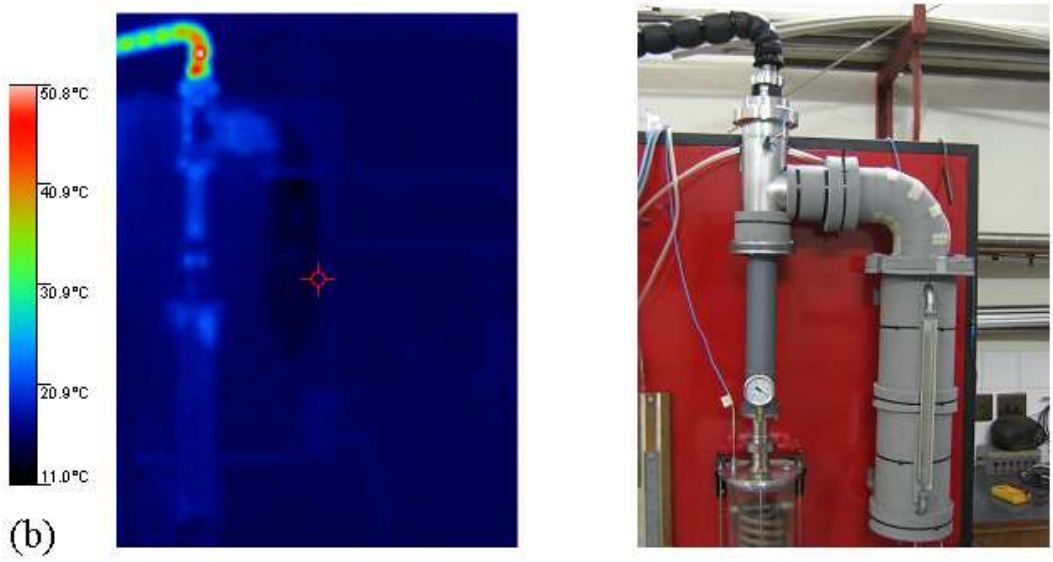

Figure B.5: IR and normal images of the evaporator
(a) The evaporator, ejector and condenser top
(b) The evaporator, ejector, condenser and steam pipe inlet

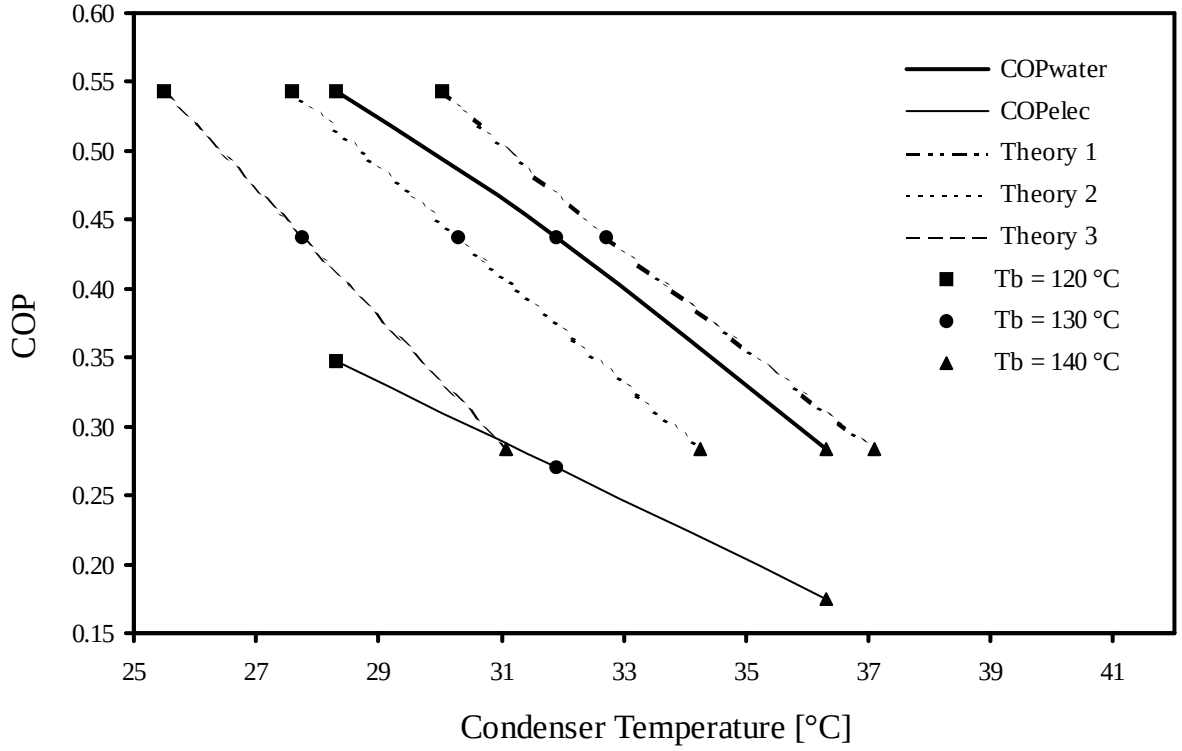

Figure B.6: Water and electric COP compared to three theoretical models. T_e = 10 °C, A_R = 81, NXP = 26 mm (Eames et al., 1995)

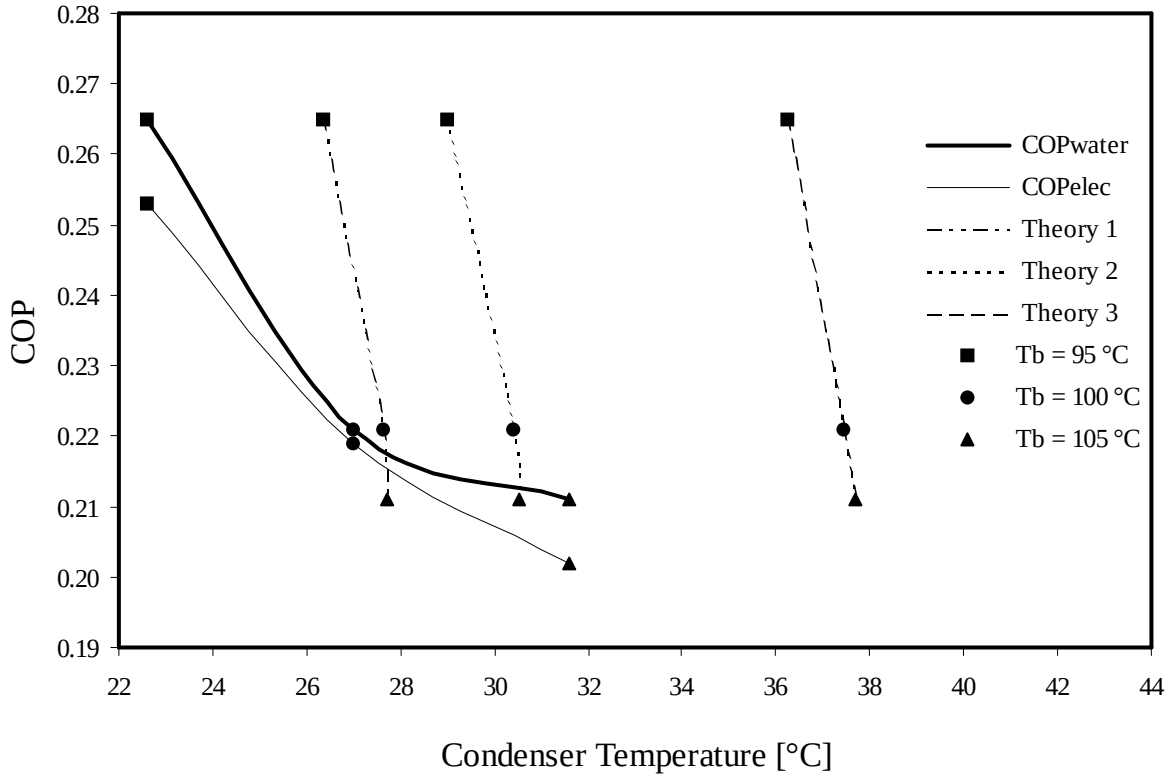

Figure B.7: Electric and water COP compared to three theoretical models. T_b = 95 °C to 105 °C, T_e = 10 °C, A_R = 26.5

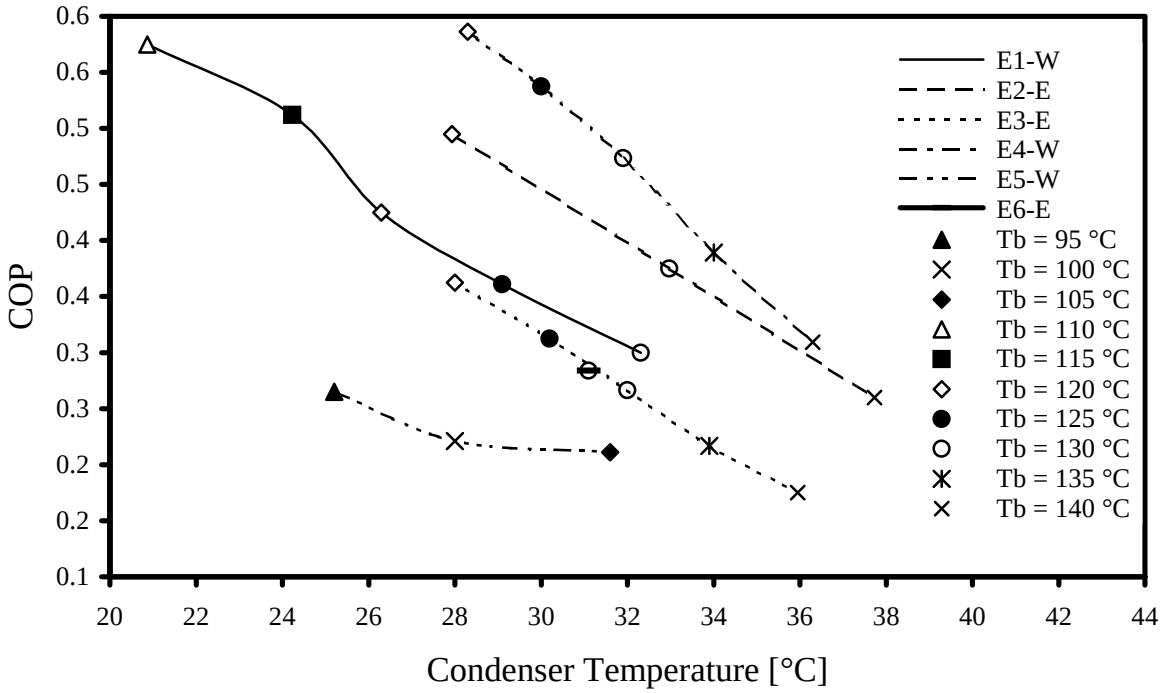

Data Series	Author*	Measured Data	System	A_R	NXP [mm]	T_e [°C]
E1-W	1	COP_{water}	Closed	81	-	10
E2-E	2	COP_{elec}	Closed	90	26.16	10
E3-E	3	COP_{elec}	Closed	81	26	10
E4-W	4	COP_{water}	Closed	90	26.16	10
E5-W	5	COP_{water}	Open	36	16	10
E6-E	6	COP_{elec}	Open	81	25	10

*1) Sun (1996)
2) Chunnanond and Aphornratana (2004)
3) Aphornratana and Eames (1997)
4) Eames et al. (1995)
5) Author – Nozzle 7
6) Author – Nozzle 3

Figure B.8: Comparison of different published data for T_b = 95 °C to 140 °C and T_c = 10 °C

APPENDIX C – EXPERIMENTAL SETUP

DRAWING TREE :

Steam Jet Ejector Complete Assembly (SteamJet06_00_00A)**
- **Boiler Assembly (SteamJet06_01_00A)**
  - Main Boiler Pipe (SteamJet06_01_01P)*
  - Flange (SteamJet06_01_02P)*
  - Flange (SteamJet06_01_03P)*
  - Male Union (SteamJet06_01_04P)*
  - Pipe (SteamJet06_01_05P)*
  - Flange (SteamJet06_01_06P)*
- **Condenser Assembly (SteamJet06_02_00A)**
  - Pipe (SteamJet06_02_01P)*
  - Flange (SteamJet06_02_02P)*
  - Flange (SteamJet06_02_03P)*
  - Pipe (SteamJet06_01_05P)*
  - Union (SteamJet06_01_04P)*
- **Evaporator Assembly (SteamJet06_03_00A)**
  - Pipe (SteamJet06_03_01P)*
  - Pipe (SteamJet06_03_02P)*
  - Flange (SteamJet06_03_03P)*
  - Flange (SteamJet06_03_04P)*
  - Flange (SteamJet06_03_05P)*
  - Elbow (SteamJet06_03_06P)*
  - Union (SteamJet06_03_07P)*
- **Steam Pipe Assembly (SteamJet06_04_00A)**
  - Pipe (SteamJet06_04_01P)*
  - Elbow (SteamJet06_04_02P)*
  - Union (SteamJet06_01_04P)*
  - Elbow (SteamJet06_04_03P)*
  - Pipe (SteamJet06_01_05P)*
  - Elbow (SteamJet06_04_04P)*
  - Union (SteamJet06_04_05P)*
- **Ejector Assembly (SteamJet06_05_00A)**
  - Ejector (SteamJet06_05_01P)
  - Flange (SteamJet06_05_02P)*
  - Flange (SteamJet06_05_03P)*
  - Union (SteamJet06_05_04P)*
  - Flange (SteamJet06_05_05P)*
  - Pipe (SteamJet06_01_05P)*
  - Union (SteamJet06_04_05P)*
  - T-Piece (SteamJet06_05_06P)*
- **Ejector Top Assembly (SteamJet06_06_00A)**
  - Flange (SteamJet06_06_01P)*

Spacer (SteamJet06_06_05P)*
Spacer (SteamJet06_06_04P)*
Nozzle (SteamJet06_06_13P)*
Union (SteamJet06_05_04P)*
Pipe (SteamJet06_01_05P)*
Union (SteamJet06_04_05P)*

Additional parts

Nozzle (SteamJet06_06_11P)
Nozzle (SteamJet06_06_12P)
Nozzle (SteamJet06_06_13P)
Nozzle (SteamJet06_06_14P)
Nozzle (SteamJet06_06_15P)
Nozzle (SteamJet06_06_16P)
Nozzle (SteamJet06_06_17P)
Spacer (SteamJet06_06_04P)*
Spacer (SteamJet06_06_05P)*
Spacer (SteamJet06_06_06P)*
Spacer (SteamJet06_06_07P)*
Spacer (SteamJet06_06_08P)*
Spacer (SteamJet06_06_09P)*
Spacer (SteamJet06_06_10P)*

*These parts are included on the data CD at the back of this thesis.

**The letter A at the end of a part number indicates that it is an assembly. The letter P indicates that it is a part.